

AD 748428

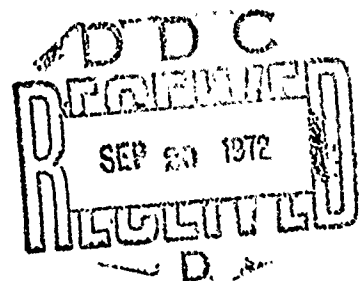
INVESTIGATION OF TARGET TRACKING ERRORS IN MONOPULSE RADARS

FINAL TECHNICAL REPORT

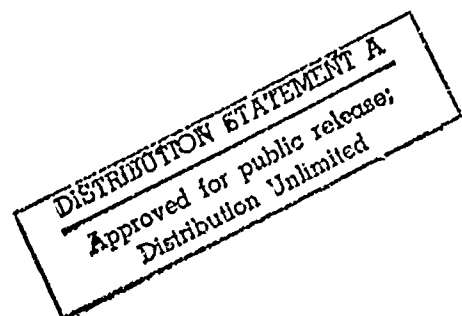
by G. W. Ewell, N. T. Alexander, and E. L. Tomberlin

July 1972

Prepared for
Advanced Sensors Directorate
Research, Development, Engineering
and Missile Systems Laboratory
U. S. Army Missile Command
Redstone Arsenal, Alabama 35809



by
Engineering Experiment Station
Georgia Institute of Technology
Atlanta, Georgia 30332



DISTRIBUTION OF THIS DOCUMENT IS UNLIMITED

Reprinted by
NATIONAL TECHNICAL
INFORMATION SERVICE
U. S. Department of Commerce
Springfield, VA 22151

ADDITIONAL TO	
THIS	<input checked="" type="checkbox"/>
DATE	<input type="checkbox"/>
BY	<input type="checkbox"/>
BY	
BY	
A	

Information and data contained in this study are based on the input available at the time of preparation. Because the results may be subject to change and concern only limited aspects of this subject, this document should not be construed to represent the official position of the U. S. Army Material Command.

The findings in this report are not to be construed as an official Department of the Army position unless so designated by other authorized documents.

Destroy this report when no longer needed. Do not return it to the originator.

UNCLASSIFIED

Security Classification

DOCUMENT CONTROL DATA - R & D

(Security classification of title, body of abstract and indexing annotation must be entered when the overall report is classified)

1. ORIGINATING ACTIVITY (Corporate author) Engineering Experiment Station Georgia Institute of Technology		2a. REPORT SECURITY CLASSIFICATION Unclassified	
		2b. GROUP N. A.	
3. REPORT TITLE Investigation of Target Tracking Errors in Monopulse Radars.			
4. DESCRIPTIVE NOTES (Type of report and inclusive dates) Final Technical Report May 1971-July 1972			
5. AUTHOR(S) (First name, middle initial, last name) George W. Ewell, Neal T. Alexander, and Edwin L. Tomberlin			
6. REPORT DATE July 1972		7a. TOTAL NO. OF PAGES 119	7b. NO. OF REFS 55
8a. CONTRACT OR GRANT NO. DAAH01-71-C-1192		8b. ORIGINATOR'S REPORT NUMBER(S) GIT-A-1336-F	
b. PROJECT NO. c. d.		9b. OTHER REPORT NO(S) (Any other numbers that may be assigned this report) Georgia Tech Project A-1336	
10. DISTRIBUTION STATEMENT Distribution of this document is unlimited			
11. SUPPLEMENTARY NOTES		12. SPONSORING MILITARY ACTIVITY U.S. Army Missile Command Redstone Arsenal, Alabama 35809	
13. ABSTRACT This Final Technical Report on Contract DAAH01-71-C-1192 discusses investigations of tracking errors associated with a particular monopulse phased-array radar system, called the Experimental Array Radar (EAR). The free-space performance of the EAR is first analyzed and degradations of performance due to particular target Doppler shifts and multipath returns are noted. A computer analysis of the tracking performance of the EAR is then presented, and it is noted that there are significant tracking errors due to multipath returns for targets at altitudes less than 1200 feet. An analysis of the effectiveness of frequency-agile operation in reducing the effects of these multipath returns is presented, and shows that the available frequency-agility bandwidth of a modified EAR would significantly reduce multipath-induced tracking errors, particularly for higher antenna and target locations. Improved MTI filters which provide more nearly uniform responses for a wide range of Doppler frequencies are then discussed and a number of representative improved filter responses presented.			

16'

DD FORM 1 NOV 66 1473

UNCLASSIFIED

Security Classification

INVESTIGATION OF TARGET TRACKING ERRORS IN
MONOPULSE RADARS

Final Technical Report

by

G. W. Ewell, N. T. Alexander, and E. L. Tomberlin

July 1972

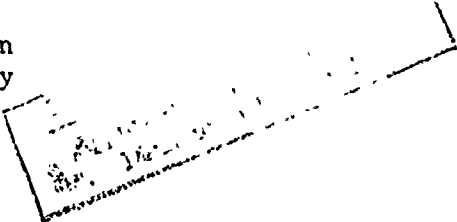
Contract DAAH01-71-C-1192

Project A-1336

Prepared for
Advanced Sensors Directorate
Research, Development, Engineering and
Missile Systems Laboratory
U. S. Army Missile Command
Redstone Arsenal, Alabama 35809

by

Engineering Experiment Station
Georgia Institute of Technology
Atlanta, Georgia 30332



Distribution of this document is unlimited

ABSTRACT

This Final Technical Report on Contract DAAH01-71-C-1192 discusses investigations of tracking errors associated with a particular monopulse phased-array radar system, called the Experimental Array Radar (EAR). The free-space performance of the EAR is first analyzed and degradations of performance due to particular target Doppler shifts and multipath returns are noted. A computer analysis of the tracking performance of the EAR is then presented, and it is noted that there are significant tracking errors due to multipath returns for targets at altitudes less than 1200 feet. An analysis of the effectiveness of frequency-agile operation in reducing the effects of these multipath returns is presented, which shows that the available frequency-agility bandwidth of a modified EAR would significantly reduce multipath-induced tracking errors, particularly for higher antenna and target locations. Improved MTI filters which provide more nearly uniform responses for a wide range of Doppler frequencies are then discussed and a number of representative improved filter responses presented.

FOREWORD

The efforts of numerous people at MICOM and at Georgia Tech have contributed substantially to the performance of the work described in this report. At MICOM the cooperation of a number of people involved with the EAR program has substantially aided the investigation described herein. The assistance and guidance provided by Mr. J. Hatcher and Mr. R. Fletcher were particularly valuable. Without the continuing interest and support of Mr. W. Lindberg and Mr. W. Low, this program would not have been possible.

At Georgia Tech, in addition to the authors, Mr. T. Brewer and Dr. R. Larson made substantial contributions to the technical effort.

Preceding page blank

TABLE OF CONTENTS

	<u>Page</u>
I. INTRODUCTION	1
II. PRELIMINARY INVESTIGATION OF EAR PERFORMANCE	3
A. Free-Space Signal-to-Noise Ratio	3
B. Tracking Errors Due to Glint and Thermal Noise	5
C. Radar Angle Tracking Errors Due to Multipath Returns	8
D. Clutter Effects on the EAR	8
III. MULTIPATH EFFECTS ON EAR ANGLE TRACKING ACCURACY	13
A. Introduction	13
B. Geometry of the Target Trajectory.	13
C. Calculation of Received Signals and Indicated Errors	15
D. Antenna Pattern Generation	17
E. Program Organization	20
F. Results of Computer Analysis	20
IV. APPLICABILITY OF FREQUENCY AGILITY TO THE EAR.	27
A. Required Overall Frequency Agility Bandwidth	33
B. Effect of Frequency Agility on Angle Tracking Performance.	36
C. Adaptive Processing for the EAR System	36
V. IMPROVED MTI PROCESSORS.	43
A. Use of Statistical Detection Theory in Developing Optimum MTI Receivers.	43
B. Optimization of MTI Processors Using Weighted Sums of Sampled Signals.	46
C. MTI Processor Design as a Filter Optimization Problem.	47
D. Conventional Digital-Filter Design Procedures.	49
E. Optimum Transversal Digital-Filter Design Procedures for Unstaggered prf Systems.	50
1. "Cost" Minimization MTI Filters.	50
2. Filter Design by Linear Programming.	52
3. MTI Clutter Rejection Filters Using an rms Error Specification.	57
a. Improvement for an Arbitrary N-Pulse Canceller	59
b. Error Statement.	60

Preceding page blank

TABLE OF CONTENTS (cont.)

	<u>Page</u>
c. Optimization	61
d. Results.	62
4. Maximally Flat Non-Recursive Digital MTI Filters . . .	67
F. MTI Processors Using Staggered prf	70
VI. CONCLUSIONS AND RECOMMENDATIONS.	79
A. Primary Conclusions.	79
B. Principal Recommendations.	79
VII. REFERENCES	81
VIII. APPENDICES	87

LIST OF FIGURES

<u>Figure</u>	<u>Page</u>
1. Average signal-to-noise ratio for the EAR system as a function of range.	4
2. Response of a conventional three-pulse canceller having filter tap weights of 1, -2, and 1	6
3. Average tracking errors due to thermal noise and glint as functions of range for the EAR system	7
4. RMS tracking errors due to multipath as a function of the ratio of direct to indirect signals at the receiver	9
5. Signal-to-clutter ratio after MTI filtering (56 dB MTI improvement) as a function of range for the EAR system using a one-microsecond pulse	11
6. Antenna/target geometry	14
7. Indicated angular error versus actual angular error for $K = 0.86$	16
8. Indicated angular error versus actual angular error for $K = 0.845 + 0.335 (\theta \text{ scan}/30)$	18
9. Typical sum (solid lines) and difference (dashed lines) patterns used in the computer analysis.	19
10. Tracking error as a function of time. $H_a = 100 \text{ ft}$, $H_t = 300 \text{ ft}$, $f = 5.5 \text{ GHz}$, $\rho = 0.5$, tilt angle = 0°	21
11. Tracking error as a function of time. $H_a = 100 \text{ ft}$, $H_t = 300 \text{ ft}$, $f = 5.5 \text{ GHz}$, $\rho = 0.5$, tilt angle = 30°	22
12. Tracking error as a function of time. $H_a = 100 \text{ ft}$, $H_t = 500 \text{ ft}$, $f = 5.5 \text{ GHz}$, $\rho = 0.5$, tilt angle = 30°	24
13. Tracking error as a function of time. $H_a = 15 \text{ ft}$, $H_t = 300 \text{ ft}$, $f = 5.5 \text{ GHz}$, $\rho = 0.5$, tilt angle = 30°	25
14. Peak-to-peak elevation tracking errors as functions of target height for 15 and 100 feet antenna heights. $\rho = 0.5$ and frequency is 5.5 GHz.	26
15. Tracking error as a function of time. $H_a = 100 \text{ ft}$, $H_t = 300 \text{ ft}$, $f = 5.3 \text{ GHz}$, $\rho = 0.5$, tilt angle = 30°	28
16. Tracking error as a function of time. $H_a = 100 \text{ ft}$, $H_t = 300 \text{ ft}$, $f = 5.4 \text{ GHz}$, $\rho = 0.5$, tilt angle = 30°	29
17. Tracking error as a function of time. $H_a = 100 \text{ ft}$, $H_t = 300 \text{ ft}$, $f = 5.5 \text{ GHz}$, $\rho = 0.5$, tilt angle = 30°	30

LIST OF FIGURES (cont.)

Figure	Page
18. Tracking error as a function of time. $H_a = 100$ ft, $H_t = 300$ ft, $f = 5.6$ GHz, $\rho = 0.5$, tilt angle = 30°	31
19. Tracking error as a function of time. $H_a = 100$ ft, $H_t = 300$ ft, $f = 5.7$ GHz, $\rho = 0.5$, tilt angle = 30°	32
20. Frequency change required to change the relative phase of the direct and reflected signals by π . Antenna height = 15 ft.	34
21. Frequency change required to change the relative phase of the direct and reflected signals by π . Antenna height = 100 ft	35
22. Tracking error as a function of target height using frequency agility. $H_a = 100$ ft	37
23. Tracking error as a function of target height using frequency agility. $H_a = 15$ ft.	38
24. Tracking error as a function of target height using frequency agility. $H_a = 100$ ft	39
25. Complex indicated angle (CIA) as a function of time for the same target-radar parameters described in Figure 17	41
26. Sum signal variations as a function of time for the same target-radar parameters described in Figure 17	42
27. Response of conventional three-pulse MTI canceller or filter as a function of Doppler frequency.	48
28. Filter response for a four-pole Butterworth high-pass filter (labelled steady-state response) and the output of the same recursive filter terminated after $N = 3, 5$, and 7 pulses were processed. The steady-state response has been offset for clarity	51
29. MTI filter responses developed using linear programming techniques. 0.8-, 1.8-, and 3-dB ripple specification. See text for details.	54
30. Effects on MTI filter response of too stringent a ripple specification. See text for details.	55
31. Ripple vs. clutter attenuation for 5-pulse filters with 500 Hz and 750 Hz lower cutoff frequencies	56
32. Bandstop filters showing effects of increasing allowable ripple on stop band characteristics. $F_c = 250$ Hz.	58

LIST OF FIGURES (cont.)

<u>Figure</u>	<u>Page</u>
33. Comparison of the response of a conventional three-pulse MTI filter and a minimum-rms-error filter designed for $I = 60$ dB, $\text{prf} = 5000$ pps, $\sigma_c = 8.0$, and $\eta = 0.1$	63
34. Comparison of responses of minimum-rms-error filters designed for $I = 10, 30$, and 60 dB. $\eta = 0.1$, $\text{prf} = 5000$ pps, and $\sigma_c = 8.0$	64
35. Comparison of minimum-rms-error filter responses for 3, 5, and 7 pulses processed. $I = 60$ dB, $\text{prf} = 5000$ pps, $\sigma_c = 8.0$, $\eta = 0.1$	65
36. Comparison of responses of five-pulse minimum-rms-error filters for $\eta = 0$ and $\eta = 0.1$. $I = 60$ dB, $\sigma_c = 8.0$, $\text{prf} = 5000$ pps. . .	66
37. Maximally flat three-pulse MTI filter response. $I = 60$ dB . . .	68
38. Comparison of responses for three-pulse maximally flat three pulse MTI filter ($I = 60$ dB) and minimum-rms-error MTI filter ($I = 60$ dB, $\eta = 0.1$, $\sigma_c = 8.0$, $\text{prf} = 5000$)	69
39. Maximally flat MTI filter responses for three- and four-pulses processed.	71
40. Maximally flat filter responses for a four-pulse MTI filter for $i = 0$, and $i = 1$	72
41. Maximally flat filter responses for a five-pulse MTI filter for $i = 0, 1$, and 2	73
42. Filter response for a conventional three-pulse MTI filter when various values of stagger, ϵ , are used	74
43. System improvement versus clutter spectral width for radar system with $f_r = 5$ kHz and $\lambda = 5.5$ cm, $K =$ stagger ratio for staggered prf.	77
44. Response of an optimum unstaggered MTI filter when used with various amount of prf stagger, ϵ	78
A-1. Three-pulse MTI filter	90
A-2. System improvement versus clutter spectral width for radar system with $f_r = 5$ kHz and $\lambda = 5.5$ cm	94
C-1. Representative received pulse shape showing the samples used in the range-tracking algorithms.	98

LIST OF FIGURES (cont.)

<u>Figure</u>	<u>Page</u>
C-2. ϵ_r/k as a function of t_o/τ for f_{3dB} $\tau = 1$ and $\Delta/\tau = 1$	100
C-3. ϵ_r/k as a function of t_o/τ for f_{3dB} $\tau = 2$ and $\Delta/\tau = 1$	101
E-1. Main computer program.	104
E-2. Subroutine GAIN.	106
E-3. Subroutine DIST.	107
E-4. Subroutine STNDEV.	108
E-5. Subroutine ERRO.	109
E-6. Subroutine RCS	111
D-1. Velocity response for frequency-agile radar using three-pulse MTI filter. $F_{start} = 5.3$ GHz, $F_{final} = 5.6$ GHz, Step = 0.05 GHz.	114
D-2. Velocity response for frequency-agile radar using three-pulse MTI filter. $F_{start} = 5.3$ GHz, $F_{final} = 5.8$ GHz, Step = 0.03125 GHz.	115
F-1. General form of non-recursive digital filters.	118

I. INTRODUCTION

This Final Technical Report describes work performed for the U. S. Army Missile Command under Contract DAAH01-71-C-1192 from May 1971 through May 1972. The investigations carried out during this period involved analyzing the Experimental Array Radar (EAR) being constructed by the Missile Systems Laboratory, and developing methods for improving its performance.

These investigations were initially based on work performed for the Missile Command under Contract DAAH01-70-C-0535 [1]*, under which Georgia Tech examined the effects of polarization agility on monopulse radar angle tracking. The techniques and target models developed under this earlier Missile Command contract formed the basis for a substantial portion of the work performed under the current contract.

The initial phase of the program was concerned with preliminary analyses of the performance of the EAR system and identification of areas of marginal performance. A modified C-Band radar at Georgia Tech was used to estimate anticipated radar cross-section of targets for incorporation into this preliminary performance analysis. Results of this preliminary analysis are presented in Section II, and indicate deterioration in the performance of the EAR when the target has a relatively low Doppler frequency and/or when strong multipath returns are being received by the system.

The effect of strong multipath returns on the tracking performance of the EAR when tracking low-flying targets is analyzed in some detail in Section III. The applicability of frequency agility to the EAR system for the purpose of minimizing these multipath-induced errors is discussed in Section IV. The analyses in both of these chapters leans heavily on a computer prediction of the EAR performance which included realistic representation of antenna beamshapes, null positions, and sidelobe levels.

The design of optimum MTI processors for use in the EAR system is treated in some detail in Section V. Previous work in digital processing is reviewed and improved procedures for design of processors having optimum responses for a range of Doppler shifts are presented.

Conclusions and recommendations resulting from this study are presented in Section VI.

*Numbers in brackets refer to References in Section VII.

II. PRELIMINARY INVESTIGATION OF EAR PERFORMANCE

The initial step in the research program was a preliminary system analysis to define the performance of the EAR and to focus attention to those areas where performance is marginal. First, the free-space signal-to-noise ratio was calculated for the EAR system, and the effect of thermal noise on angle-tracking accuracy was analyzed. Next, the effect of multipath returns entering the antenna sidelobes (the high angle tracking case) was considered, and finally signal-to-clutter ratios were calculated for the EAR system

A. Free-Space Signal-to-Noise Ratio

The system parameters assumed in the preliminary analysis of the free-space signal-to-noise ratio for the EAR system were:

P_t = peak transmitted power = 75 kW;

G = antenna gain (assumed to be same for both transmit and receive modes) = 25 dB;

λ = wavelength = 5.45×10^{-2} meters (5.5 GHz); and

N = noise power = -93 dBm (10-dB noise figure, 10-MHz bandwidth).

The free-space, single-pulse, signal-to-noise ratio (S/N), is given by

$$S/N = \frac{P_t G^2 \lambda^2 \sigma}{N (4\pi)^3 R^4} = \frac{2.245 \times 10^{16} \sigma}{R^4},$$

where

R = range in meters, and

σ = target radar cross-section in square meters.

The average signal-to-noise ratio (averaged over all Doppler frequencies and relative phases) is unaffected by MTI processing. This can be seen readily by considering that the average power gain of a two-channel MTI processor is six, and that six noise samples are added during processing, so that the output signal-to-noise is unaffected. In a single-channel processor, the average gain is reduced to three (due to the necessity of averaging over all relative phases) but now only three noise pulses are added, so the output signal-to-noise ratio remains unchanged.

When processing in triplets, as in the EAR system [2], the 48 pulses on a target produce 16 independent samples. Approximately 10 dB should be added to the signal-to-noise ratio calculated earlier to account for effects of integration of these 16 samples. Figure 1 shows the average free-space signal-to-noise ratio as a function of range for several values of target radar cross-section.

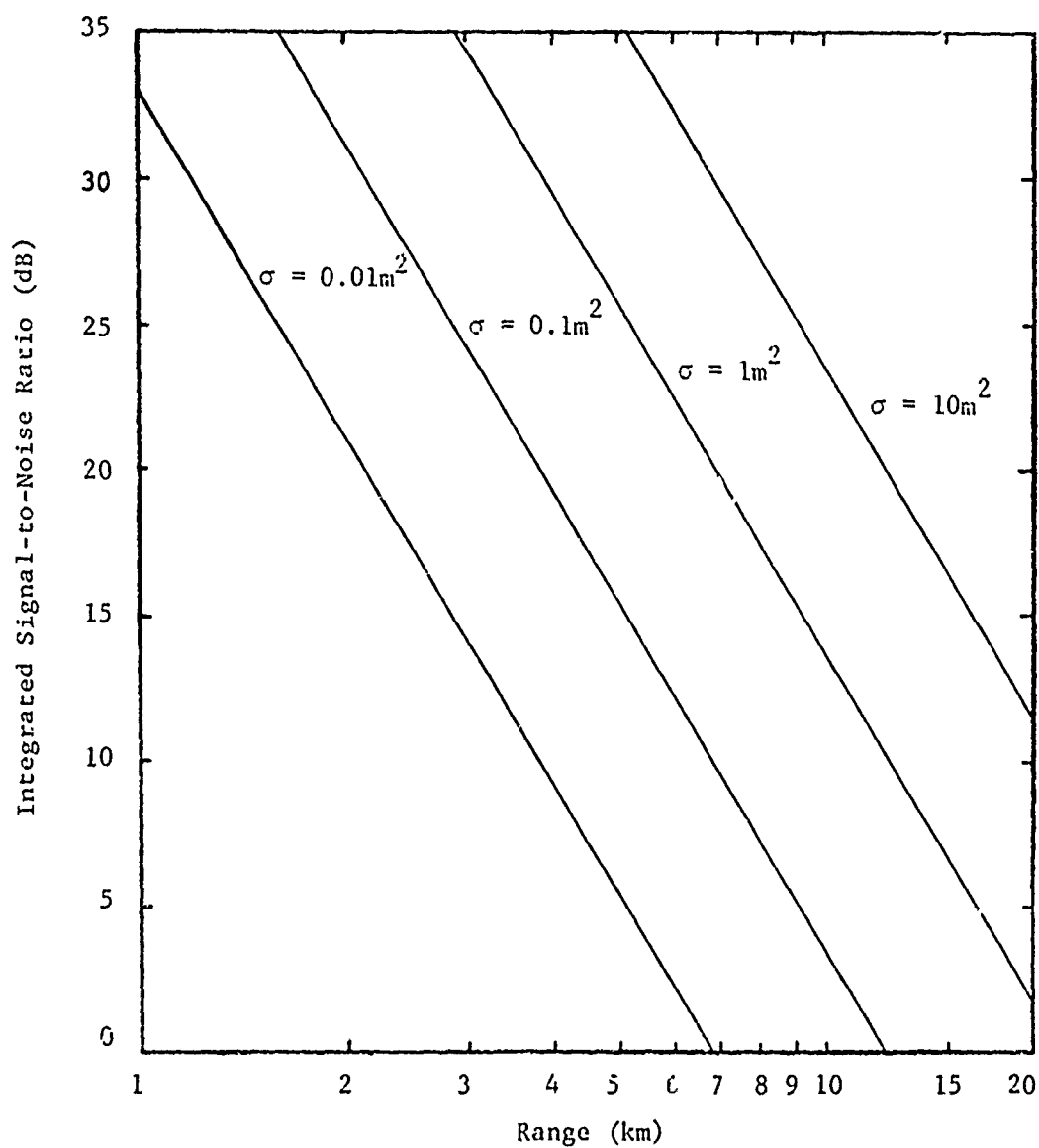


Figure 1. Average signal-to-noise ratio for the EAR system as a function of range. These values should be modified by the response at the specific target Doppler frequency obtained from Figure 2.

The average signal-to-noise ratio is given by the above expression; however, the response at a particular Doppler frequency may be considerably different from this average value. The frequency response for the conventional three-pulse MTI filter is derived in Appendix A and plotted in Figure 2. Figure 2 has been normalized so that the signal-to-noise ratio for a given target may be determined by adding the response at the desired Doppler frequency from Figure 2 to the values read from Figure 1. For very slow targets and for targets near the blind speed, substantial reductions in performance are possible. The design of improved MTI filters having more nearly uniform response is discussed in Section V.

B. Tracking Errors Due to Glint and Thermal Noise

The rms tracking error due to thermal noise has been derived by a number of authors to be [3]

$$\sigma_t = \frac{\theta}{k_m \sqrt{B\tau(S/N)}},$$

where

σ_t = rms angle-tracking error,

θ = 3 dB antenna beamwidth,

k_m = difference-channel error slope,

B = i-f bandwidth,

τ = pulse length, and

S/N = signal-to-noise power ratio.

If one assumes $B\tau = 2$, $k_m = 1.57$, and $\theta = 2^\circ$, which might be reasonable choices, then

$$\sigma_t = \frac{0.9}{\sqrt{S/N}},$$

where σ_t is expressed in degrees.

This rms tracking error in degrees is plotted as a function of range in Figure 3 for a number of target radar cross-sections. The 10 dB of integration gain included in Figure 1 is also incorporated into the results shown in Figure 3. The signal-to-noise ratio used was the average over all Doppler frequencies; at some particular frequencies, the performance may be appreciably worse due to the frequency response of the MTI processor.

The treatment of rms error due to target glint may be considerably simplified by characterizing the target by an "rms effective length," L_{eff} .

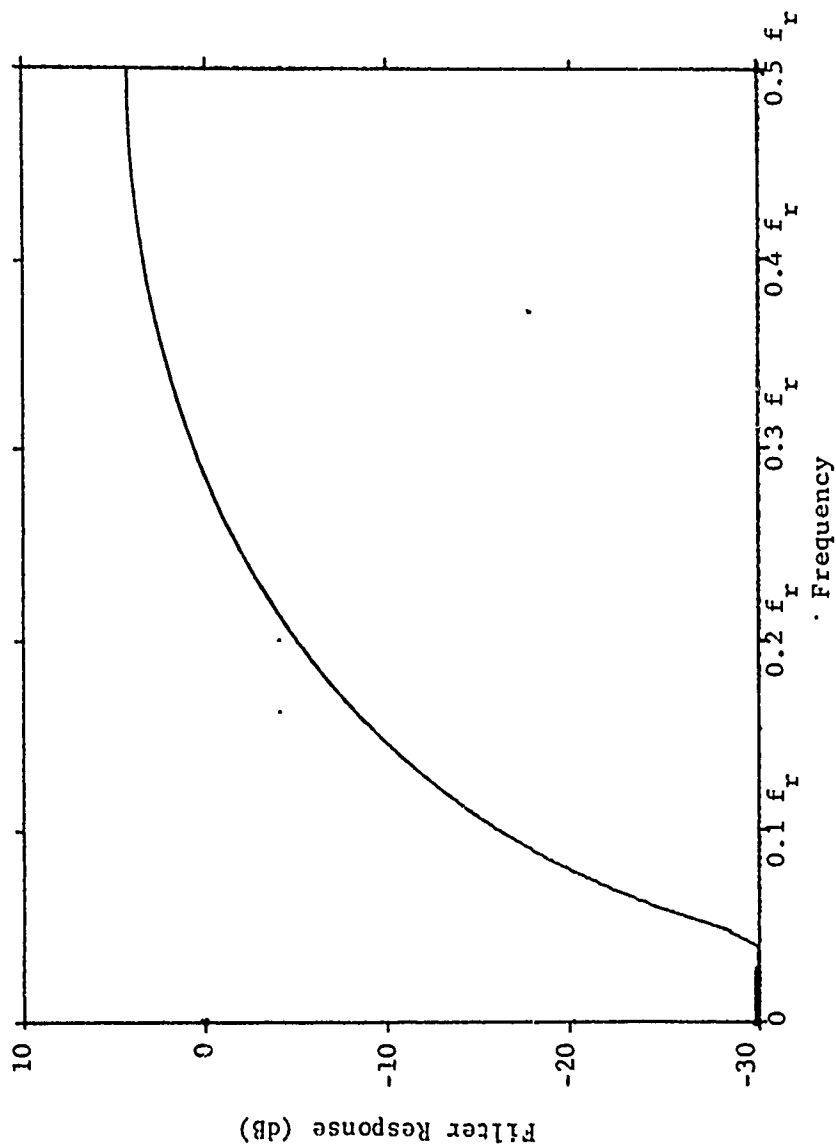


Figure 2. Response of a conventional three-pulse canceller having filter tap weights of 1, -2, and 1. The response has been normalized so the signal power averaged over all Doppler frequencies is 0 dB.

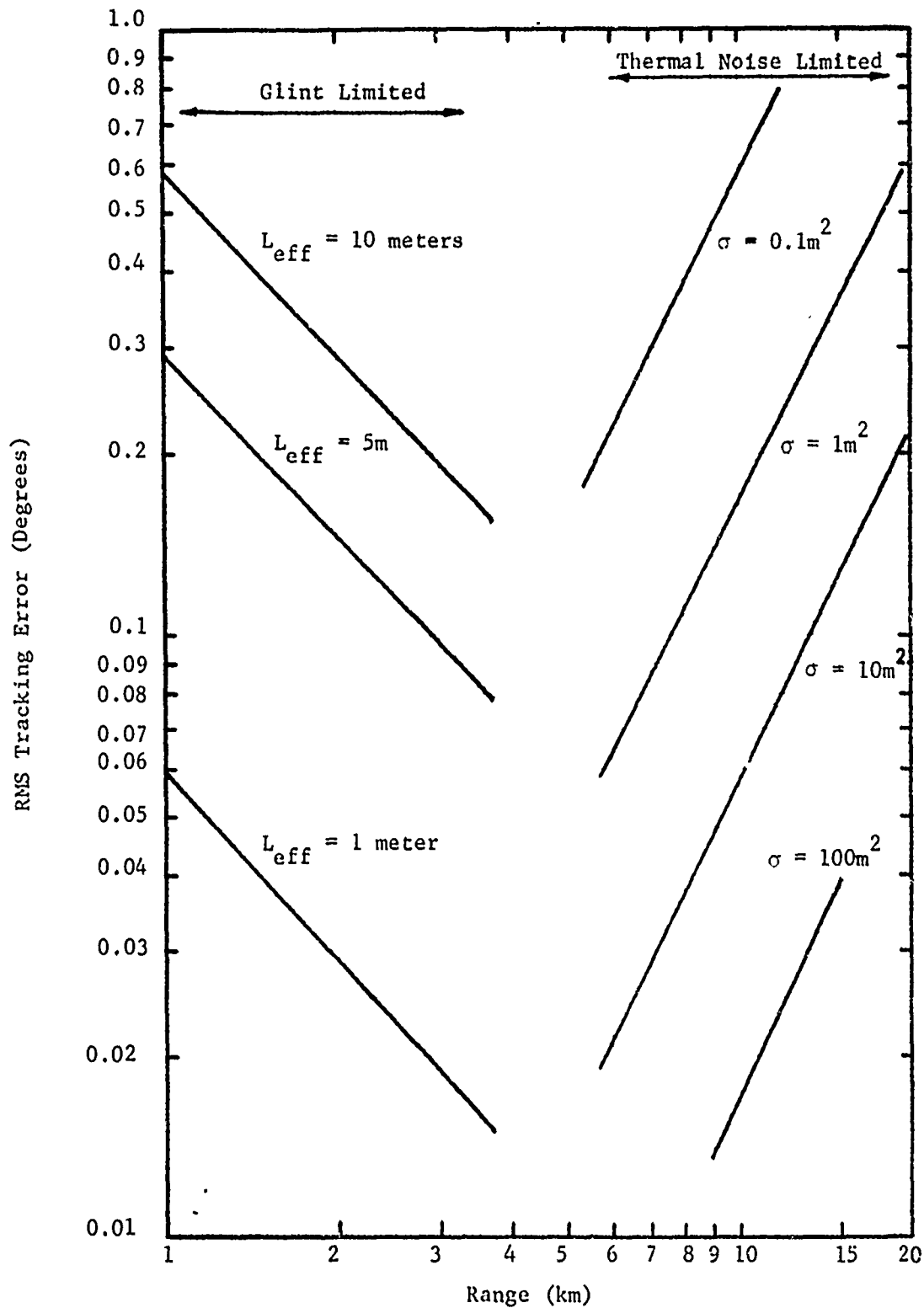


Figure 3. Average tracking errors due to thermal noise and glint as functions of range for the EAR system. Integration improvement in signal-to-noise ratio of 10 dB is included.

The rms angular error in degrees as a function of range is also plotted in Figure 3 for targets having several values of L_{eff} . Results of analyses performed during earlier contracts at Georgia Tech and surveys of the available literature indicate that an effective length of from 5 to 10 meters in azimuth is representative of values to be expected from many targets of interest. The effective length in elevation will probably be somewhat less; reasonable values probably lie between 1 and 3 meters.

Figure 3 indicates that the region of maximum average angle tracking accuracy lies roughly between 3 and 7 km, depending upon the specific choices of target radar cross-section and effective target length assumed.

C. Radar Angle Tracking Errors Due to Multipath Returns

The preceding analyses indicate the magnitude of errors to be expected when targets are being tracked under free-space conditions. Additional tracking errors are introduced by reflections from the surface of the earth. Two different methods of analysis have been used to study these tracking errors. Barton [3] discusses the case where the interfering signal is considered to be noiselike with random phase, and with amplitude determined both by the sidelobe ratio for the direction of arrival of the multipath signal and by the reflection coefficient of the reflecting surface. Another method of analysis assumes the multipath signal to be a return from a second target whose amplitude is given by the product of the sidelobe ratio and the reflection coefficient of the reflecting surface. The errors are then those of this two-scatterer target as their relative phase changes. Comparing results of these two analyses, plotted in Figure 4, shows them to be in substantial agreement.

For high elevation angles, an average sidelobe level of 25-dB and a surface reflectivity of 0.5 results in a multipath signal approximately 31 dB down. From Figure 4, this corresponds to an error of approximately 0.018 beamwidths or 0.04 degrees; such errors will only limit the tracking accuracy for targets having large cross-sections near the region of maximum accuracy. While this limits the maximum accuracy attainable for 1-10 m² cross-section targets for ranges approximately 5 - 10 km, the problem becomes worse for low-angle targets, where the image target is more strongly illuminated and the multipath return represents a target which is stronger and less random in nature. A more detailed computer analysis of radar tracking performance in this region is discussed in Section III.

D. Clutter Effects on the EAR

The limitations on clutter cancellation with digital MTI as implemented in the EAR system appear to be due to quantization errors in the analog-to-digital conversion process, rather than the actual clutter residue associated with the frequency response of the filter and the width of the clutter spectra. The calculations in Appendices A and B indicate the clutter residue produced by a conventional three-pulse canceller processing return from wooded hills in a 20-knot wind is approximately -83 dB, while the limitation on cancellation due to analog-to-digital quantization error for an eight-bit-plus-sign conversion is approximately -53 dB.

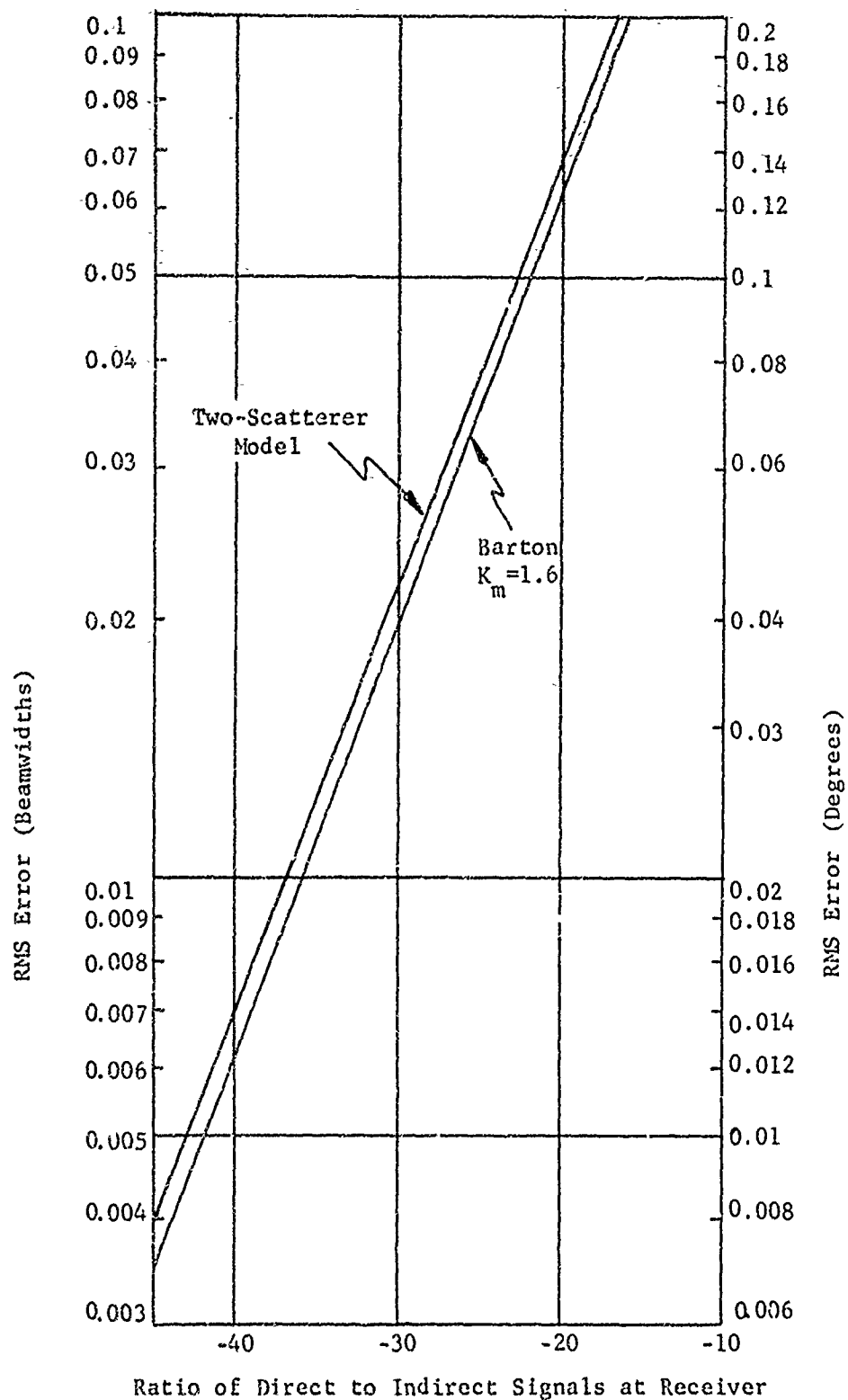


Figure 4. RMS tracking errors due to multipath as a function of the ratio of direct to indirect signals at the receiver.

The received signal-to-clutter power ratio (S/C) before MTI processing may be approximated by

$$S/C = \frac{\sigma S_{rt} S_{rg}}{\sigma^o} \times \frac{1}{R \theta_A} \times \frac{2}{\tau c}$$

where

σ = target radar cross-section,

S_{rt} = gain in the sum channel on reception for target,

S_{rg} = gain in the sum channel on reception for reflected energy,

σ^o = radar cross-section per unit area of clutter,

R = range,

θ_A = azimuth 3-dB beamwidth,

τ = pulse length, and

c = velocity of light.

For the vertical array, where the broad azimuth beamwidth (approximately 30°) results in large clutter power and the broad transmitting pattern is assumed to illuminate the clutter and the target with approximately equal intensity, the S/C ratio is a function of elevation angle. However, if elevation greater than approximately 2° , the gain for the clutter signal will be approximately the average gain in the sidelobes of the vertical array. For simplicity, assume that this gain is approximately -25 dB. Values of S/C ratio may now be calculated and then modified by the clutter cancellation of the system.

A plot of the average signal-to-clutter ratio after cancellation for a one-microsecond pulse and various ratios of σ/σ^o valid for elevation angles greater than approximately 2° is presented in Figure 5. These values must be modified by the response of the MTI processor for the particular target velocity.

To illustrate the use of Figure 5, consider $\sigma = 1 \text{ m}^2$ and $\sigma^o = -20 \text{ dB}$ or $\sigma/\sigma^o = 100 \text{ m}^2 = 20 \text{ dBsm}$. The average signal-to-clutter ratio is approximately 43 dB at a range of 10 km. However, the frequency response of the MTI processor must be added to this value; since the processor response may be substantially smaller than -20 dB, the value obtained from Figure 5 may be modified substantially. This reduction of signal-to-clutter ratio is another manifestation of nonuniform Doppler responses produced by conventional MTI processors, and illustrates the need for improved MTI filter responses as discussed in Section V.

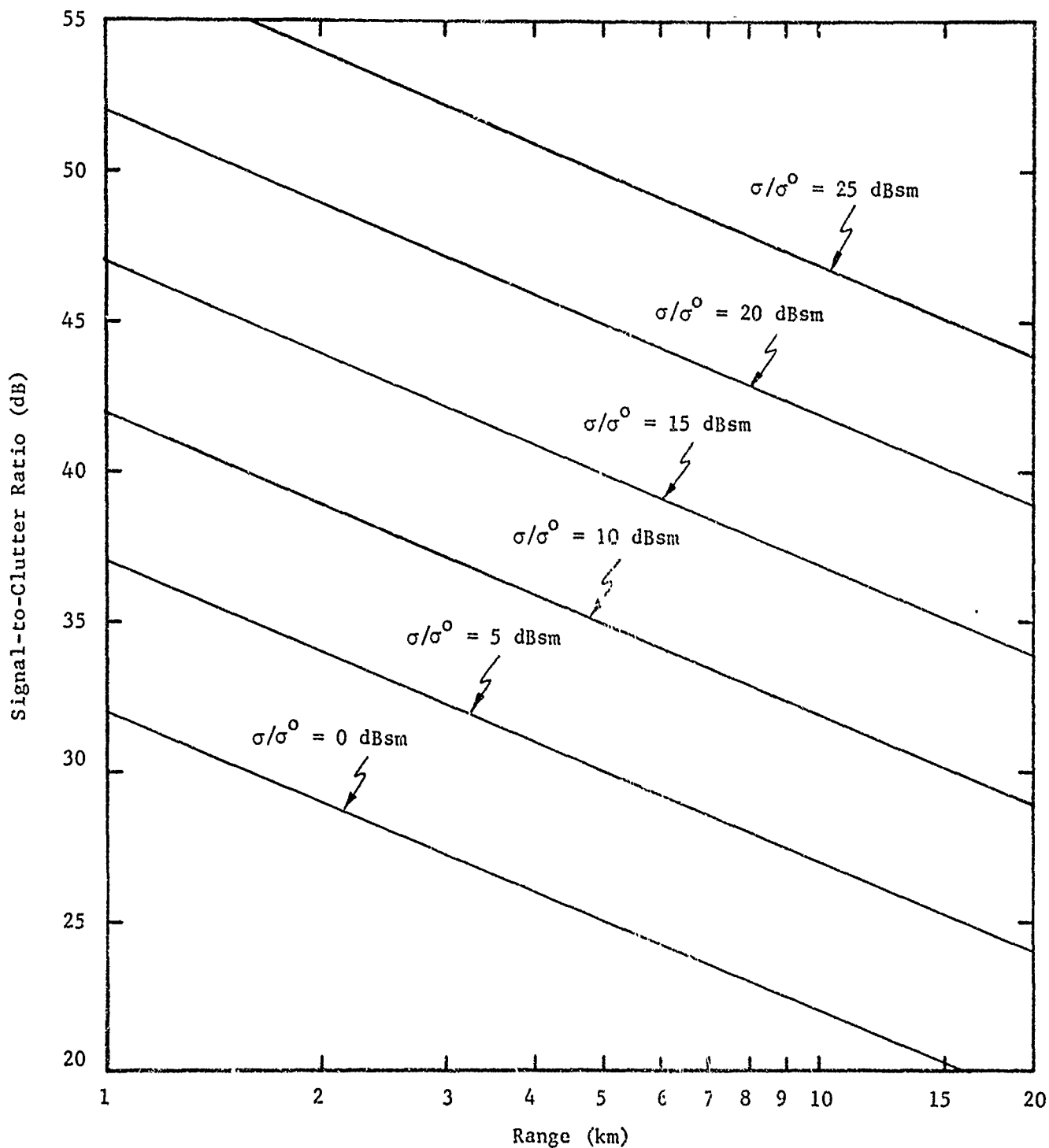


Figure 5. Signal-to-clutter ratio after MTI filtering (56 dB MTI improvement) as a function of range for the EAR system using a one-microsecond pulse.

III. MULTIPATH EFFECTS ON EAR ANGLE TRACKING ACCURACY

A. Introduction

In the previous section, it was noted that multipath reflections returned to the antenna through the low-amplitude sidelobes of the EAR antenna do not limit system performance except for the case of large targets near the region of maximum accuracy. However, when target elevation is reduced, multipath returns become stronger, errors are less random in nature, and tracking accuracy lessens; consequently, multipath signals in this situation can seriously limit EAR system performance.

Characteristics of the target, reflecting surface, tracking antenna, and radar data processor all influence the nature and severity of multipath-induced tracking errors. A computer program was written to assist in determining the effects of these factors on tracking performance of the EAR in multipath situations. The program permits calculation of elevation-angle tracking error, and signal amplitude and phase variations, and allows implementation of various processing techniques.

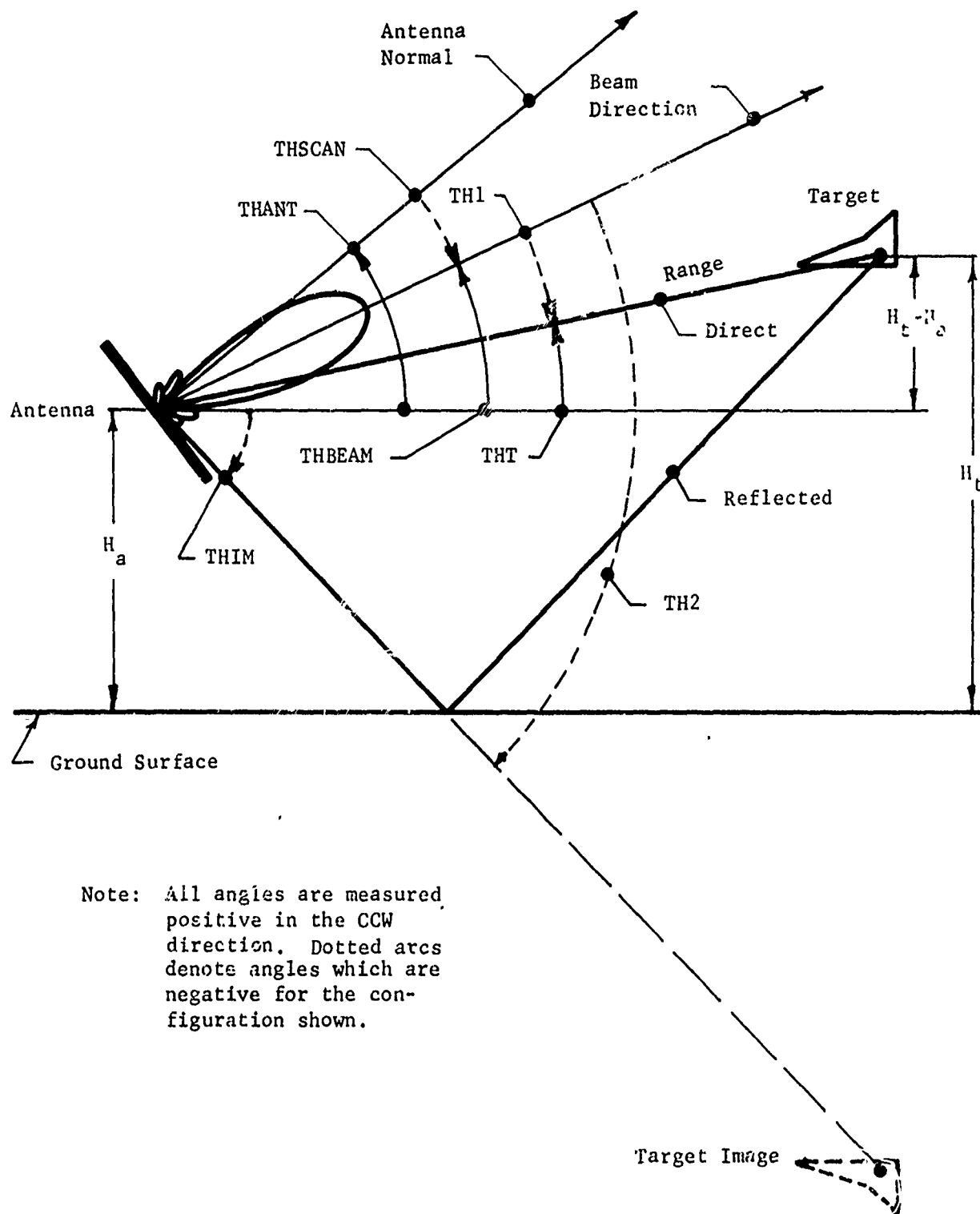
The geometry of the target trajectory, calculation of received signals and indicated errors, antenna pattern generation, program organization, and results of this computer analysis are discussed in the following paragraphs.

B. Geometry of the Target Trajectory

The analysis assumes a target flying at constant altitude on a radial path toward the antenna as shown in Figure 6. Target altitude is denoted by H_t and the antenna is located at height H_a . The surface is assumed to be flat, so that simple specular reflection occurs, and to have a reflection coefficient ρ (in most of the analyses ρ was assumed to be real). The angles necessary to define the geometry are indicated in Figure 1 as follows:

THT	Angle between antenna and target measured from horizontal
THIM	Angle between antenna and target image measured from horizontal
THANT	Pointing angle of antenna normal measured from horizontal
THSCAN	Angle at which antenna beam is scanned from antenna normal
THBEAM	Pointing angle of antenna beam measured from horizontal
TH1	Angle between antenna beam and target measured from antenna base
TH2	Angle between antenna beam and target image measured from antenna beam

Preceding page blank



Note: All angles are measured positive in the CCW direction. Dotted arcs denote angles which are negative for the configuration shown.

Figure 6. Antenna/target geometry.

C. Calculation of Received Signals and Indicated Errors

In the EAR system, the signals are transmitted through the horizontal array and received through both the horizontal and vertical arrays; therefore, different antenna gains apply on transmission and reception when tracking with the vertical array. With reference to Figure 6, let S_{α} and D_{α} represent the sum-pattern gain and difference-pattern gain, respectively, of the phased-array antenna upon reception in the α direction; similarly S_{α} will denote the transmitting antenna gain in the α direction. The subscript α will denote either the direction of the direct ray to the target ($\alpha = t$) or the ray reflected from the ground to the target ($\alpha = g$). When reflections are present, the total signal received by the antenna will be a combination of signals which traverse four paths. The first path is that directly to the target and back to the antenna, the second and third are paths having one reflection from the ground surface, and the fourth involves two reflections from the ground surface. Thus, the total signal received at the antenna (for the sum channel) is given by

$$S = S_{tt} e^{-jkR} S_{rt} e^{-jkR} + S_{tt} e^{-jkR} \rho S_{rg} e^{-jk(R + \delta R)} S_{rt} e^{-jkR} \\ + S_{tg} \rho e^{-jk(R + \delta R)} \rho S_{rg} e^{-j(kR + \delta R)},$$

where ρ is the ground reflection coefficient and δR is the range difference between direct and reflected paths to the target. The decrease in signal level due to the increase in range by an amount δR is neglected as a second-order effect. Simplifying and changing the phase reference to delete the factor e^{-j2kR} there results:

$$S = S_{tt} S_{rt} (S_{tt} S_{rg} + S_{tg} S_{rt}) \rho e^{-jk\delta R} + \rho^2 S_{tg} S_{rg} e^{-j2k\delta R}.$$

In a similar fashion, the difference signal strength is found to be:

$$D = S_{tt} D_t + \rho S_{tt} D_g e^{-jk\delta R} + \rho S_{tg} D_t e^{-jk\delta R} + \rho^2 S_{tg} D_g e^{-jk\delta R}.$$

The indicated error, θ_e , may then be calculated from the ratio of the difference signal to the sum signal as

$$\theta_e = K \operatorname{Im} \left(\frac{D}{S} \right),$$

where K is a constant chosen to give unity error slope at boresight and is a function of antenna pattern beamwidth and beamshape. A typical plot of indicated angular error versus actual angular error is presented in Figure 7 for $K = 0.86$. Because the error functions become less sensitive as the antenna

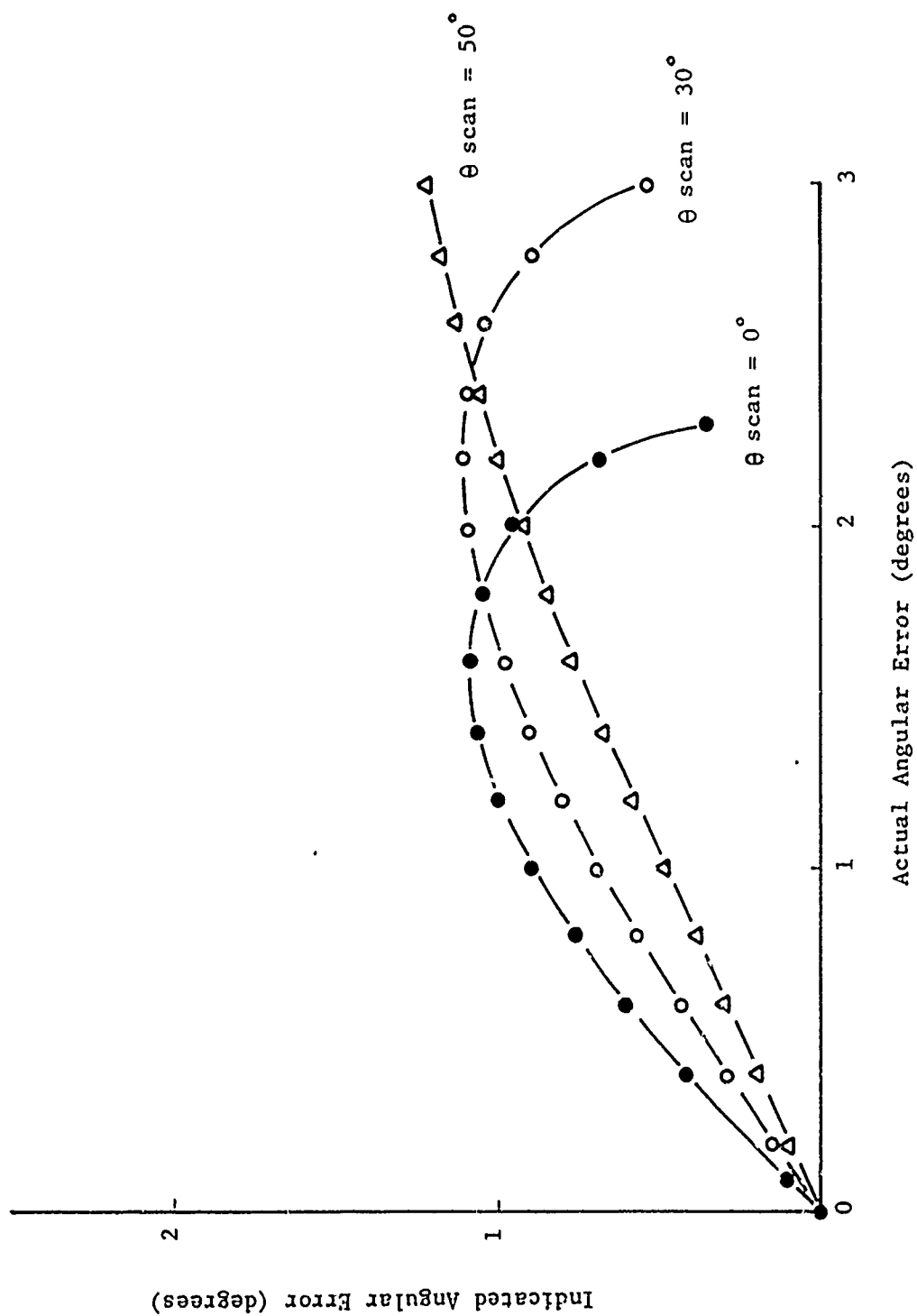


Figure 7 . Indicated angular error versus actual angular error for $K = 0.86$.

is scanned (due to increasing antenna beamwidth) it may be advantageous to make K a function of scan angle so the curves for all scan angles have approximately unity slope at the origin. Curves for this case are shown in Figure 8 where $K = 0.845 + 0.335 (\theta \text{ scan}/30)$.

D. Antenna Pattern Generation

For the system simulation, it was decided to use a simple scheme that would give an adequate representation of the antenna patterns to be approximated. The characteristics of the antenna pattern used for the computer analysis of vertical array are shown in Table I, and compared with measured values given in parentheses:

Table I - Antenna Pattern Characteristics

Parameter	Boresight	50° Scan
Sum 3 dB BW	2° (2)	3° (3)
Gain Reduction	0 dB (0)	4 dB (3.5)
Sidelobe Level	-27 dB (-28)	-30 dB (-28)
Peak Difference Pattern Level (referred to peak of sum patterns)	-2 dB (-2.7)	-2.5 dB (-2.7)

The patterns were generated using assumed aperture illuminations of the form

$$f(x) = A \cos \frac{\pi x}{a} ,$$

which result in far-field patterns having the form

$$g(u) = k_1 F \frac{\cos u}{\frac{\pi}{2} - u^2} ,$$

where

$$u = k_2 F \sin \theta_1 .$$

To generate the sum and difference patterns, θ_1 is assigned values θ and $\theta + \theta_0$, where θ_0 is the offset angle of the beam. The two patterns thus created are added and subtracted to produce sum and difference far-field patterns (see Figure 9). In order to cause the patterns to vary with scan angle, both θ_0 and F are made to be functions of scan angle, the specific function being determined empirically to produce the desired pattern variation.

The transmitted signal is radiated through the horizontal array which has very nearly constant gain over a wide range of elevation angles. The elevation pattern for this antenna was simulated as being that of an isotropic radiator.

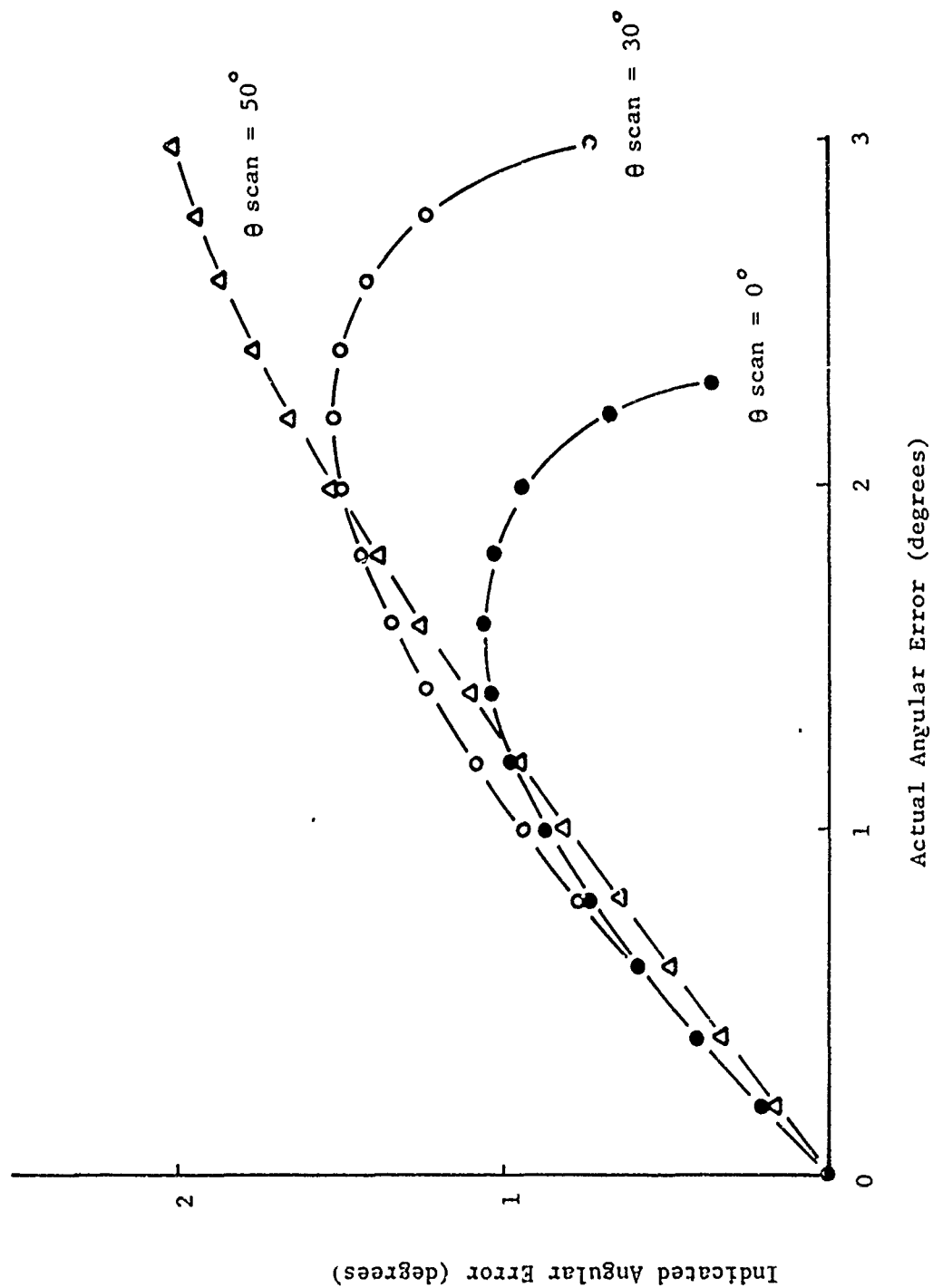


Figure 8. Indicated angular error versus actual angular error for
 $K = 0.845 + 0.335 (\theta \text{ scan}/30)$.

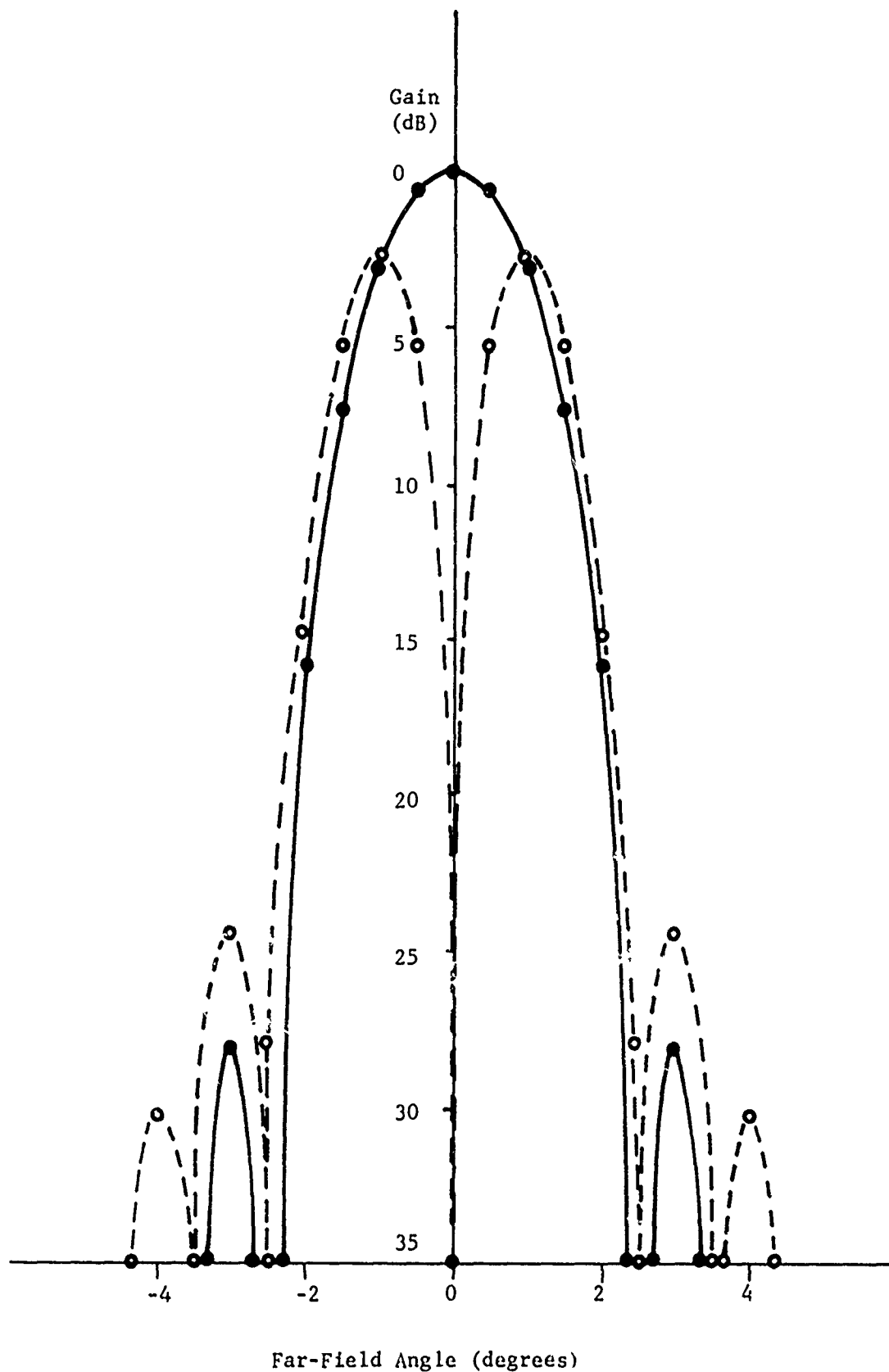


Figure 9. Typical sum (solid lines) and difference (dashed lines) patterns used in the computer analysis.

E. Program Organization

The computer program used for analysis (Appendix E) consists of a large main program which performs input and output tasks with several subroutines to do specialized computations. All parameters are initialized in the main program; this program controls the execution of the various subroutines. The subroutine ERRO, for example, provides for calculation of the indicated angular error between antenna and target and returns this information to the main program for antenna beam-pointing calculations. Trajectory predictions are computed in the main program, while frequency-agility calculations and signal processing are performed in subroutine ERRO. The subroutine GAIN calculates antenna pattern data (see Section E) and feeds this information to ERRO. The remaining subroutines are used to perform statistical analyses on the calculated data and produce output plots.

Various versions of the program include provision for different beam-pointing calculations (including linear and parabolic predictions and predictor-corrector filters) and the implementation of frequency agility. The trajectory prediction programs fit linear and parabolic curves, respectively, to a set of three data points to predict where the antenna beam should be pointed for the next look. The frequency-agility program permits selection of start and stop frequencies and the frequency step size. Each frequency is transmitted for three pulses and then stepped; when the stop frequency is reached a new cycle is begun. Since a total of 48 pulses are transmitted for each look at the target, the frequency parameters are normally chosen such that 16 frequencies are transmitted before a new cycle is begun in order to maximize the information obtained. Data from all frequencies may be averaged to calculate the indicated angular position of the target or adaptive-processing techniques may be used to select data samples from the available set.

F. Results of Computer Analysis

From the computer analysis are obtained plots of the elevation tracking error in feet as a function of time. These results are affected by antenna height and tilt angle, target height and backscattering characteristics, radar frequency, and the properties of the reflecting surface. A representative plot of tracking error is shown in Figure 10; this particular run was calculated for an isotropic-scatterer target having a radial velocity of 250 mph, and was initiated at a distance of ten miles. The frequency of operation was chosen to be 5.5 GHz, and the physical face of the antenna was vertical (antenna normal horizontal). The reflection at the earth surface was characterized by a (voltage) reflection coefficient of 0.5.

The beamshape produced by the antenna varies with scan angle, beamwidth being minimum when the beam is normal to the face of the array, and broader for non-zero scan angles. Therefore, the physical orientation of the antenna may be chosen so as to minimize antenna beamwidth and maximize tracking accuracy for the region of most interest. Figure 11 shows the effect of tilting the antenna back, which enhances accuracy at high angles at the expense of low-angle accuracy (compare with Figure 10). The most desirable tilt angle for the antenna depends upon a number of factors and may differ with mission

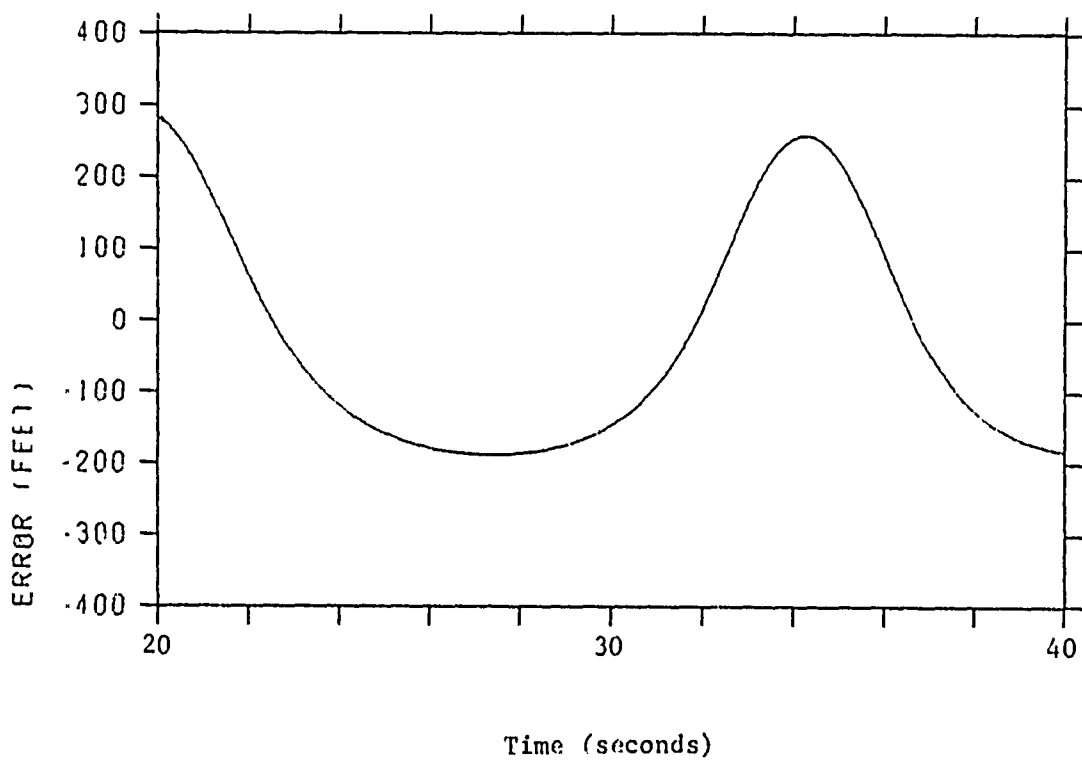
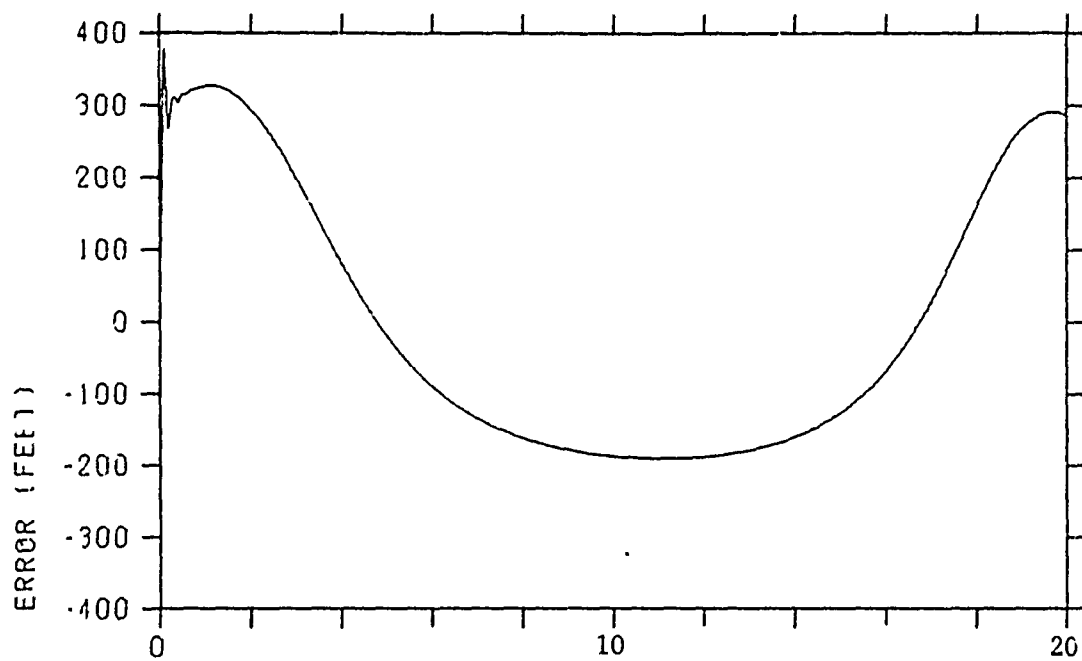


Figure 10. Tracking error as a function of time, $H_a = 100$ ft, $H_t = 300$ ft.
 $f = 5.5$ GHz, $\sigma = 0.5$, tilt angle = 0° .

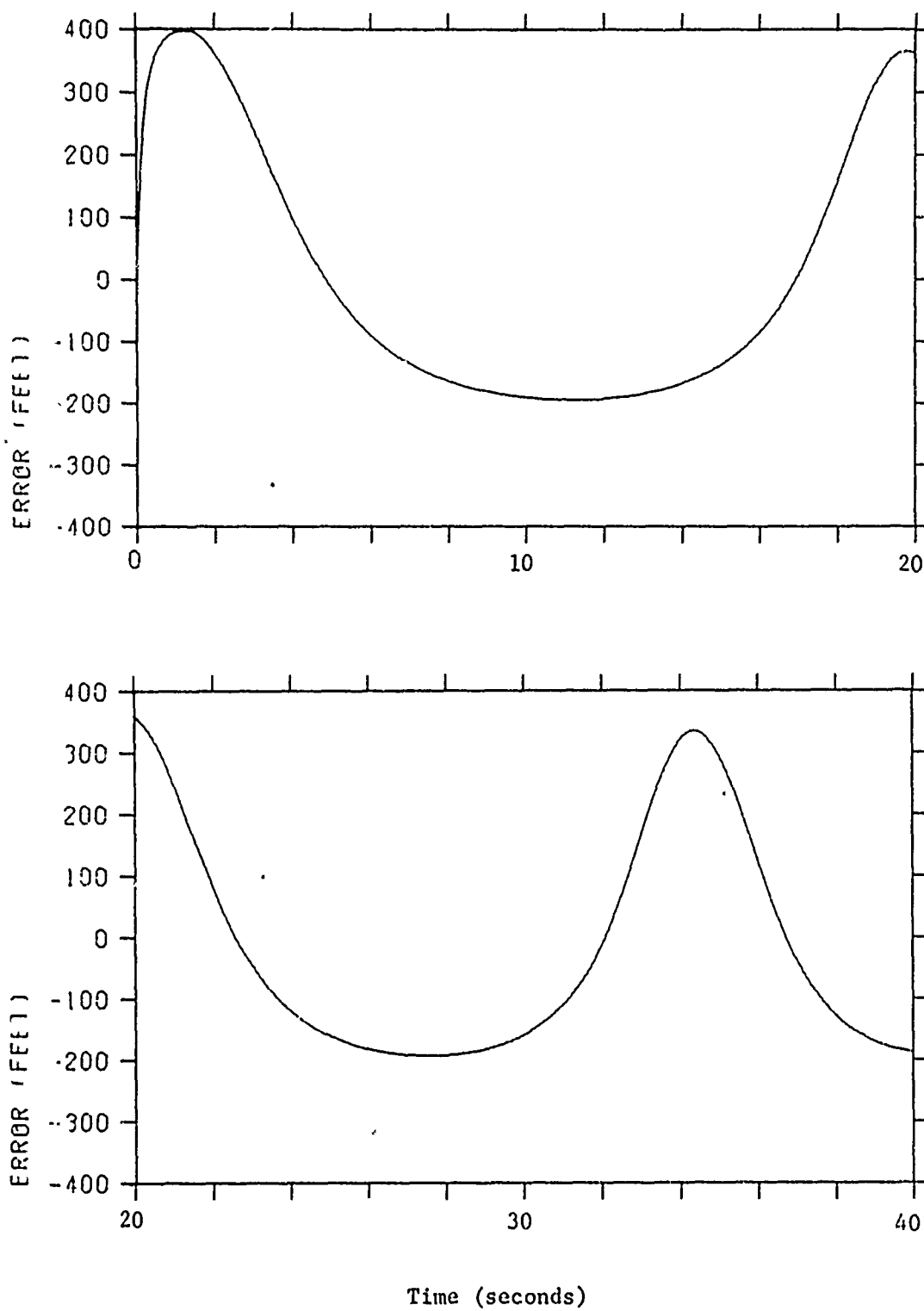


Figure 11. Tracking error as a function of time. $H_a = 100$ ft, $H_c = 300$ ft, $f = 5.5$ GHz, $\rho = 0.5$, tilt angle = 30° .

requirements. An angle of 30° was chosen arbitrarily for use in most of the remaining computer analyses.

Figures 11 and 12 present a comparison of results for $H_t = 300$ ft and $H_t = 500$ ft for an antenna tilt angle of 30° . These two figures illustrate the influence of target height on the multipath-induced tracking errors. The target height is seen to influence both the amplitude and frequency of these multipath-induced errors. These errors are also affected by changes in antenna height: Figure 13 shows the same situation as Figure 11 (on a different time scale), but with antenna height reduced to 15 feet. The peak amplitude of the tracking error is somewhat less at the lower antenna height, and the frequency of the excursions is significantly lower.

Numerous runs of the type shown in Figures 9 - 13 were performed in order to define more clearly the effect of multipath returns on the tracking accuracy of the EAR system. An antenna tilt angle of 30° was selected for most of these analyses, and an isotropic-scatterer target having a radial velocity of 250 mph was used. A surface reflection coefficient of 0.5 was chosen for all of these analyses. Figure 14 summarizes the results as plots of peak-to-peak tracking error as a function of target height for two values of antenna height chosen to approximate the heights of the initial EAR Test Bed site and a similar antenna mounted on a tracked vehicle. Figure 14 indicates that multipath error is significant for targets below 1200 feet, and is maximum at altitudes of about 400 to 800 feet.

Figure 14 shows that tracking error due to multipath can be of such a magnitude as to severely limit radar system performance. Various methods for alleviating the effect of multipath returns have been proposed, and are discussed at length in an earlier Georgia Tech report [4]. The most practical method for implementation with the EAR is frequency agility, and the applicability of this approach to the EAR system is discussed in detail in the next section.

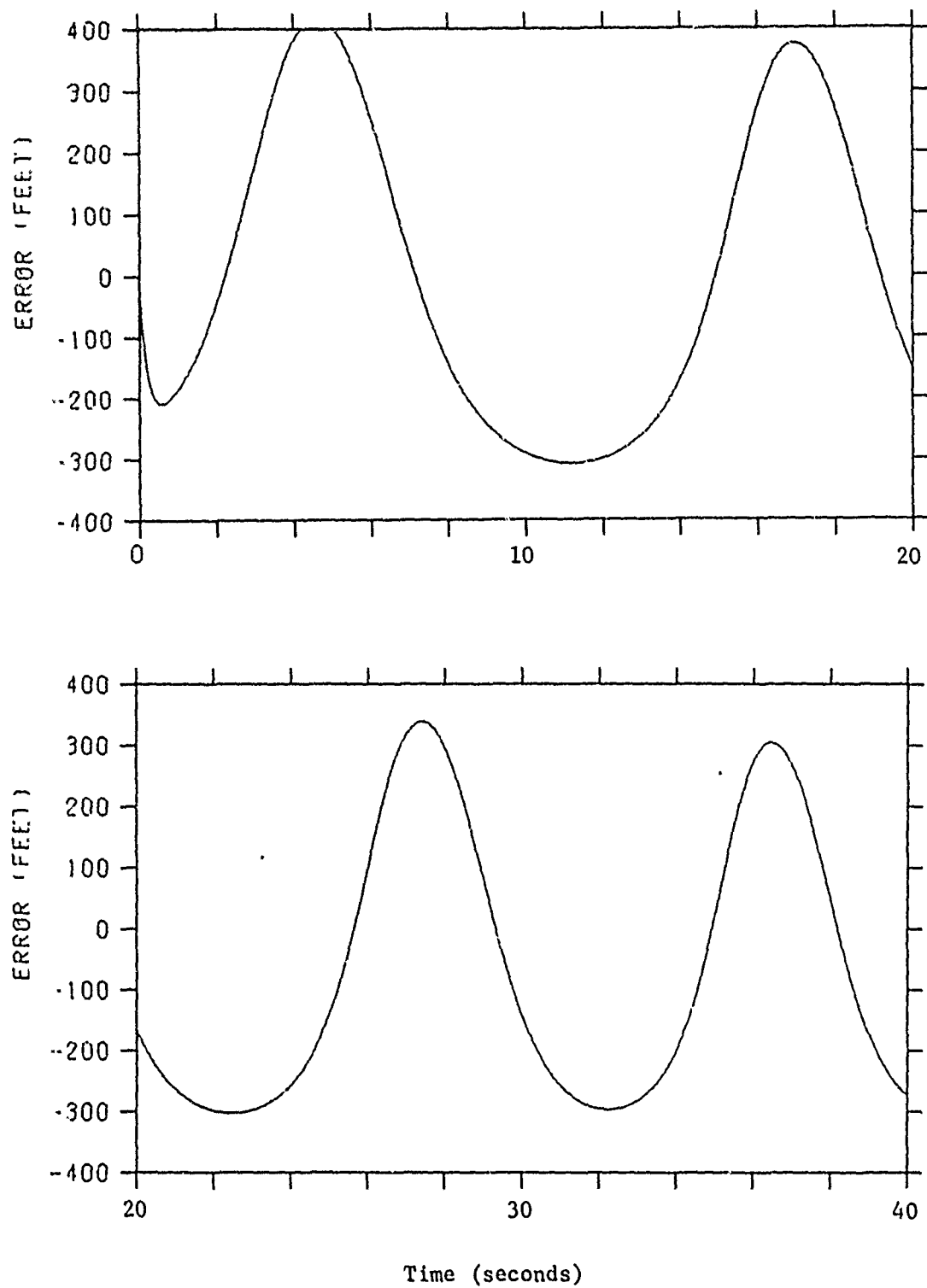


Figure 12. Tracking error as a function of time. $H_a = 100$ ft, $H_t = 500$ ft, $f = 5.5$ GHz, $\rho = 0.5$, tilt angle = 30° .

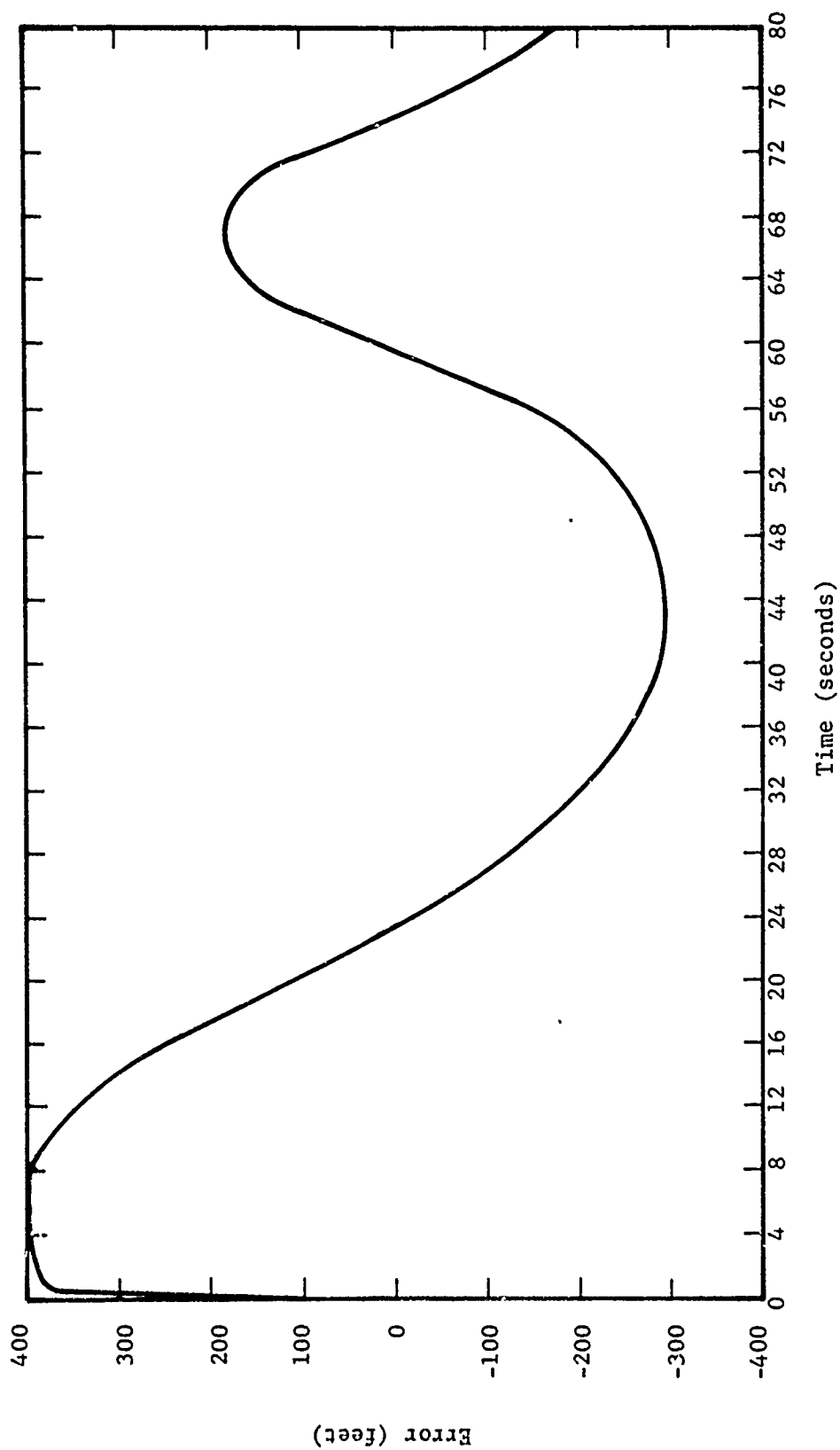


Figure 13. Tracking error as a function of time. $H_a = 15$ ft, $H_t = 300$ ft, $f = 5.5$ GHz, $\rho = 0.5$, tilt angle $= 30^\circ$.

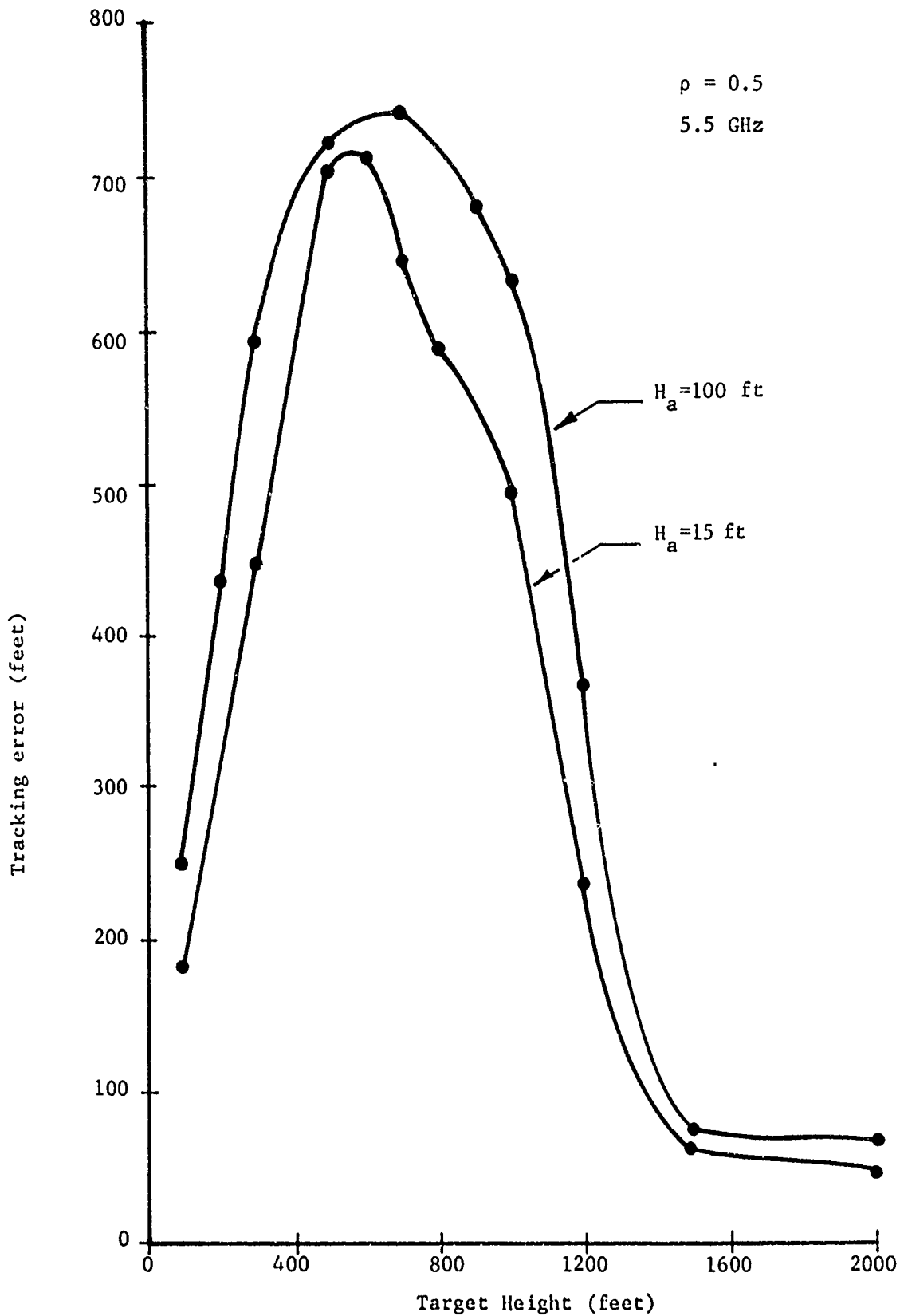


Figure 14. Peak-to-peak elevation tracking errors as functions of target height for 15 and 100 foot antenna heights. $\rho = 0.5$ and frequency is 5.5 GHz.

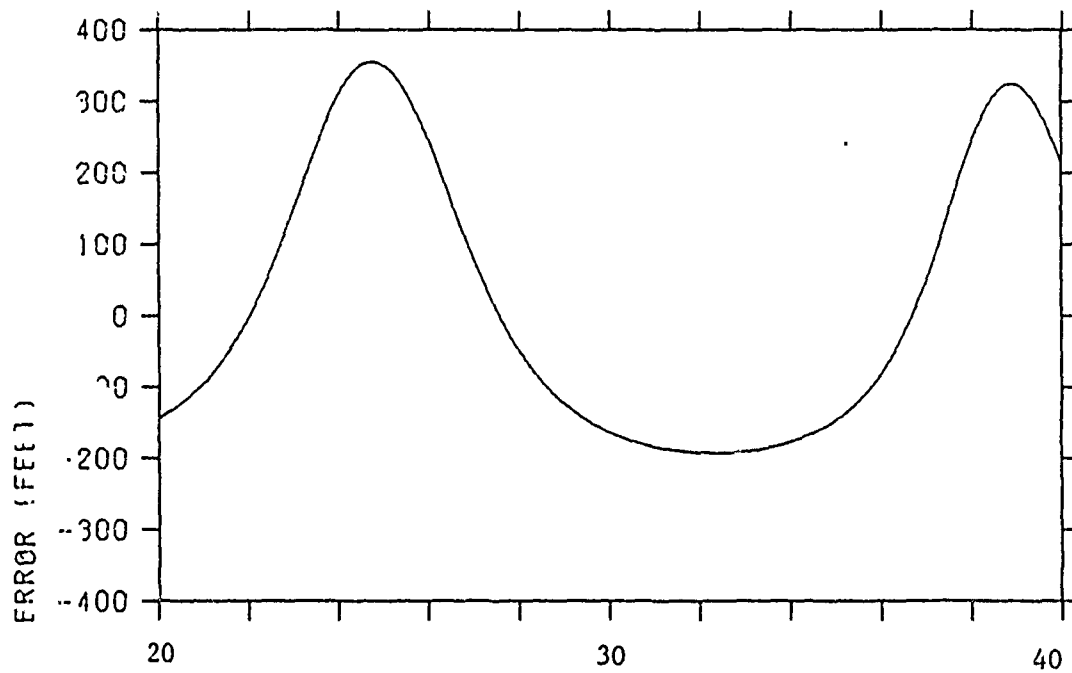
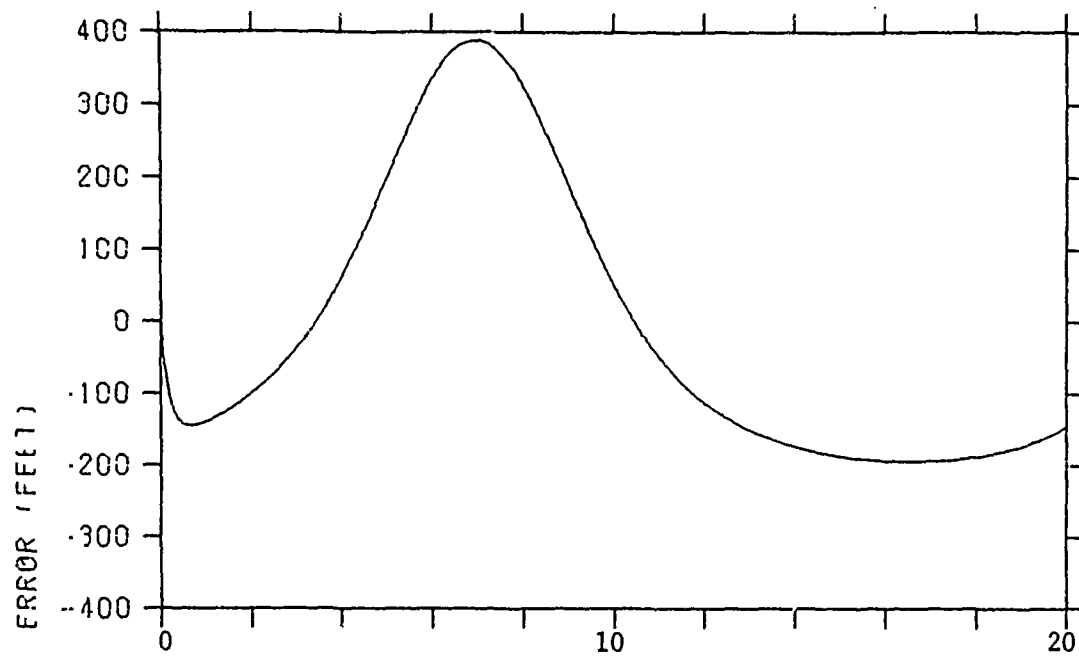
IV. APPLICABILITY OF FREQUENCY AGILITY TO THE EAR

Frequency agility is often proposed as a method for reducing effects of both glint and multipath on radar tracking accuracy. The effectiveness of frequency agility on glint-induced tracking errors has been investigated in an earlier Georgia Tech report [4]. While the EAR presents a somewhat different situation (C-band vs X-Band), the results set forth in that report are generally indicative of what could be achieved if frequency agility were used with the EAR system in tracking a free-space target.

The analysis presented in Section III shows that the effect of multipath returns on the EAR system performance is significant for targets at altitudes less than 1200 ft. Numerous methods for reducing the tracking error have been proposed; these include multiple-height antennas, space diversity (in the azimuth plane), high-resolution antennas, polarization agility, shaped antenna beams, and frequency agility. The discussions in an earlier Georgia Tech Report [5], coupled with the physical constraints of the EAR system, make frequency agility seem to be a promising candidate technique for reducing multipath-induced tracking errors. Therefore, an investigation of the effectiveness of frequency agility in reducing these multipath-induced tracking errors was begun.

When frequency agility is used, a set of pulses is radiated in sequence with frequency changed from pulse to pulse; the received pulses are either averaged to obtain a more accurate, stable, and repeatable indication of target position, or a selection rule is used to select optimum data from the available set. In the remainder of this section, the term "frequency agility" will be used to describe the averaging process, and the term "adaptive processing" used to denote the selection process.

Changing the transmitted frequency permits the acquisition of a number of independent samples of target location by changing the relative phase between direct and indirect rays (altering their electrical path lengths), by changing the amplitude and phase of the reflection coefficient of the reflecting surface, or by affecting the scattering characteristics of the target. Within the normally achievable bandwidths of most frequency-agile radars, the reflection coefficient of many reflecting surfaces remains essentially unchanged. The effect of small frequency changes on target characteristics has not been exhaustively investigated, but should be small for most low-altitude targets, particularly in the vertical plane [5]. Thus, the principal mechanism by which frequency changes affect tracking error is the change in relative phase of direct and indirect signals received at the antenna. These changes in electrical path length produce what are often substantial shifts in the location in range of the extremes of the tracking errors. Figures 15 through 19 show the tracking errors for the EAR system with operating frequencies of 5.3, 5.4, 5.5, 5.6, and 5.7 GHz. The changes in the pattern of the tracking error with changes in frequency are clearly seen, and these changes indicate that practical frequency changes may indeed be effective in obtaining a number of independent samples for further processing.



Time (seconds)

Figure 15. Tracking error as a function of time. $H_a = 100$ ft, $H_t = 300$ ft, $f = 5.3$ GHz, $\rho = 0.5$, tilt angle = 30° .

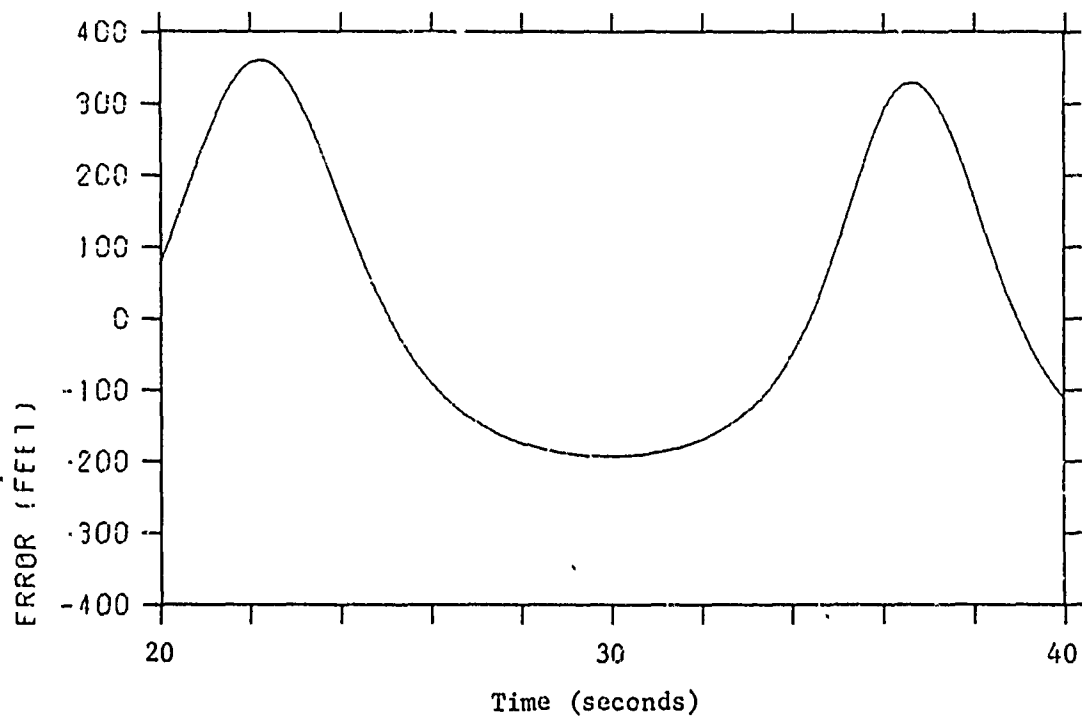
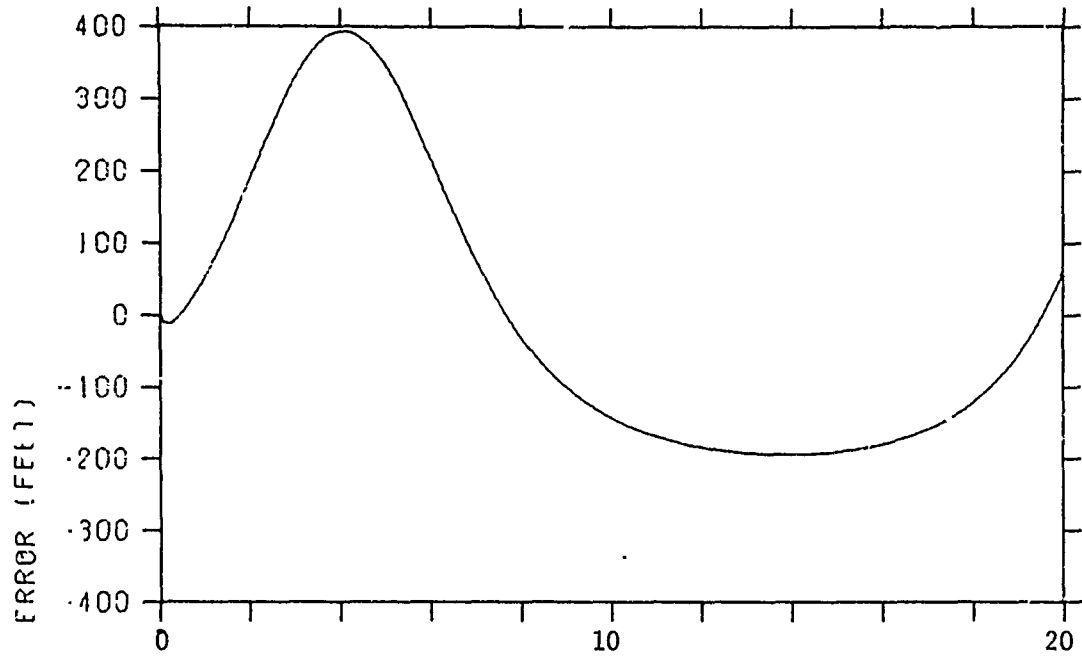


Figure 16. Tracking error as a function of time. $H_a = 100$ ft, $H_t = 300$ ft, $f = 5.4$ GHz, $\rho = 0.5$, tilt angle = 30° .

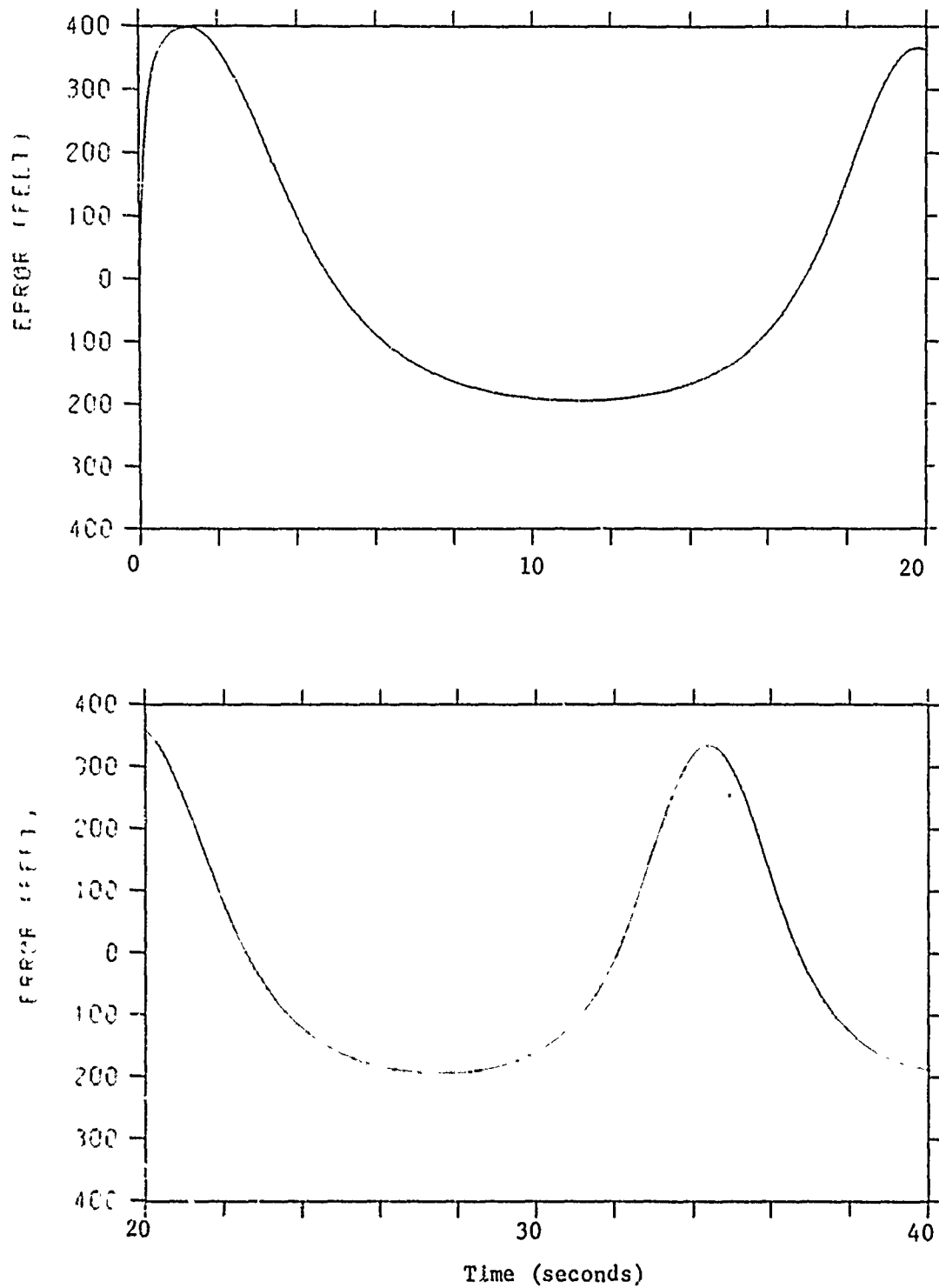


Figure 17. Tracking error as a function of time. $H_a = 100$ ft, $H_t = 300$ ft, $f = 5.5$ GHz, $\rho = 0.5$, tilt angle = 30° .

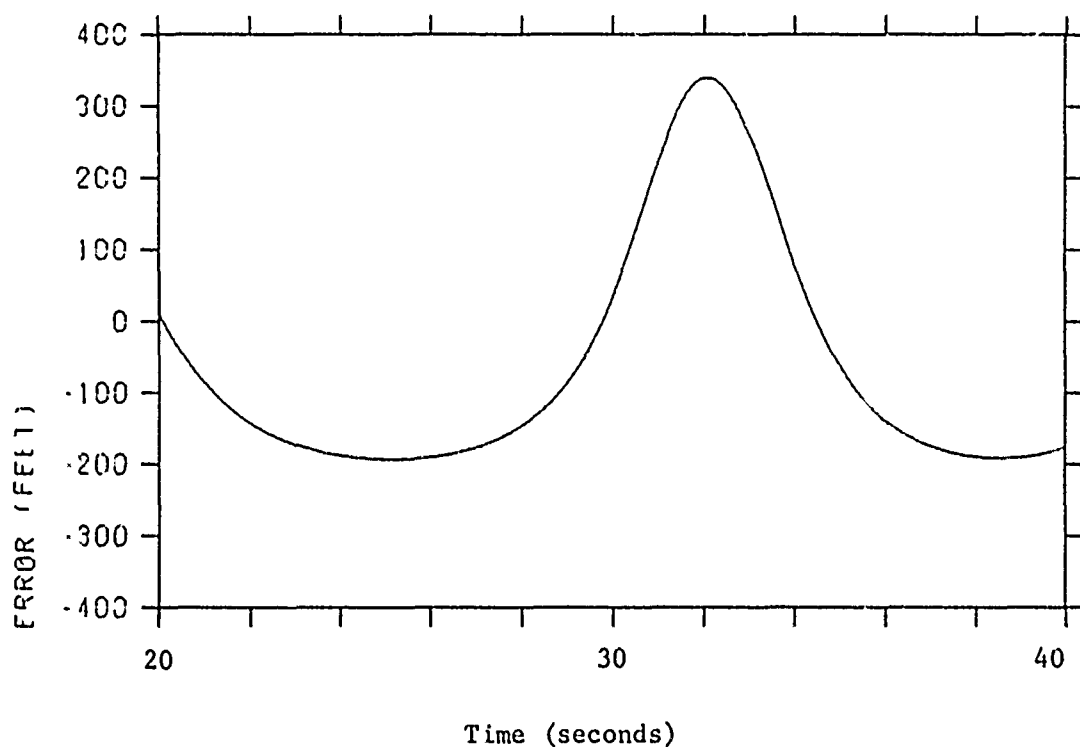
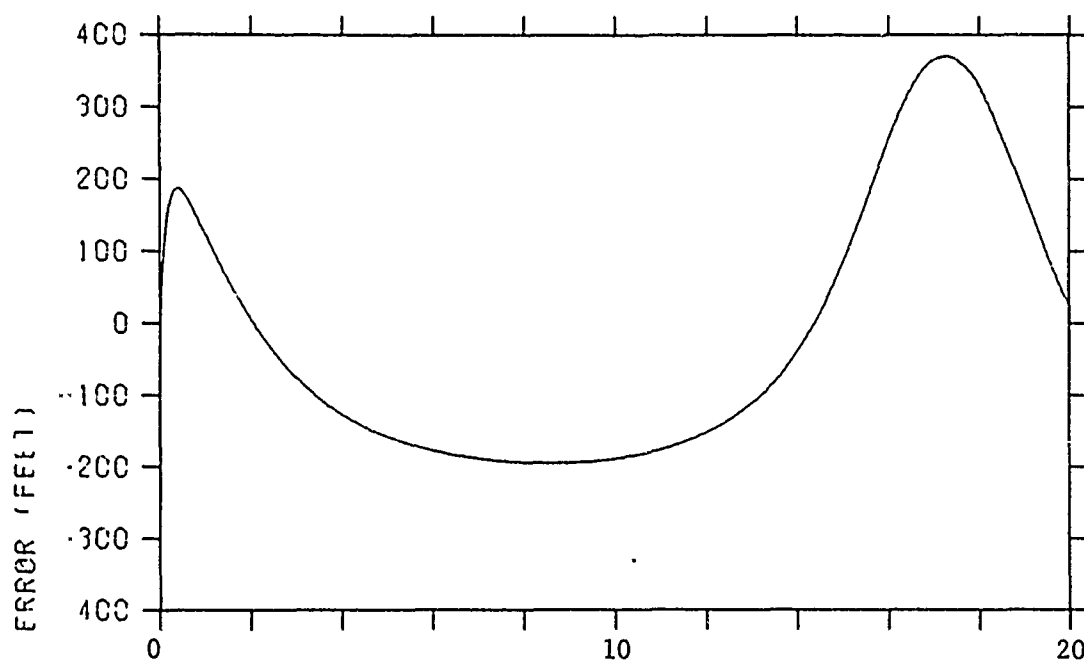


Figure 18. Tracking error as a function of time. $H_a = 100$ ft, $H_t = 300$ ft, $f = 5.6$ GHz, $\rho = 0.5$, tilt angle = 30° .

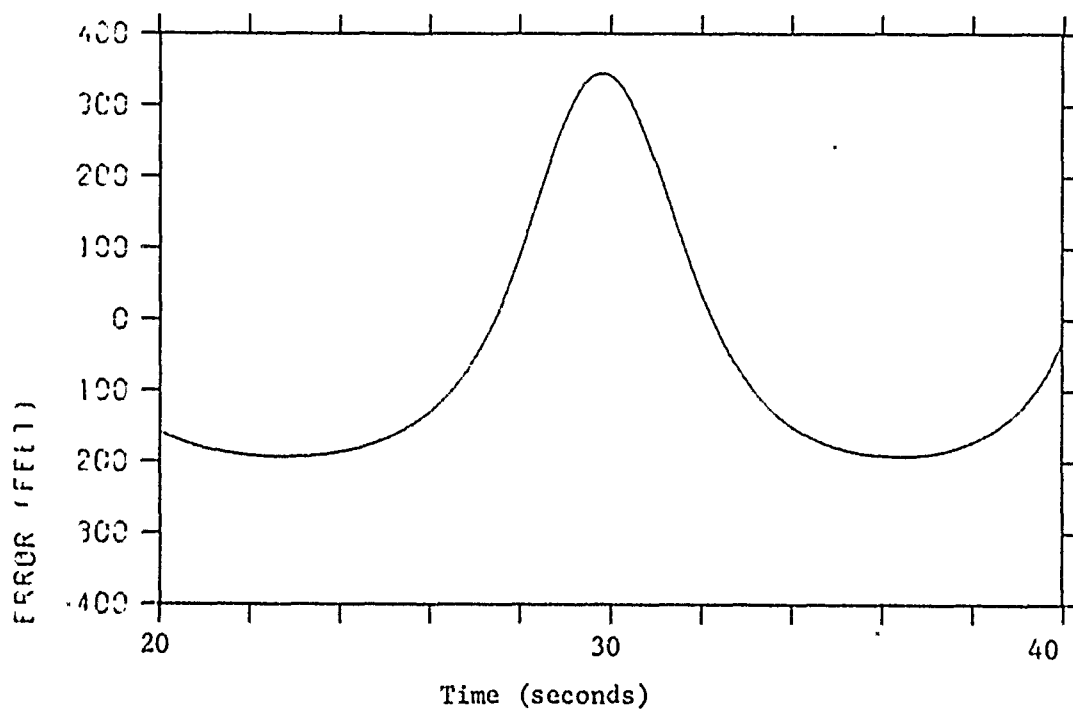
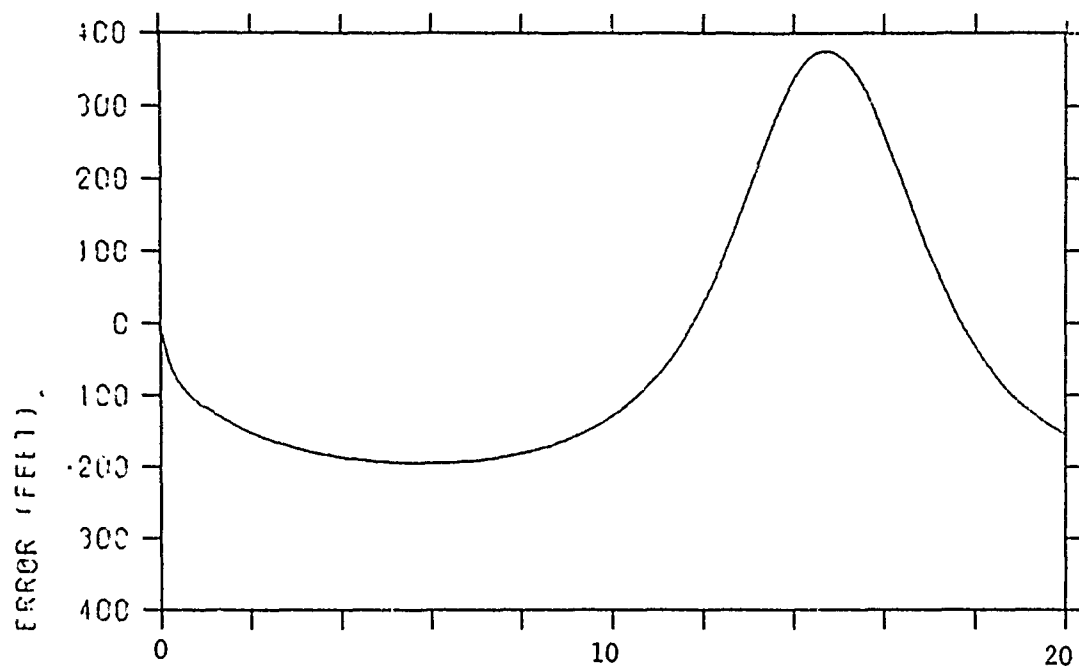


Figure 19. Tracking error as a function of time. $H_a = 100$ ft, $H_t = 300$ ft, $f = 5.7$ GHz, $\rho = 0.5$, tilt angle = 30° .

While coherent systems such as the EAR may usually be modified for frequency agility with a minimum of transmitter and antenna changes, care must be taken not to degrade the system MTI performance. In the EAR degradation is circumvented by use of a "triplet" canceller as opposed to the normal "sliding window" canceller [6]. A central consideration in implementing such a system is the amount of frequency agility bandwidth required; this topic is discussed in the next section.

A. Required Overall Frequency Agility Bandwidth

An approximate estimate of the amount of overall frequency change required may be arrived at by considering the relative phase of indirect and direct rays. The relative phase, ϕ , between signals which traverse two paths whose physical lengths differ by ΔR is given by

$$\phi = \frac{2\pi \Delta R}{\lambda} = 2\pi \frac{f}{c} \Delta R \quad .$$

When frequency agility is used, in order to sample all possible indicated target positions, it is necessary to change ϕ by π ; the corresponding required frequency change, Δf , may be arrived at as follows:

$$\phi + \pi = 2\pi \frac{(f + \Delta f)}{c} \Delta R \quad ,$$

or

$$\Delta f = \frac{c}{2\Delta R} \quad .$$

Taking $c = 3 \times 10^8$ m/sec, then

$$\Delta f = \frac{3 \times 10^8}{2\Delta R} \quad ,$$

and if Δf is MHz and ΔR in meters,

$$\Delta f = 150/\Delta R \quad .$$

Since for multipath situation [7],

$$\Delta R \approx \frac{2H_a(H_a + H_t)}{R} \quad ;$$

the required frequency change becomes

$$\Delta f \approx \frac{75f}{H_a(H_a + H_t)} \quad .$$

The required changes for $H_a = 15$ feet and 100 feet have been calculated and are plotted in Figures 20 and 21. These data indicate that the 400 to

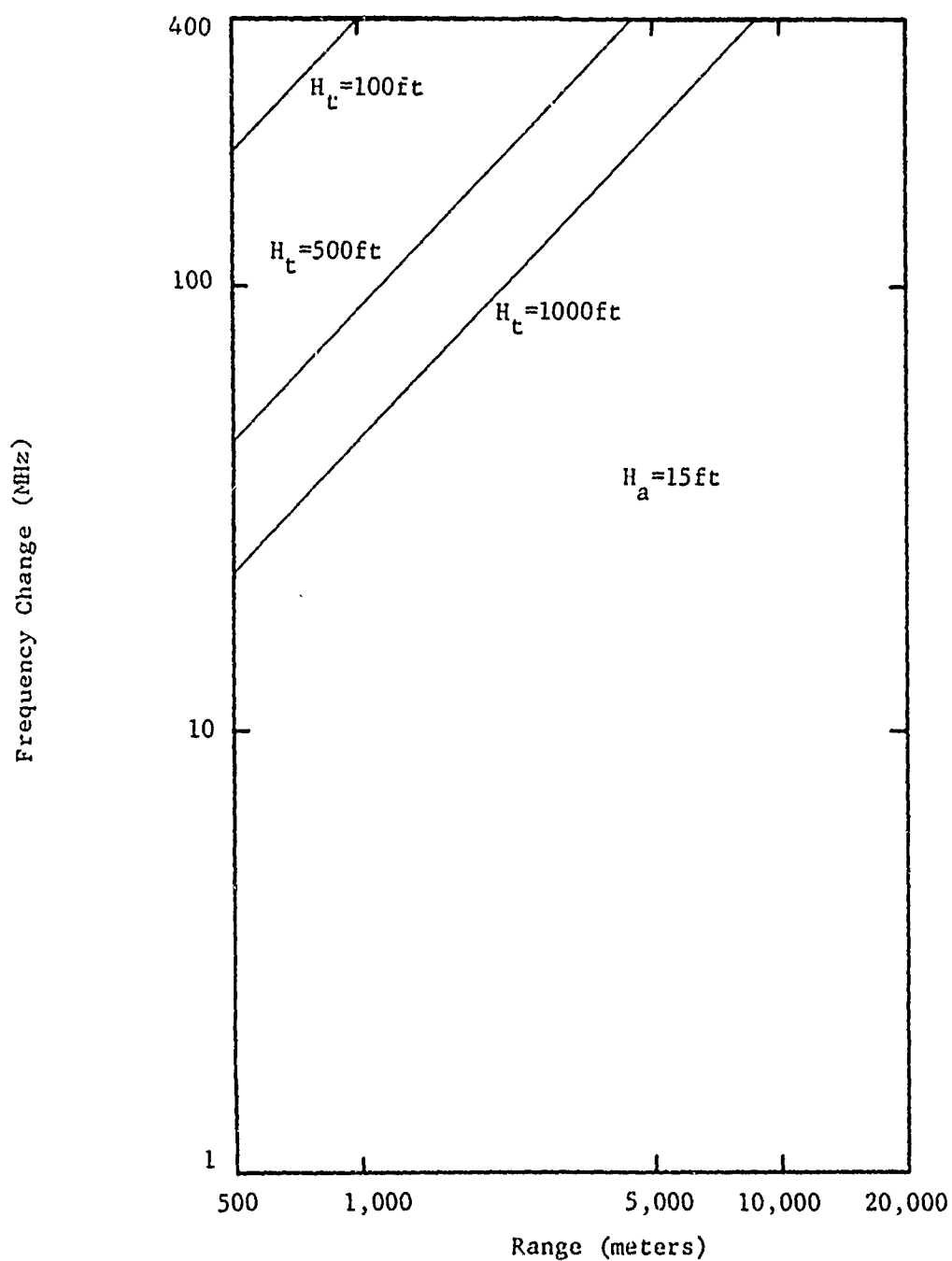


Figure 20. Frequency change required to change the relative phase of the direct and reflected signals by π . Antenna height = 15ft.

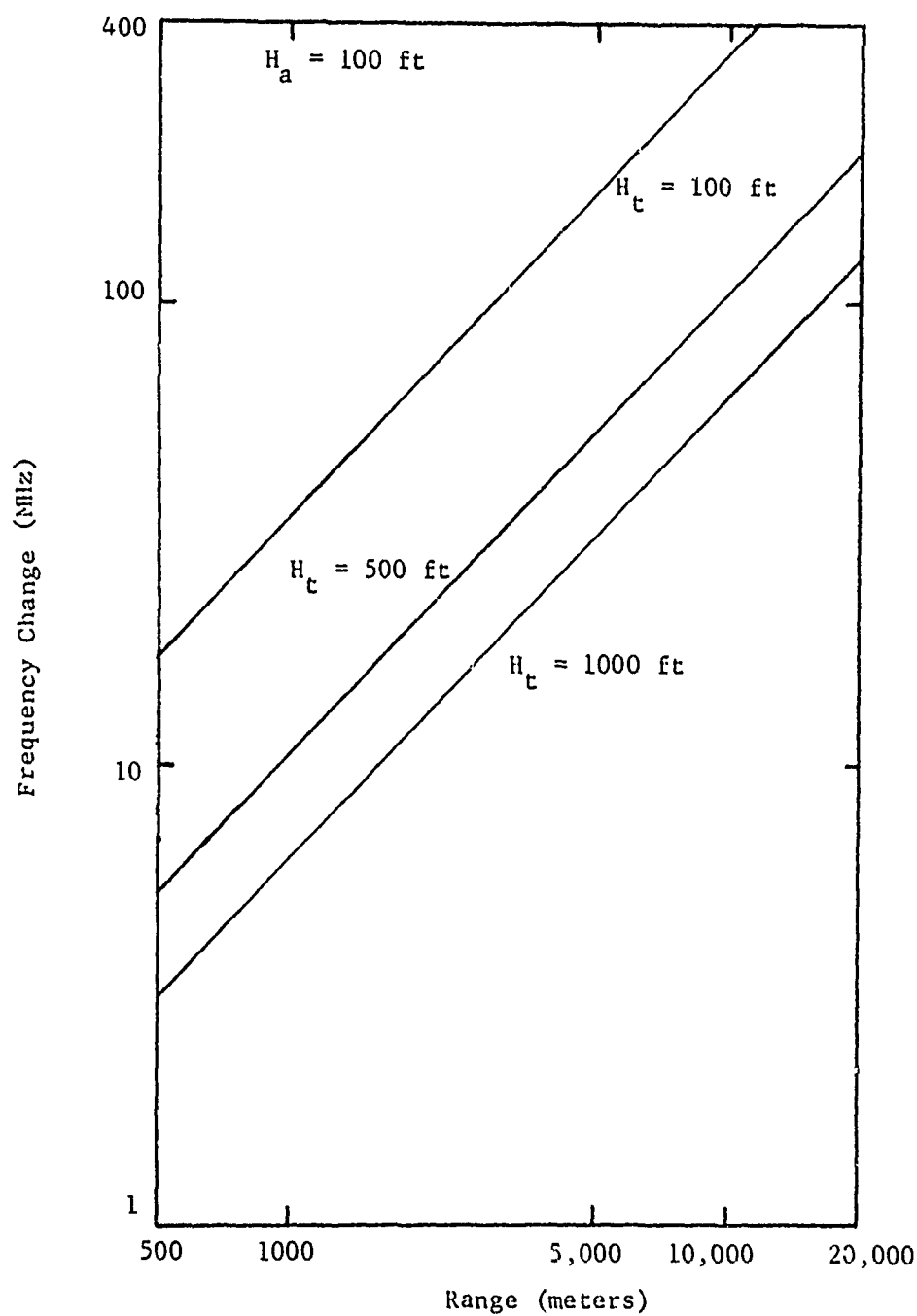


Figure 21. Frequency change required to change the relative phase of the direct and reflected signals by π . Antenna height = 100ft.

500 MHz potential frequency agility bandwidth of the EAR system is sufficient to be at least partially effective in reducing multipath effects on the EAR, particularly for higher altitude targets, higher antenna site, and shorter ranges.

B. Effect of Frequency Agility on Angle Tracking Performance

The computer analysis of EAR tracking performance described earlier was used as tool to examine the effectiveness of frequency agility in reducing multipath-induced angle tracking errors. The format selected was to radiate 16 frequencies and wait 0.1 seconds between looks at the target. The indicated angular errors for each of the 16 frequencies were then averaged together to provide an estimate of true target position.

The degree of improvement that may be realized with frequency agility is a function of target and antenna heights, and of the frequency-agility bandwidth (overall frequency excursion). Data from a number of runs have been summarized by presenting peak-to-peak tracking error as a function of target height for various frequency-agility bandwidths and antenna heights.

Figure 22 shows one such set of data, indicating the effectiveness of various frequency-agility bandwidths in reducing multipath-induced tracking error. The three curves plotted in Figure 22 represent the performance achievable with fixed-frequency operation, 200-MHz bandwidth frequency-agile operation, and 400 MHz bandwidth frequency-agile operation for a 100-foot antenna height. The 400-MHz bandwidth is particularly effective in reducing these errors, especially for higher targets.

As discussed earlier and shown in Figures 20 and 21, the antenna height influences the amount of frequency excursion necessary. Figure 23 shows the results obtained when frequency agility was used with a 15-foot antenna height. While tracking performance was improved with frequency agility, the improvement is not as dramatic as seen in Figure 22 for 100-foot antenna height.

The reflection coefficient also influences the tracking performance of the EAR in a multipath situation. A reflection coefficient of $\rho = 0.5$ was used for most of these analyses, however, both higher and lower values of ρ were also used during the course of the analysis. Figure 24 shows the results obtained when a value of $\rho = 0.7$ was used, indicating the while the magnitude of the errors increases with increasing ρ , the relative effectiveness of frequency agility remains essentially the same.

These data indicate that substantial reduction in angle tracking error is possible when frequency agility is used in the EAR system, provided the full frequency agility bandwidth of the EAR system is utilized.

C. Adaptive Processing for the EAR System

Use of the relative phase difference between sum and difference signals as an indication of the acceptability (or quality) of the tracking information is based on the fact that when tracking a single target in free space, the

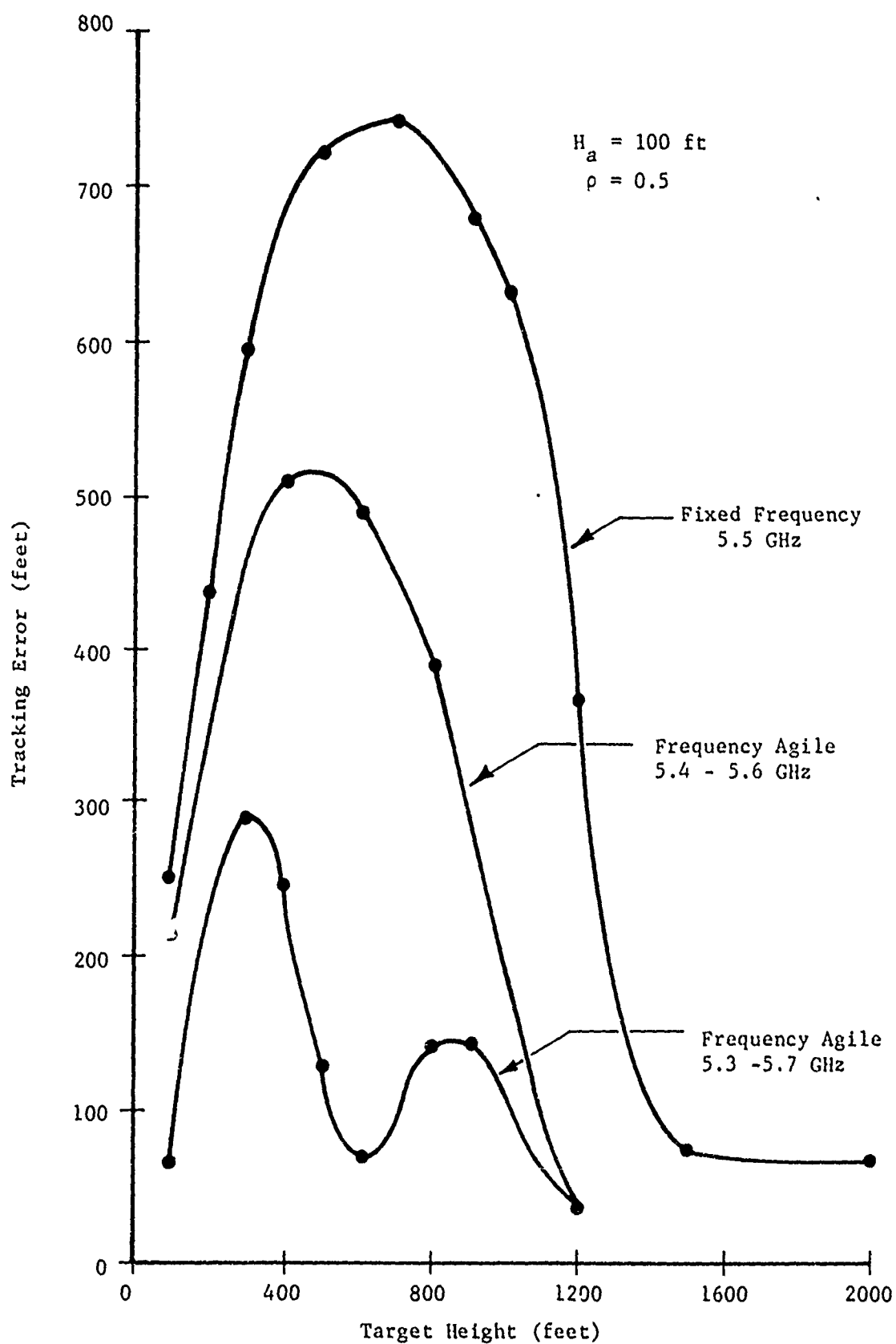


Figure 22. Tracking error as a function of target height using frequency agility. $H_a = 100 \text{ ft}$.

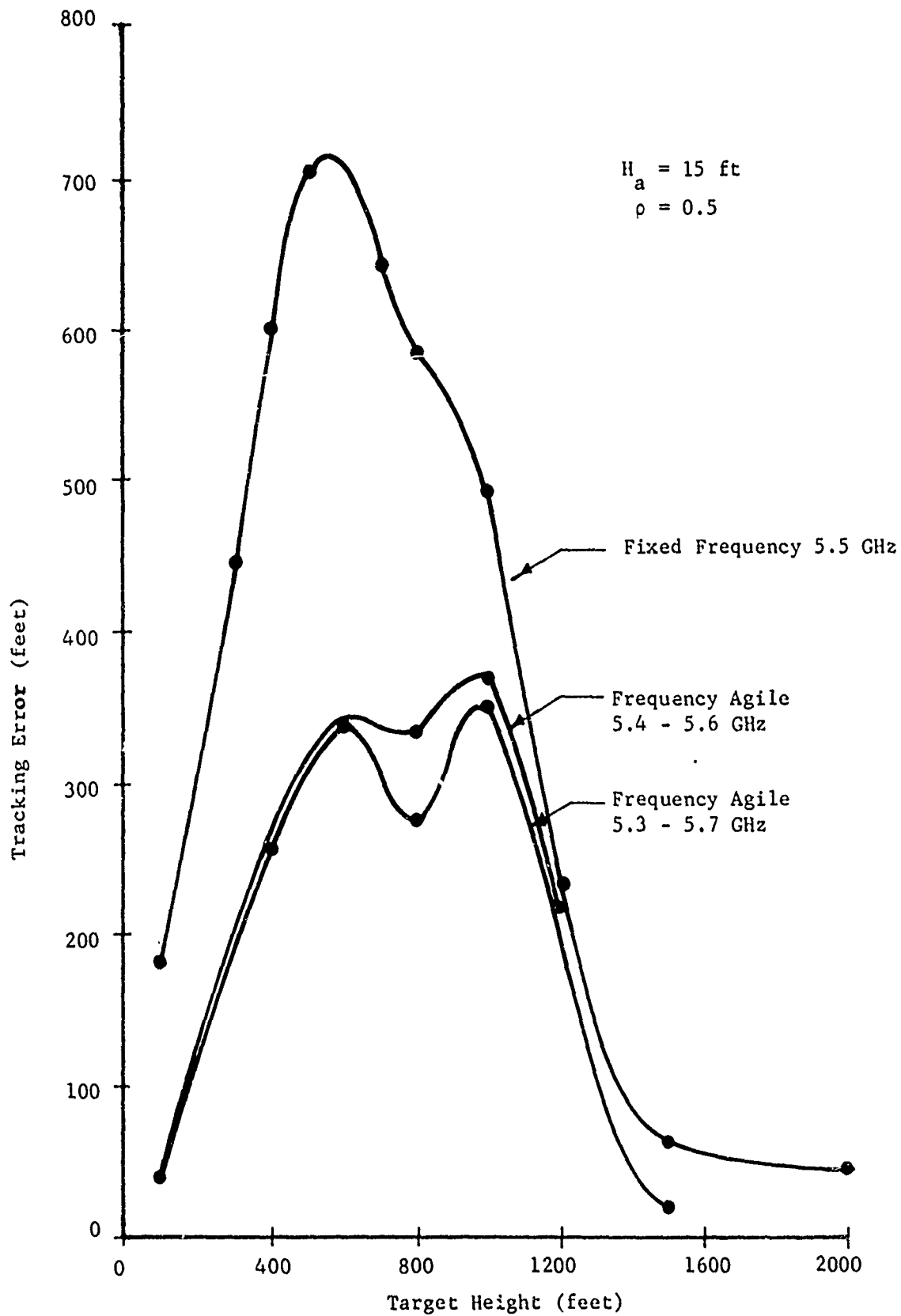


Figure 23. Tracking error as a function of target height using frequency agility. $H_a = 15 \text{ ft}$.

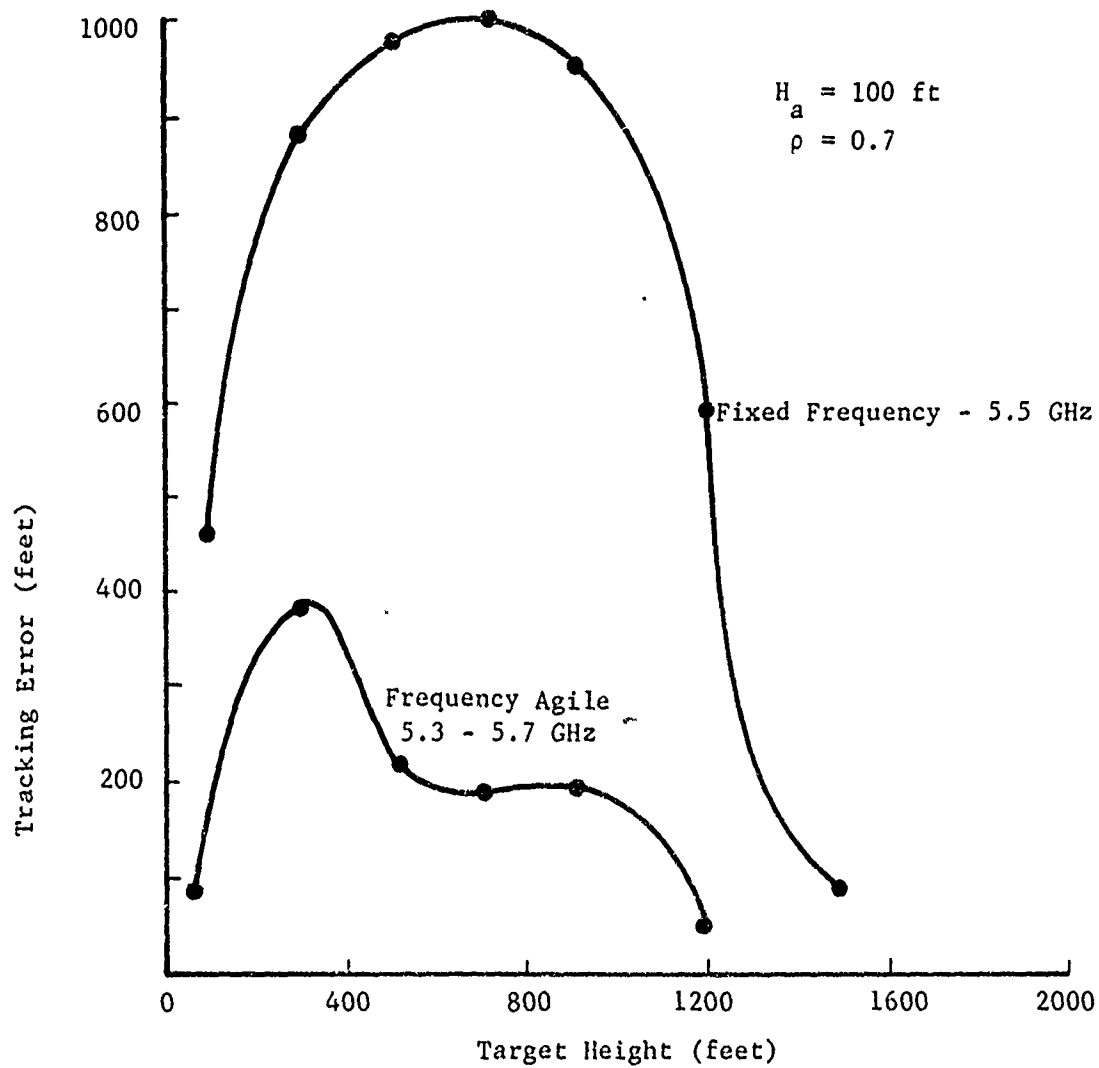


Figure 24. Tracking error as a function of target height using frequency agility. $H_a = 100 \text{ ft}$.

difference signal has relative phase of 0 or 180° (depending on which side of the axis the target lies) when compared with the sum signal. When several unresolved targets (or a single target and its image) are illuminated by the radar, this phase relationship no longer holds. The basis of one adaptive processing scheme is to use this relative phase between sum and difference signals, the so-called Complex Indicated Angle (CIA) [8] as a measure of the quality of the position data. A plot of the CIA as a function of time for the same run shown in Figure 17 is given in Figure 25. A correlation is seen between the phase deviations of the CIA from 0 and 180° and the peaks of the tracking error. However, these phase variations are rather small and the presence of thermal noise, random target characteristics, and equipment inaccuracies would probably make it difficult to appreciably improve the quality of the track data by using the CIA.

Use of the amplitude of the received sum signal as a means of identifying acceptable track data has also been proposed [9]. Figure 26 shows the amplitude of the sum signal for the same situation shown earlier in Figure 17. Comparing these two figures indicates a high degree of correlation between the minimum of the received signals and the peaks of large tracking error. This is probably the most significant correlation which may be used to assess the quality of tracking information, and on which has been proposed to reduce glint-induced tracking errors. In the multipath situation, when tracking a complex target, variations in target cross-section with frequency may be as large or larger than the variations in received power due to multipath signals. Thus, there is no guarantee that optimum processing is obtained by selecting the signal of minimum amplitude. However, weighting of the track information based on the amplitude of the received sum signal appears to be a reasonable approach, since it has a high likelihood of improving the overall quality of track data, if for no other reason than that low-amplitude signals likely to be corrupted by thermal noise will be deemphasized. Computer analysis of more complex target models in a multipath situation using adaptive processing has shown no clearly identifiable improvement in the quality of track data over conventional frequency agility. While there were cases where track data improved appreciably, there were also cases where it did not, depending upon details of the lobing of the target and the lobing due to multipath.

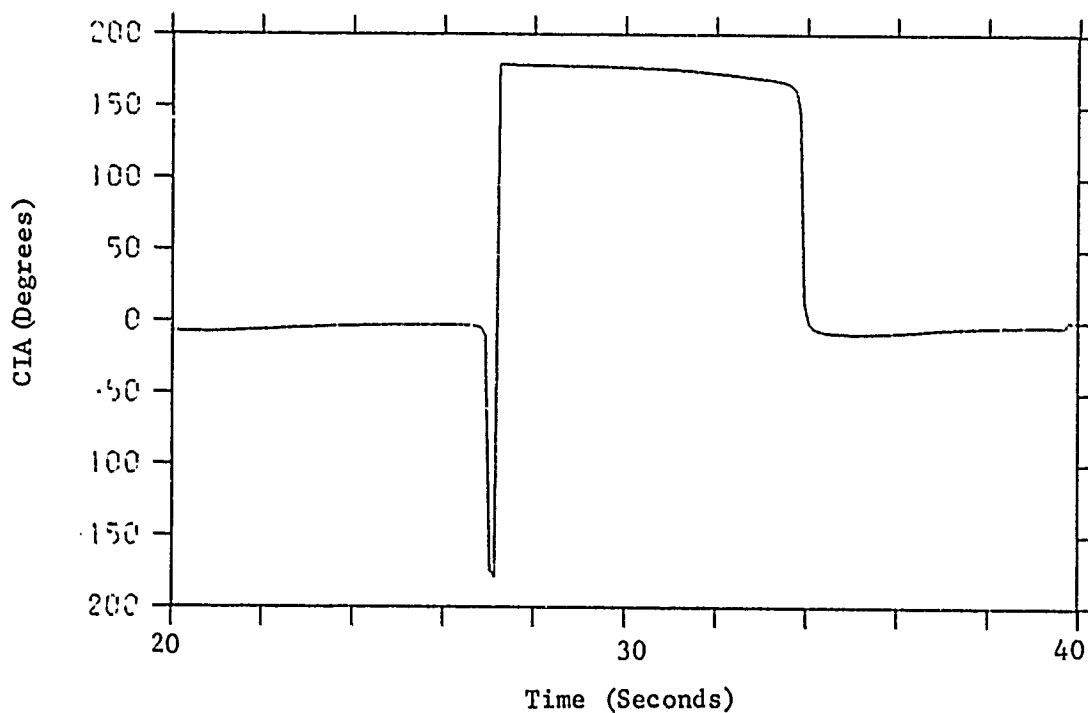
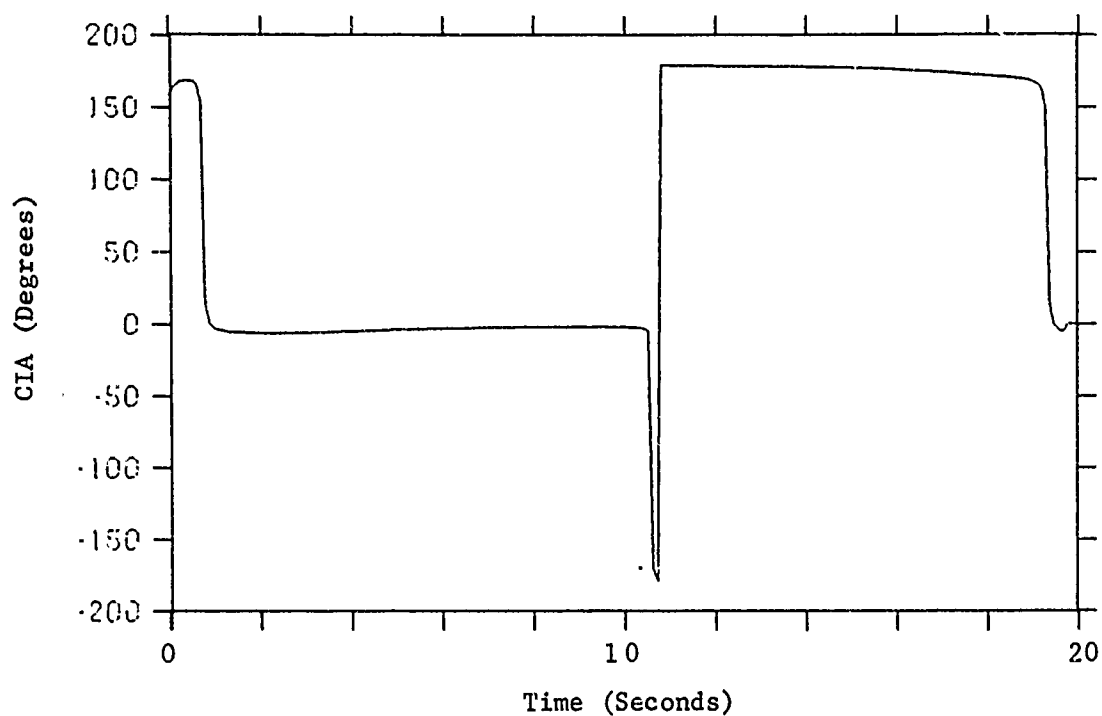


Figure 25. Complex indicated angle (CIA) as a function of time for the same target-radar parameters described in Figure 17.

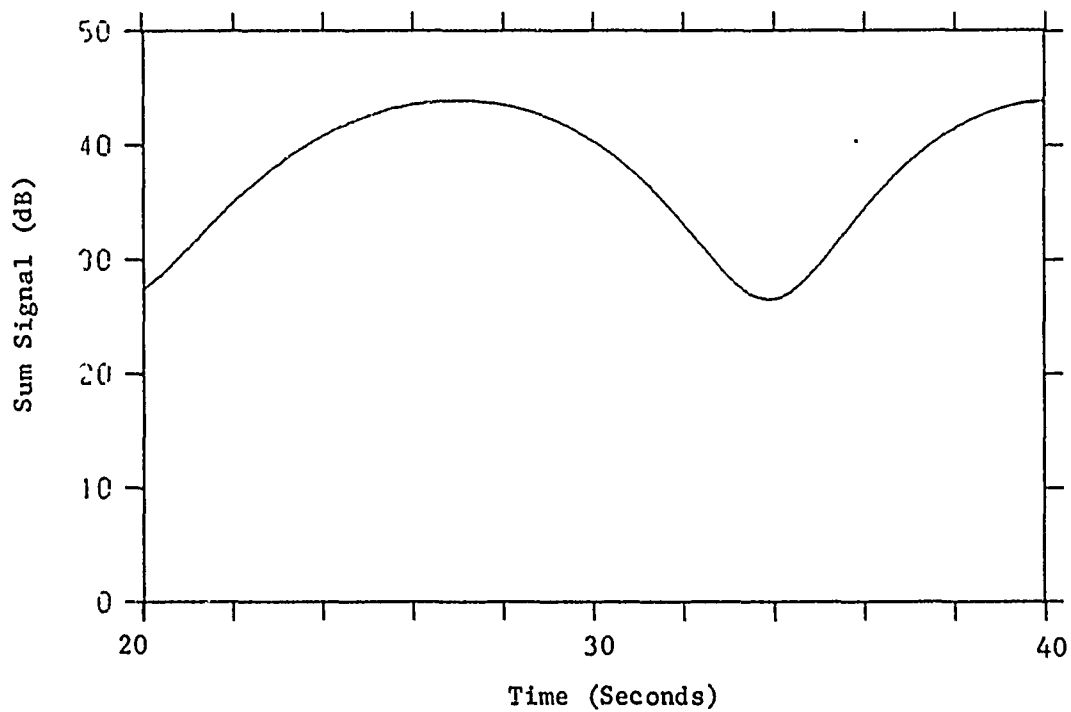
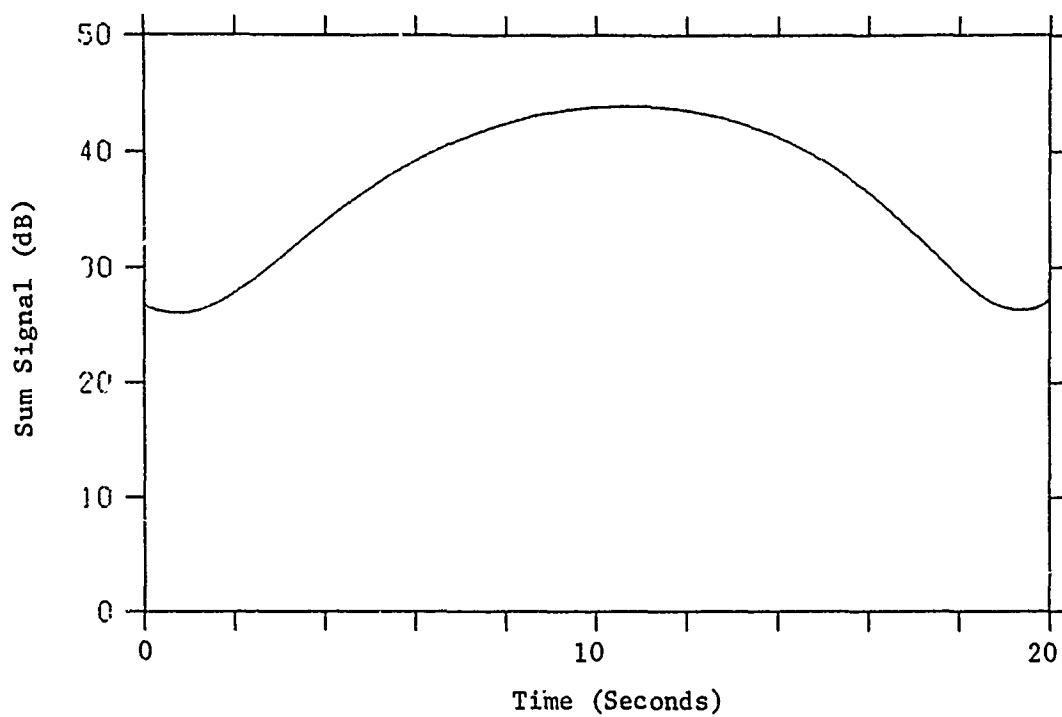


Figure 26. Sum signal variations as a function of time for the same target-radar parameters described in Figure 17.

V. IMPROVED MTI PROCESSORS

A number of factors enter into the design and specification of the data processor for an MTI radar system. Among the constraints are requirements that the system have sufficient clutter attenuation for operation in a heavy clutter environment, that the target detectability remain relatively constant for the range of expected Doppler frequencies, and that processing be performed using some specified number of received pulses. The motivation for the first two requirements are rather obvious, and the last requirement is dictated by the desire to minimize the number of pulses required on a given target (and consequently to maximize the number of targets which can be investigated) in a beam-agile radar such as a phased-array radar, or by the desire to optimize performance when frequency agility is used (by minimizing the number of pulses transmitted at one frequency).

The basic points to be developed in this section are these: (1) The optimum MTI processor (optimum from a point of view of statistical detection theory) which operates on more than two received pulses has not yet been developed. (2) If such a processor had been developed, its performance would be limited by practical equipment considerations. (3) Several improved filter designs for unstaggered prf systems have been developed which offer substantial clutter attenuation while maintaining more nearly uniform response to various Doppler frequencies. (4) Similar improved filter designs are needed for the staggered prf case.

In this section, several design procedures are presented for the realization of improved MTI processors (cancellers, or clutter filters), and characteristics of processors designed using these procedures are discussed. Section A reviews receivers that are optimum from the point of view of statistical detection theory. Previous work directed toward development of optimum digital MTI processors is presented in Section B, where difficulties in obtaining acceptable MTI processor performance are discussed, and realistic constraints set by equipment limitations and by system performance specifications are outlined. MTI processors that are optimum from a filter-design point of view are developed in Section C, and conventional filter design procedures are reviewed in Section D. In Section E, several design procedures for use in unstaggered MTI radar systems are outlined. Some representative results of filter responses developed using these design procedures will be presented, and the limitations of each approach discussed.

MTI filters for use in systems employing staggered prf are briefly discussed in Section F. The effect of using several different pulse stagger ratios in a staggered prf system is analyzed, and available design procedures for staggered systems are summarized.

A. Use of Statistical Detection Theory in Developing Optimum MTI Receivers

Development of optimum receivers has been of substantial interest since radar was first developed. The earliest optimum receiver was for detection of a single pulse in white noise. This concept led to the development of the

so-called "matched filter" [10,11,12], namely, one which maximizes peak signal-to-noise ratio, and has a frequency response given by the complex conjugate of the voltage spectrum of the received pulse.

If the power spectrum of the noise plus received clutter varies with frequency (so-called colored noise), then the optimum filter response becomes (except for a constant time delay) the complex conjugate of the voltage spectrum of the received pulse divided by the power spectrum of the receiver noise plus received clutter [13,14]. This fact was used by Urkowitz [15] to derive optimum receivers for detection of targets in clutter.

Rihaczek [16] has pointed out that the class of filters developed by Urkowitz is optimum only when thermal noise may be neglected, and that the presence of both fluctuating clutter and thermal noise requires more complex filters than those developed by Urkowitz.

If desired targets and unwanted clutter returns are separated in time (range) and/or in frequency, substantial improvement in performance is possible using combined signal and filter optimization. DeLong and Hoffstader [17,18] consider the problem of detection of a point target in random clutter using combined signal-receiver optimization. The detection of a target of known Doppler shift has been treated by Stuart and Westerfield [19] and by Van Trees [20]. Spafford [21,22], Stutt and Spafford [23], and Rummler [24] have treated the optimum receiver when clutter and target signals have different areas of occupancy on the range-frequency plane.

In many cases the expected Doppler shift of the received signal is not known, a priori, and the expected range of signals overlaps the clutter in both range and in frequency. The optimum estimation receiver for this case becomes essentially a bank of matched filters, one for each expected Doppler frequency [25]; this configuration is very similar to the pulsed Doppler radar which employs a comb filter or a filter bank followed by a threshold for both velocity estimation and target detection.

The optimum detection receiver corresponding to the conventional MTI radar system appears to have been first discussed in the radar context by Wainstein and Zubakov [26]. Because of the importance of this work, their basic approach to this problem will be briefly reviewed.

The formulation of the optimum MTI receiver is one of testing general Gaussian hypotheses for the case of a nonfluctuating target and interfering signals which are Gaussian random variables. Two hypotheses H_0 and H_1 are defined in terms of the received signal as follows:

$$H_0: r(t) = n(t)$$

$$H_1: r(t) = n(t) + m(t) \quad ,$$

where $m(t)$ is a received signal reflected from a point target; in general $m(t)$ will have experienced some Doppler shift. The interfering signal $n(t)$ is due to both thermal noise and reflections from clutter.

Define several matrices:

the observation matrix,

$$\underline{r} = \begin{bmatrix} r_1 \\ r_2 \\ \vdots \\ r_n \end{bmatrix},$$

the mean of the matrix \underline{r} ,

$$\underline{m} = E(\underline{r}),$$

the covariance matrix

$$\underline{\Lambda} = \text{Cov}(\underline{r}) = E \left[(\underline{r} - \underline{m}) (\underline{r} - \underline{m})^T \right],$$

and the inverse covariance matrix

$$\underline{Q} = \underline{\Lambda}^{-1}.$$

The optimum Bayes and Neyman-Pearson tests are both likelihood ratios. The likelihood ratio (which is a function of both the Doppler shift ω_d due to target radial velocity and the initial phase of the received signal θ) is given by Van Trees [27];

$$L(\underline{r}(\theta, \omega_d)) = \exp \left[-\frac{1}{2} \left[(\underline{r} - \underline{m})^T \underline{Q} (\underline{r} - \underline{m}) - \underline{r}^T \underline{Q} \underline{r} \right] \right],$$

under the assumption that the mean value of $n(t) = 0$.

Since \underline{Q} is symmetric about its diagonal, that is, $\underline{Q}^T = \underline{Q}$, then $\underline{m}^T \underline{Q} \underline{m} = \underline{r}^T \underline{Q} \underline{r}$. Using this fact, the likelihood ratio may be written

$$L(\underline{r}(\theta, \omega_d)) = \exp \left[-\frac{1}{2} (\underline{m}^T \underline{Q} \underline{m}) \right] \exp (\underline{m}^T \underline{Q} \underline{r}).$$

Since both the anticipated Doppler shift, ω_d , and the initial phase θ are unknown, the average likelihood ratio test then becomes, assuming all ω_d and θ are equally probable,

$$L(\underline{r}) = \int_0^{2\pi} \int_{\omega_d} \exp \left[-\frac{1}{2} (\underline{m}^T \underline{Q} \underline{m}) \right] \exp (\underline{m}^T \underline{Q} \underline{r}) d\omega_d d\theta.$$

The evaluation of this likelihood ratio in a closed form is a formidable task. The first integration introduces Bessel functions of the second kind of order zero, making the second integration difficult. Wainstein and Zubakov [26] have applied the addition formula for Bessel functions and evaluated this integral exactly for the case where the observation consists of two pulses.

The optimum MTI receiver derived by Wainstein and Zubakov for processing two received signals consists of optimum processing of both the in-phase and quadrature components of the received signal, pairwise subtraction of these two in-phase and quadrature samples, formation of the square of each of these differences, and comparison of the sum of these squares with the threshold [26]. This processing corresponds to the conventional two-pulse MTI canceller.

Selin [28] expanded the Bessel function of the second kind of order zero in a power series valid for small ratios of signal to interfering signal in order to simplify integration of the Bessel functions. Selin then further confines his discussion to the case of white noise interference (which is uncorrelated from pulse to pulse). The results of this analysis have limited applicability due to their complexity and because in many cases of interest, the interfering signal is highly correlated from pulse to pulse due to the presence of strong clutter returns.

Brennon, Reed, and Sollfrey [29] approximate the integral of the Bessel function by a finite sum. This approximation is used to compare the performance of optimum receivers under various conditions, but it does not give information concerning how to construct an optimum MTI receiver; only how to approximate its performance by means of a Doppler filter bank.

From this review, it becomes evident that the specification of the optimum MTI processor from the point of view of statistical detection theory is a formidable task, and one which has been solved exactly only for the case of the two-pulse processor. Because of the difficulty in specifying the performance of the optimum MTI receiver, considerable attention has been focused on the design of optimum weighted sums for processing sampled sequences of the return from moving targets in a clutter environment. This work is summarized in the following section.

B. Optimization of MTI Processors Using Weighted Sums of Sampled Signals

It was brought out in the previous section that the optimum MTI receiver, from the point of view of statistical detection theory, is known only for the two-pulse case. The receiver for larger numbers of received pulses has often been approximated as a linear combination of a number of sample values of either the in-phase or the quadrature component of the received signal. Maximization of the ratio of average output signal (averaged over all expected values of Doppler frequency shifts, ω_d) to interfering signal has been treated by Capon [30]. Capon shows that the optimum weight functions, defined as those which optimize the average-output-signal-to-interfering-signal ratio (called the reference gain, G_n , or more commonly the MTI improvement I) depend only upon the covariance matrix of the interfering signal. For highly correlated pulse-to-pulse interference, such as that due to slowly moving clutter, these

optimum weight functions reduce to the conventional three-pulse canceller for the case of processing three received pulses. Capon also shows that the reference gain for the three-pulse canceller closely approximates that for a large number of received pulses when processing signals in a background of strongly correlated clutter.

There are two main objections to Capon's approach. First, there is no reason to believe that the optimum processor may be realized in the general configuration assumed by Capon; and second, the concept of the average system gain, \bar{G}_n , produces poor signal detectability at some Doppler frequencies of interest. It is perhaps appropriate to note that if the linear processing format discussed by Capon were the configuration of the optimum processor, then the optimum Neyman-Pearson test would be the one which maximizes G_n (see, for example, Spafford [22]).

The average gain \bar{G}_n , is maximized by increasing gain at frequencies where clutter return is small and decreasing it at frequencies where clutter is significantly present. Thus, processors designed to maximize G_n may have unacceptably low responses to targets with Doppler frequencies in the same region as the clutter. The problem of optimizing the response of MTI systems for a wide range of target Doppler frequencies may be approached by considering the processor as a filter. This approach is developed in the next section.

C. MTI Processor Design as a Filter Optimization Problem

As discussed in the preceding section, maximization of the average system gain, I , is often not a very satisfactory method for optimizing the processing scheme for an MTI radar, since this leads to poor detectability of targets having some particular range of Doppler frequency shifts. This leads one to consider uniformity of response of the processor as a function of ω_d as an important consideration in system design. This approach leads naturally to considering the processor to be a filter having as inputs a signal at the Doppler frequency and a signal from clutter plus thermal noise with known power spectral density. Then the filter output can be plotted as a function of input Doppler frequency; one such representation is shown in Figure 27 for the conventional three-pulse canceller. As one can see, the response is very non-uniform, and considerable improvement may be made in the shape of the curve while still maintaining a substantial value of I .

The second reason why maximizing I is not always entirely suitable for optimizing system response is that there are often substantial practical limitations which are not included in the theory. Most modern high-performance MTI processors utilize digital processing, mainly to obtain storage without recirculating analog delay lines. While round-off error in the quantization or digitizing process does not usually appreciably limit performance, analog-to-digital quantization errors usually constrain I to be substantially less than its theoretically achievable maximum value. A comprehensive treatment of the limitations in improvement due to quantization errors is given in Appendix F. Therefore, it is often possible for I to be reduced somewhat, providing more uniform detectability of targets of different Doppler shifts, without substantially affecting overall system performance.

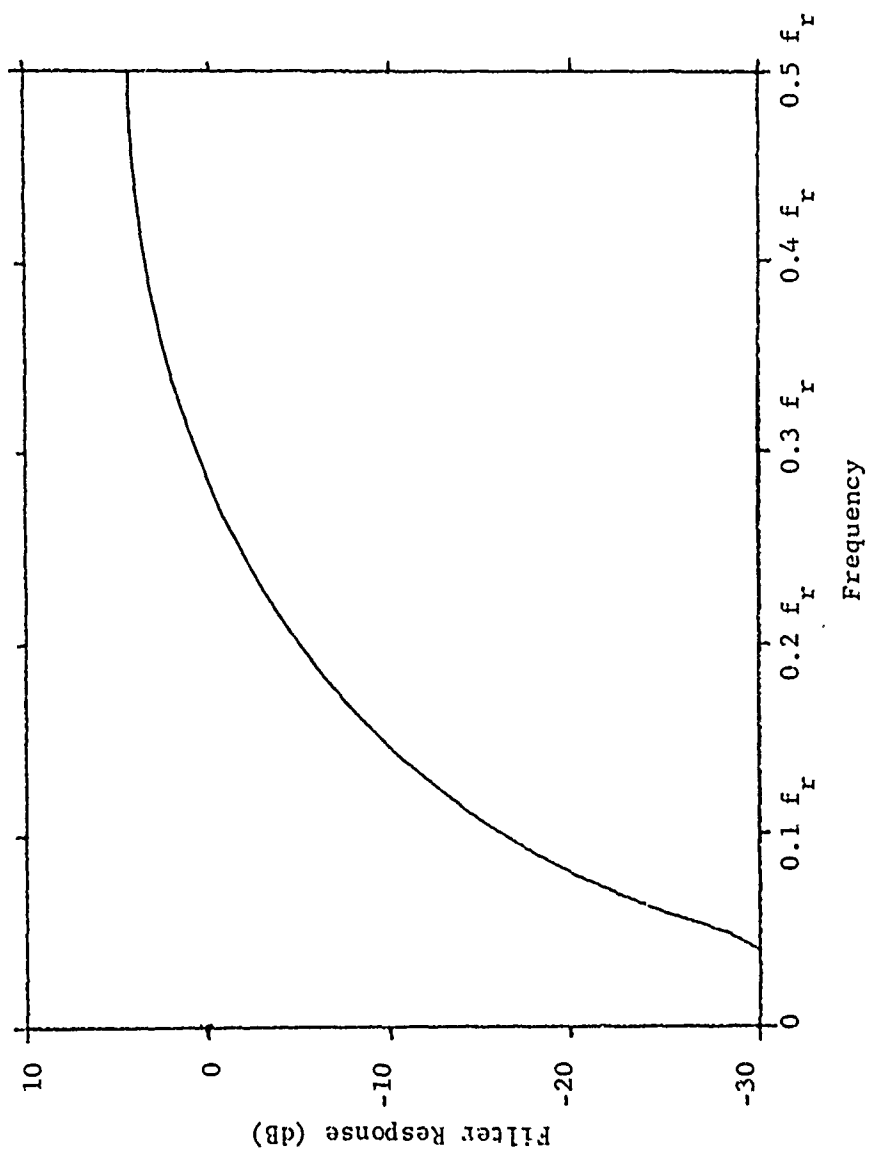


Figure 27. Response of conventional three-pulse MTI canceller or filter as a function of Doppler frequency.

Another factor which limits the performance of some real radar systems is the presence of slowly moving discrete targets such as birds, insects, and automobiles [31,32]. The presence of these extraneous targets sometimes requires that a "stop-band" be established, usually centered about zero frequency, in order to reject these unwanted returns which would otherwise completely overload the system.

Therefore, one might conclude from these remarks that a practical design procedure for digital MTI filters would be: (1) establish a desired and achievable value of I , based both on desired system performance and on practical equipment limitations, (2) within this constraint, produce an optimally uniform response for all Doppler frequencies of interest, while (3) rejecting unwanted returns. The filter responses are a function of the shape of the clutter spectrum, the optimization criteria applied to the response (such as minimum rms error, equal ripple in the pass band, etc.) and the expected range of velocities of the desired and undesired targets.

The following discussions will be largely confined to consideration of transversal filters [33,34] (nonrecursive filters or those with no internal feedback loops), because in a real application only limited number of pulses may be processed from each target. Several constraints determine the number of pulses that may be processed from a given target. In a beam-agile radar such as a phased-array system, minimizing the number of pulses on a given target maximizes the number of targets the radar can accommodate. If frequency agility is used, the radar must remain at a given frequency for a sufficient number of pulses to extract the desired information concerning a target; minimizing the number of pulses on target thus maximizes the number of available frequencies the radar may radiate in a specified time. The performance of several conventional transversal digital MTI filters is discussed as Appendix A. While a recursive filter (one containing feedback loops) could be used and its transient response truncated after the desired number of pulses, the response of such a truncated recursive filter may always be realized as a transversal filter. The difference between the two lies in the practical implementation of the filter.

D. Conventional Digital-Filter Design Procedures

Various methods have been developed for designing digital filters [35,36]. Their design is often approached by defining an analog filter prototype and appropriately transforming the response to obtain the z-transform of the desired filter. In general, this approach yields a recursive filter; while this filter's output may be truncated after the desired number of pulses, there is generally little control over the number of pulses required to closely approximate the desired steady-state response.

To illustrate the errors in filter response that may occur due to truncation of a recursive filter designed for a certain steady-state response, a four-pole Butterworth filter response was considered. Its z-transform was expanded to powers of z^{-1} by long division and the series truncated after a selected number of terms. The impulse response of the filter represented by

this series was then calculated to determine the truncated frequency response. Figure 28 compares the steady-state response and responses obtained by truncating the filter response after 3, 5, and 7 pulses. As can be seen, the response of the truncated series is a poor extreme case, due to the rapid low-frequency roll-off of the filter, but it serves to illustrate the need for specialized design procedures where the number of available samples is limited.

Three procedures are commonly used in designing transversal digital filters [35-43]. The first involves specifying the sampled finite impulse response of a filter (obtained as an input specification or as a transform of a frequency-sampled response) and utilizing an impulse-invariant transformation to specify the digital filter. Various weighing windows may be used to smooth the ripples in the resulting frequency response. The second method uses a Fourier-series approximation (with appropriate windows often incorporated) to a desired response, while the third method is a direct-search method using linear programming techniques to optimize the desired response. These techniques are not particularly applicable to the design of MTI processing filters, since they do not incorporate clutter characteristics into the filter design procedure as a design specification. In many cases they accept a specific filter shape as the design goal, rather than developing optimum processing for a predetermined number of received pulses, a constraint which is determined by the energy budget of the overall radar system. Four techniques that have been developed for design of optimum MTI processing filters for radars using unstaggered prf's will be outlined in the next section. The staggered prf case is considerably more complex; however, some related work has been done in this area and will be reviewed in Section F.

E. Optimum Transversal Digital-Filter Design Procedures for Unstaggered prf Systems

The design of optimum MTI filters should take into account a number of factors, including maintaining desired values of I , providing uniformity of response for some range of Doppler frequencies, and in some cases providing a stop-band (usually centered about zero frequency) for rejection of unwanted targets. In this section four different design procedures are described which take some of these factors into account.

1. "Cost" Minimization MTI Filters

Jacomini [44] has developed a design procedure that takes into account the clutter attenuation in the pass band, the response in a stop-band, and ripple in the pass band. A "cost" is assigned to each of these factors and designs developed which minimize the overall "cost" of the filter. This approach has the disadvantage that there is usually no straightforward means for selecting the various costs. In practice, when the filter is being designed, the improvement, I , is constrained to be some constant, the cost is apportioned between the pass and stop bands, and the relative costs adjusted until an intuitively satisfying filter response is obtained.

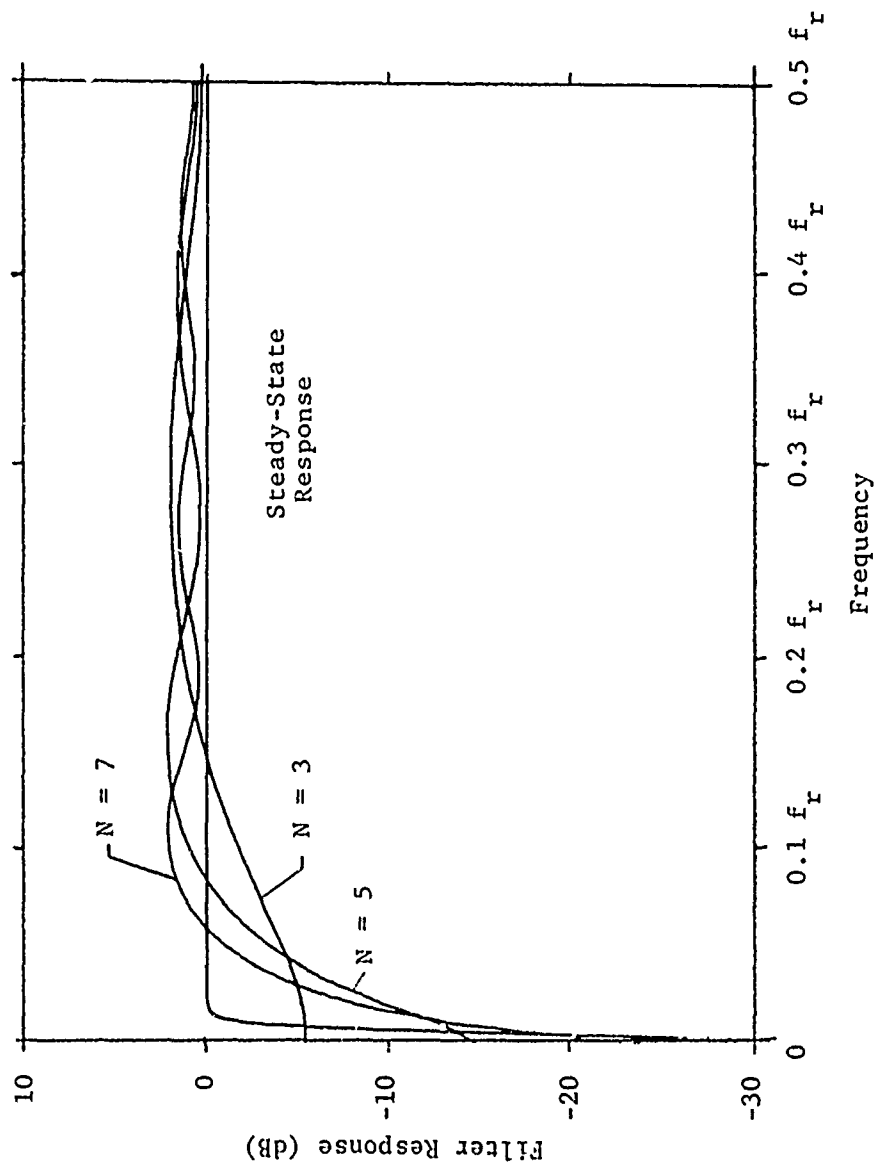


Figure 28. Filter response for a four pole Butterworth high-pass filter (labelled steady-state response) and the output of the same recursive filter terminated after $N = 3, 5$, and 7 pulses were processed. The steady-state response has been offset for clarity.

More straightforward means for obtaining the same types of results are described in following sections.

2. Filter Design by Linear Programming

The frequency response of transversal filters can be completely specified by an equation which is a linear function of the C's (see Appendix F). This fact simplifies the design of this class of filters, permitting use of well-established linear programming techniques. Optimization by linear programming makes use of the fact that, given a set of linear constraint equations, along with an "objective function" which is also a linear equation, the extreme value of the linear objective function lies on the boundary of the "feasible region" which is defined by this set of constraint equations. This important fact gives rise to the "simplex" method of linear programming; an optimization scheme which methodically searches the boundary of the feasible region for the extremum of the linear objective function.

When a desired filter response is to be approximated, several techniques may be used to determine the appropriate filter coefficients: two of these are the "least-mean-square-error" (LMSE) method and the "minimax" method. The LMSE minimizes the least-mean-square error between the specified response and the approximation for all frequencies of interest.

In the LSME method, if $Q(\omega)$ is the specified response function and $G(\omega)$ is the response of the filter, the goal is to minimize

$$\int_R [G(\omega) - Q(\omega)]^2 d\omega ,$$

where R is the frequency range of interest [45]. For many applications this method of filter design is desirable and is treated in Section 3. However, simplex methods are not applicable for LSME specification since the resulting equations are not linear.

The "minimax" method is used to reduce the maximum deviation from the filter specification at a number of selected frequencies. The minimax formula reduces

$$|G(\omega) - Q(\omega)|_{\max}$$

for a number of discrete values of ω contained in R , the frequency range of interest. For example, a typical application might be to design MTI filters with bounded ripple over some specified frequency range while maximizing attenuation for undesired targets and clutter.

Such a minimax program was implemented on the Univac 1108 using a well-known linear programming scheme [46]. The procedure used was to identify a number of frequencies at which the frequency response would be controlled. At each of these frequencies, minimum and maximum values of frequency response were specified. In addition, a linear objective function (LOF) was defined.

For this work, the clutter attenuation divided by C was chosen as the LOF; since $C \approx 1$ for most practical filters, minimizing the LOF corresponded to maximizing the clutter cancellation. The linear programming technique which was used minimized the LOF, subject to the constraint that the frequency response remain within the bounds established earlier. One substantial problem encountered using this technique was that roundoff error seriously influenced the clutter attenuation that could be calculated. Nevertheless, practical filter responses could be developed using these techniques. A second difficulty involved the large number of equations that had to be entered into the program. Successful results were obtained for three- and five-pulse filters, but greater than five pulses was beyond the scope of this program.

This linear programming scheme has been used to design a number of filter responses. Most of the results discussed here will be for five-pulse filters. The filter response for these five-pulse filters were specified in 250-Hz intervals from zero to 2500 Hz, and the constraint at zero frequency was that the response be non-negative.

Figure 29 shows three of the MTI filter responses were developed using the program. The tradeoff between ripple and low-frequency clutter attenuation can be seen clearly. The 3-dB filter has sharper low-frequency cutoff than the 0.8- and 1.8-dB filters, thus increasing the attenuation for clutter and slowly moving targets. With more available pulses, the cutoff slope could be further increased (thus increasing clutter attenuation) while retaining constant ripple.

The ripple constraint in the pass band can be made so restrictive that the filter provides essentially no clutter attenuation, as is seen in Figure 30. When the ripple constraint for this particular filter was changed from 3 dB to 0.8 dB, it failed to provide appreciable attenuation for low frequencies. The minimum specified frequency was 250 Hz.

This relationship between ripple and clutter attenuation was investigated for five-pulse radar filters, resulting in the graph shown in Figure 31. The curves show the ripple vs clutter attenuation relationship for 500 Hz and 750 Hz filters calculated using a 36-bit computer. Extensions to these curves and slightly increased accuracy could have resulted if more computing accuracy had been available. It is possible to project the clutter attenuation for a wide variety of filters by using curves of this type.

All the filters previously discussed have been developed to suppress clutter having a spectral width that is narrow in comparison with the system bandpass; the clutter has been treated essentially as an impulse at zero frequency. However, situations often arise in which targets or clutter lying somewhat higher in frequency need to be suppressed. This may be caused by unusual clutter conditions or by the presence of undesired slowly moving targets. A stop band which will suppress these frequencies can be synthesized easily by simply rewriting the system constraint equations to define these new requirements. This will usually require that the ripple constraint be relaxed

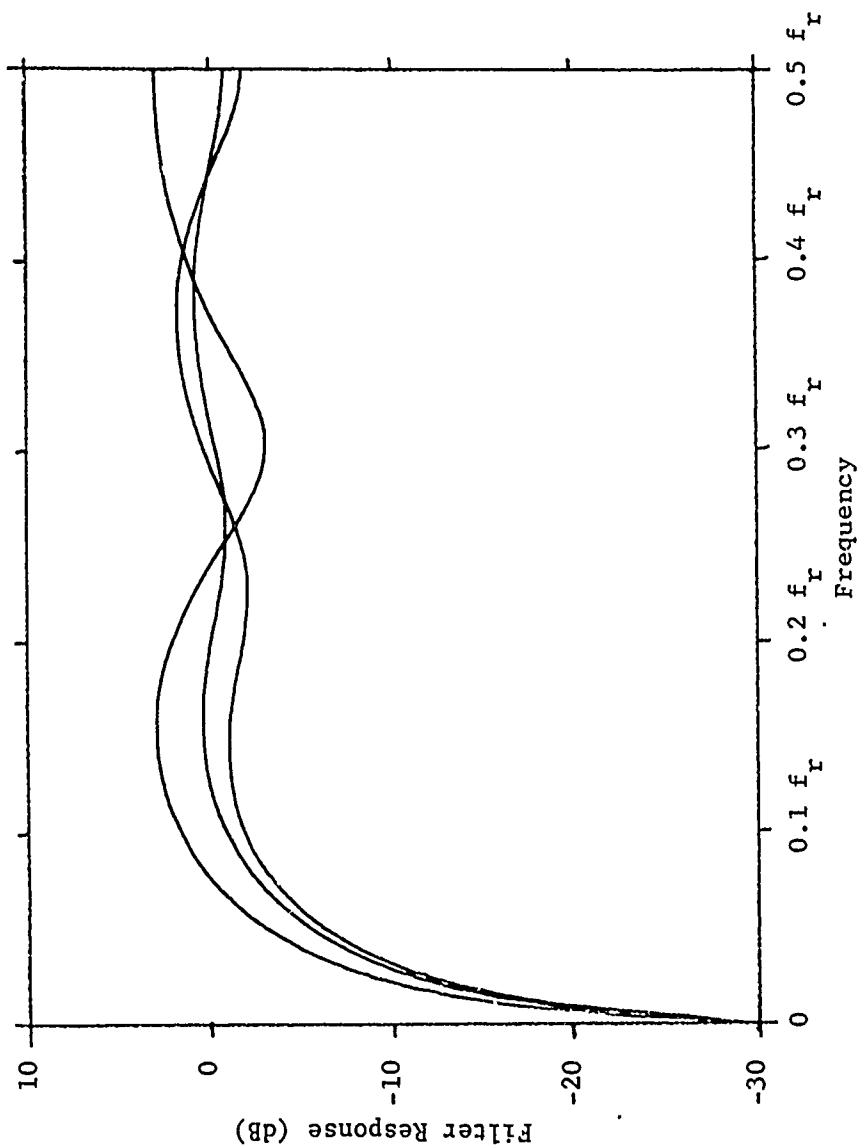


Figure 29. MTI filter responses developed using linear programming techniques.
0.8-, 1.8-, and 3-dB ripple specification. See text for details.

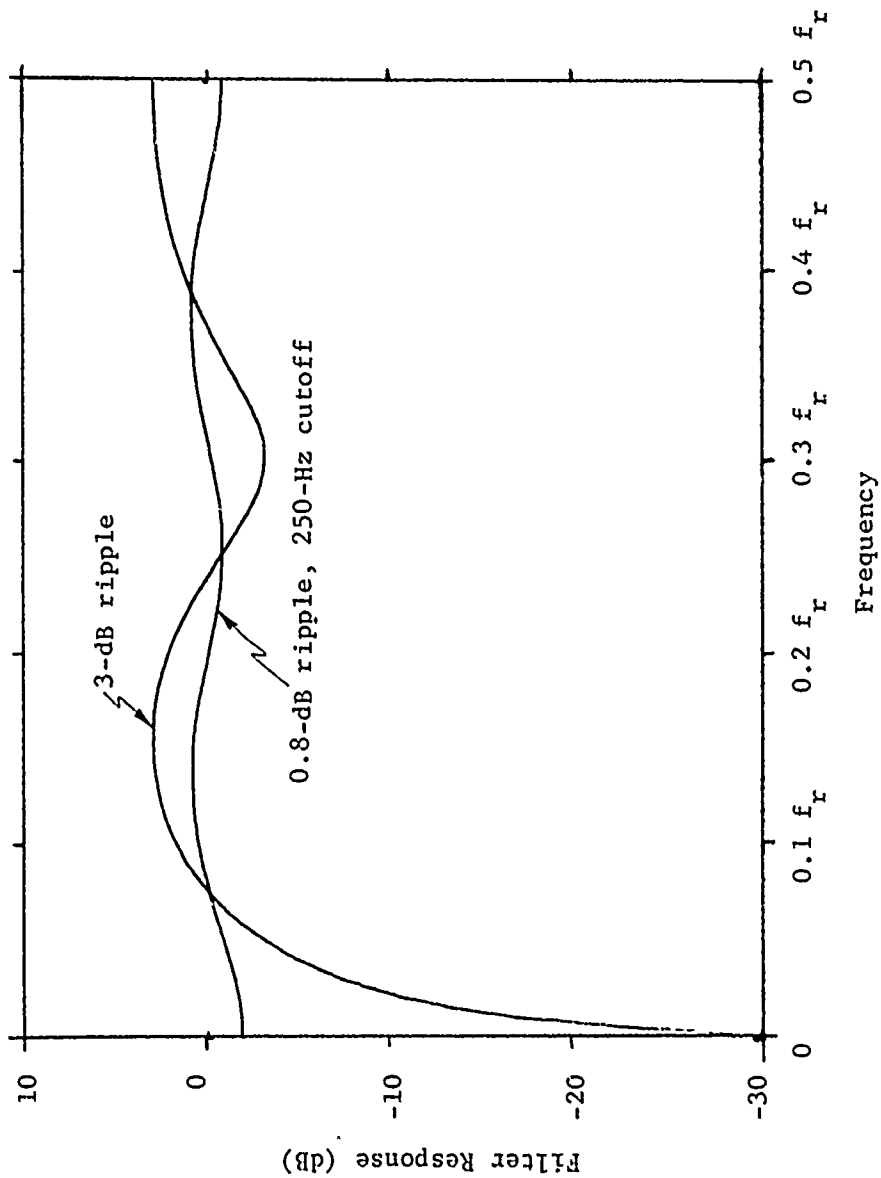


Figure 30. Effects on MTI filter response of too stringent a ripple specification. See text for details.

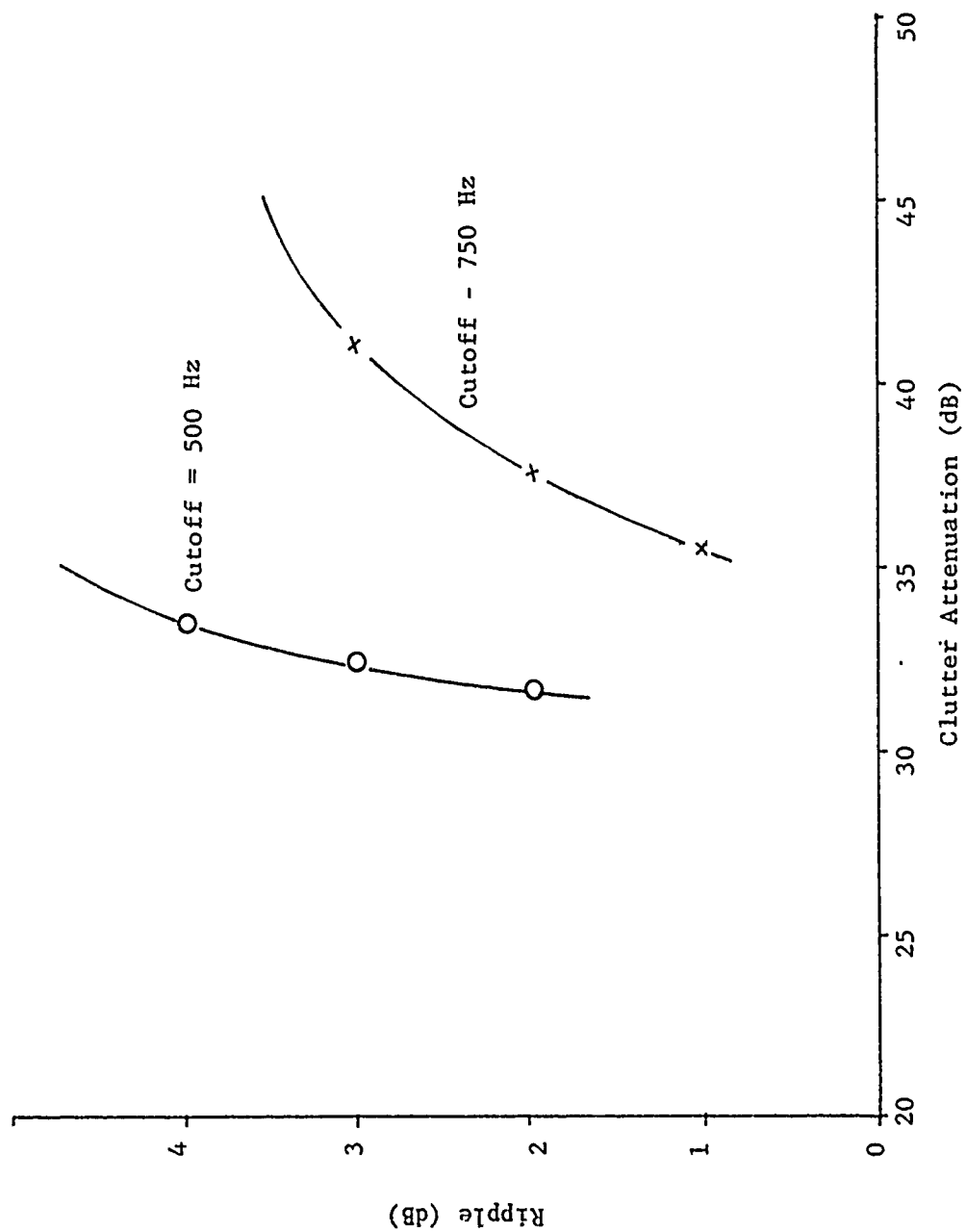


Figure 31. Ripple vs. clutter attenuation for 5-pulse MTI filters with 500 Hz and 750 Hz lower cutoff frequencies.

somewhat. In Figure 32 some low-frequency stopband filters with ripples of 1, 2, and 3 dB which were developed using linear programming techniques are plotted. Not shown, however, are the low-frequency attenuation characteristics below 30-dB attenuation. The 3-dB ripple filter achieved approximately 10 dB more attenuation in the stop band than the 2-dB ripple filter. Similar differences were noted between the 1- and 2-dB cases.

These cases show the relationship which exists between ripple and clutter attenuation for some practical filters, give guidelines for filter performance, and demonstrate the use of filters with stop bands. In all of these filters, performance was ultimately limited by the number of pulses available, and processing larger numbers of pulses would have resulted in filters having more desirable performance.

3. MTI Clutter Rejection Filters Using an rms Error Specification

The specific problem investigated was to maximize detectability of moving targets over some range of Doppler frequencies while maintaining some minimum clutter attenuation. The procedure used was to constrain the target-to-clutter ratio improvement factor, I , to be some selected value while minimizing the function

$$\int_{\eta f_r}^{f_r/2} (G(f) - \overline{G(f)})^2 df, \quad ,$$

where

f_r = the pulse repetition frequency,

η = a fraction $0 < \eta < 0.5$,

$G(f)$ = the power response of the filter, and

$\overline{G(f)}$ = average response of the filter.

The choice of η amounts to establishing a pass band of interest; for the EAR parameters, $\eta = 0.1$ corresponds to minimizing the error for targets above approximately 30 mph. The value of $G(f)$ was chosen equal to one.

The problem now posed is one which may be solved readily by Lagrange multiplier techniques. The steps involved in solution of the problem are (1) write an expression for the improvement, I , (2) write an expression for the error, (3) apply Lagrange multiplier techniques, and (4) solve for the coefficients. These steps are outlined in the following sections. It is worth noting a related analysis has been performed by Martin [33], for cases considered here, his analysis is a special case of the work which follows with $\eta = 0$.

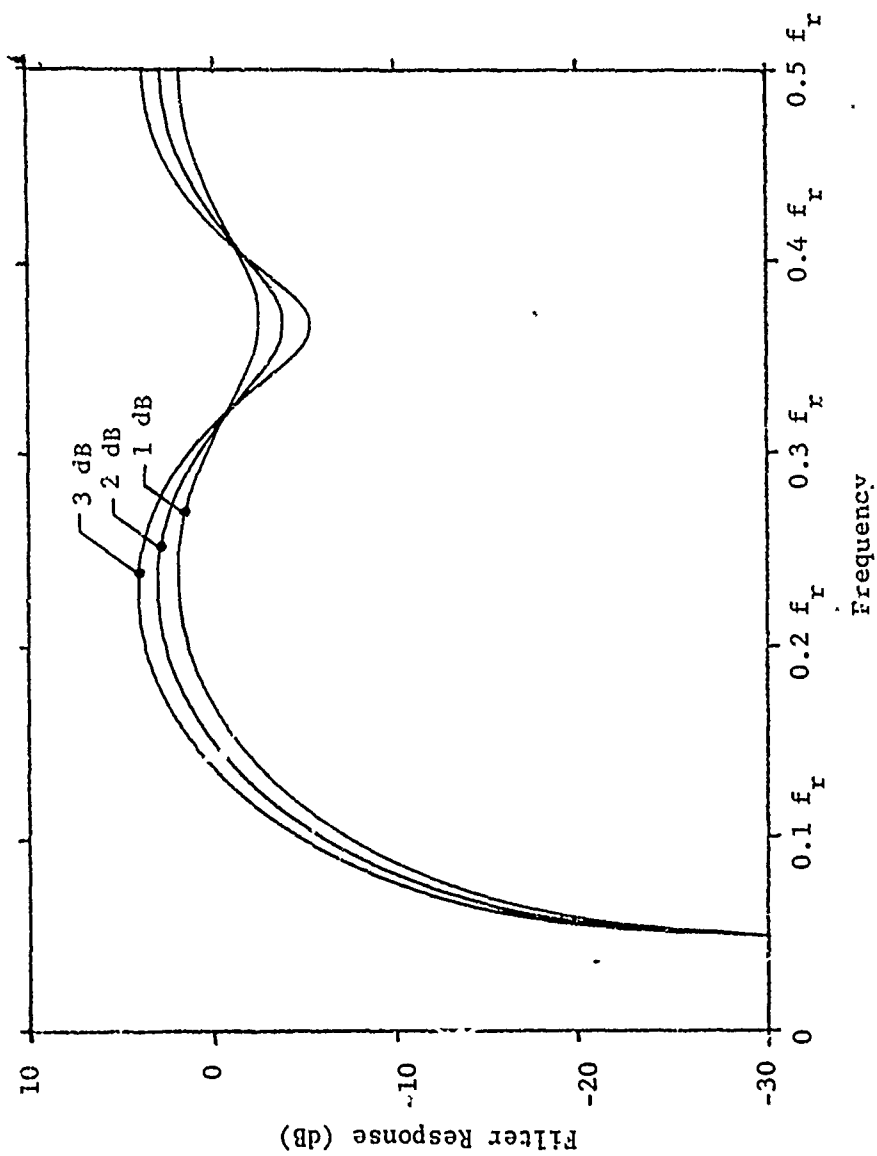


Figure 32. Bandstop filters showing effects of increasing allowable ripple on stop band characteristics. $F_c = 250$ Hz.

a. Improvement for an Arbitrary N-Pulse Canceller

As shown in Appendix F, the power response is

$$G(\omega) = C_0 + 2 \sum_{q=1}^N C_q \cos q\omega T$$

and a Gaussian clutter power spectral density input is assumed,

$$C_I = \frac{C}{\sigma_c \sqrt{2\pi}} e^{-f^2/2\sigma_c^2}$$

The clutter output is given by C_{out} , where

$$\begin{aligned} C_{out} &= \int_{-f_r/2}^{f_r/2} (C_0 + 2 \sum_{q=1}^N C_q \cos q\omega T) \left(\frac{C}{\sigma_c \sqrt{2\pi}} e^{-f^2/2\sigma_c^2} \right) df \\ &= 2 \int_0^{f_r/2} (C_0 + 2 \sum_{q=1}^N C_q \cos q\omega T) \left(\frac{C}{\sigma_c \sqrt{2\pi}} e^{-f^2/2\sigma_c^2} \right) df \end{aligned}$$

Since $\sigma_c \ll f_r$,

$$C_{out} \approx \int_0^{\infty} (C_0 + 2 \sum_{q=1}^N C_q \cos q\omega T) \left(\frac{C}{\sigma_c \sqrt{2\pi}} e^{-f^2/2\sigma_c^2} \right) df$$

or

$$C_{out} \approx \frac{2C}{\sigma_c \sqrt{2\pi}} \left[\int_0^{\infty} C_0 e^{-f^2/2\sigma_c^2} df + 2 \sum_{q=1}^N \int_0^{\infty} (C_q \cos q\omega T) (e^{-f^2/2\sigma_c^2}) df \right]$$

$$C_{out} = C \left[C_0 + 2 \sum_{q=1}^N C_q e^{-2q^2 \pi^2 T^2 \sigma_c^2} \right],$$

which is the desired result.

The average target output power, T_o , is

$$\begin{aligned} T_o &= \frac{T_i}{f_r} \int_0^{f_r} G(f) df \\ &= \frac{T_i}{f_r} \int_0^{f_r} \left[C_0 + 2 \sum_{q=1}^N C_q \cos 2\pi f q T \right] df \\ &= C_0 T_i \end{aligned}$$

Then

$$I = \frac{C_0}{C_0 + 2 \sum_{q=1}^N C_q e^{-2q^2 \pi^2 T^2 \sigma_c^2}} .$$

This expression checks with earlier results if the exponentials are expanded in a Taylor series and the first non-zero terms retained. Consider the three-pulse canceller where $C_0 = 6$, $C_1 = -4$, $C_2 = 1$. Then

$$\frac{1}{I} = \frac{1}{6} \left[6 - 8 e^{-2\pi^2 T^2 \sigma_c^2} + 2 e^{-8\pi^2 T^2 \sigma_c^2} \right]$$

substituting $e^x \approx 1 + x + \frac{x^2}{2}$,

$$I = \frac{f_r^4}{8\pi^4 \sigma_c^4} \quad \text{as before.}$$

If

$$f_r = 5 \times 10^3$$

$$\sigma_r = 0.22$$

$$\lambda = 5.5 \text{ cm}$$

are used to calculate I for the three-pulse canceller ($C_0 = 6$, $C_1 = -4$, and $C_2 = 1$), a value $I = 83.01$ dB is obtained, which agrees closely with earlier results.

b. Error Statement

The error we have chosen to minimize over the region πf_r to $f_r/2$ is the function

$$E = \int_{\pi f_r}^{f_r/2} (G(f) - 1)^2 df .$$

Now,

$$[G(\omega) - 1]^2 = [C_0 - 1 + 2 \sum_{q=1}^N C_q \cos q\omega T]^2$$

$$= (C_o - 1)^2 + 4C_o \sum_{q=1}^N C_q \cos q\omega T - 4 \sum_{q=1}^N \cos q\omega t +$$

$$4 \sum_{q=1}^N \sum_{k=1}^N C_q C_k \cos q\omega T \cos k\omega T .$$

Therefore,

$$E = \int_{\eta f_r}^{f_r} [G(f) - 1]^2 df$$

$$= (C_o - 1)^2 (f_r/2) (1 - 2\eta) - 2C_o \sum_{q=1}^N \sum_{k=1}^N C_q C_k f_r \sigma_{qk} +$$

$$2 \sum_{q=1}^N \frac{C_q f_r}{\pi q} \sin 2\pi \eta q + 4 \sum_{q=1}^N \sum_{k=1}^N C_q C_k f_r \sigma_{qk} ,$$

where

$$\alpha_{qk} = \begin{cases} -\frac{\sin 2\pi \eta (q - k)}{4\pi (q - k)} - \frac{\sin 2\pi \eta (q + k)}{4\pi (q + k)} & q \neq k \\ \frac{1}{4} [1 - 2\eta] - \frac{\sin 4\pi \eta}{2} & q = k \end{cases}$$

c. Optimization

Using standard Lagrange multiplier techniques, we wish to minimize

$$F = E - \left(\frac{1}{I} - \gamma \right) f_r C_o$$

subject to the constraint that

$$\frac{1}{I} = \text{constant} = \gamma$$

This is done by solving the system of equations

$$\frac{\partial F}{\partial C_o} = 0$$

$$\vdots$$

$$\frac{\partial F}{\partial C_N} = 0$$

$$\left(\frac{1}{I} - \gamma \right) = 0$$

Noting that $\alpha_{qk} = \alpha_{kq}$, these expressions are somewhat simplified; for a three-pulse filter, this becomes

$$\begin{aligned}
 C_0(1 - 2\eta) - 2C_1 \frac{\sin 2\pi\eta}{\pi} - 2C_2 \frac{\sin 4\pi\eta}{2\pi} + \lambda(1 - \gamma) &= 1 - 2\eta \\
 -2C_0 \frac{\sin 2\pi\eta}{\pi} + C_1 8\alpha_{11} + C_2 8\alpha_{12} + \lambda(2e^{-2\pi^2 T^2 \sigma_c^2}) &= -2 \frac{\sin 2\pi\eta}{\pi} \\
 -2C_0 \frac{\sin 4\pi\eta}{2\pi} + C_1 8\alpha_{21} + C_2 8\alpha_{22} + \lambda(2e^{-8\pi^2 T^2 \sigma_c^2}) &= -2 \frac{\sin 4\pi\eta}{2\pi} \\
 (1 - \gamma) C_0 + C_1 2e^{-2\pi^2 T^2 \sigma_c^2} + C_2 2e^{-8\pi^2 T^2 \sigma_c^2} &= 0
 \end{aligned}$$

The system of equations readily expands for larger numbers of received pulses. A computer program was written to solve for the C's for up to 100 pulses. Results obtained using this program are discussed in the next section.

d. Results

The filter responses for the conventional three-pulse MTI filter and one of the minimum-error filters designed for $I = 60$ dB is shown in Figure 33. The improvement in detectability for targets having low-frequency Doppler returns is evident.

The shape of the filter response is a function of the exact value of I specified; Figure 34 shows results for optimum responses for $I = 10$ dB, 30 dB, and 60 dB, indicating the increased ripple associated with larger values of I . This illustrates the desirability of choosing I no greater than necessary because of the consequent compromises in filter responses.

The flatness of the filter increases as the number of pulses processed increases, but the number of ripples also increases. This is illustrated in Figure 35 which shows responses for $I = 60$ dB for 3, 5, and 7 pulses processed.

Differences in responses for $\eta = 0$ and $\eta = 0.1$ are not particularly great, but the case $\eta = 0.1$ does show a slight improvement in flatness of response. Figure 36 compares results for 5-pulse response with $I = 60$ dB for $\eta = 0$ and $\eta = 0.1$.

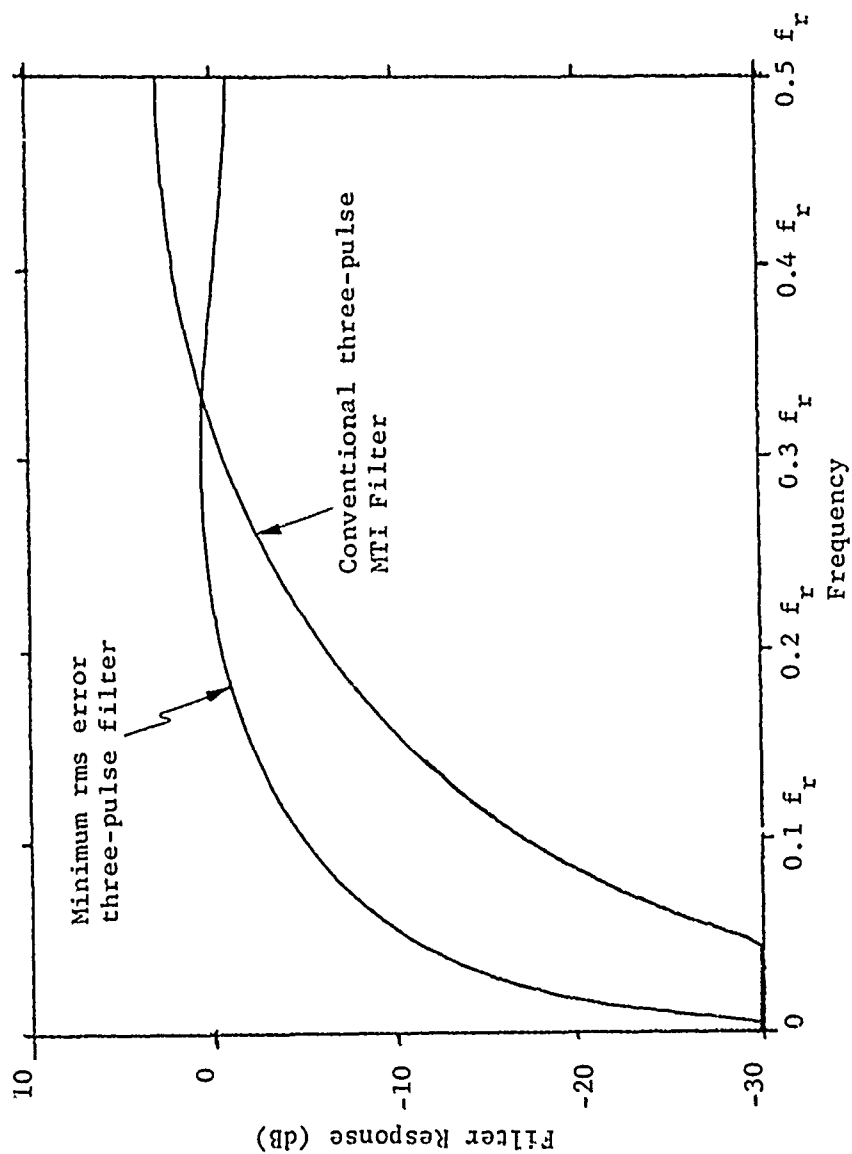


Figure 33. Comparison of the response of a conventional three-pulse MTI filter and a minimum rms error filter designed for $I = 60$ dB, $\text{prf} = 5000$ pps, $\sigma_c = 8.0$, and $\eta = 0.1$.

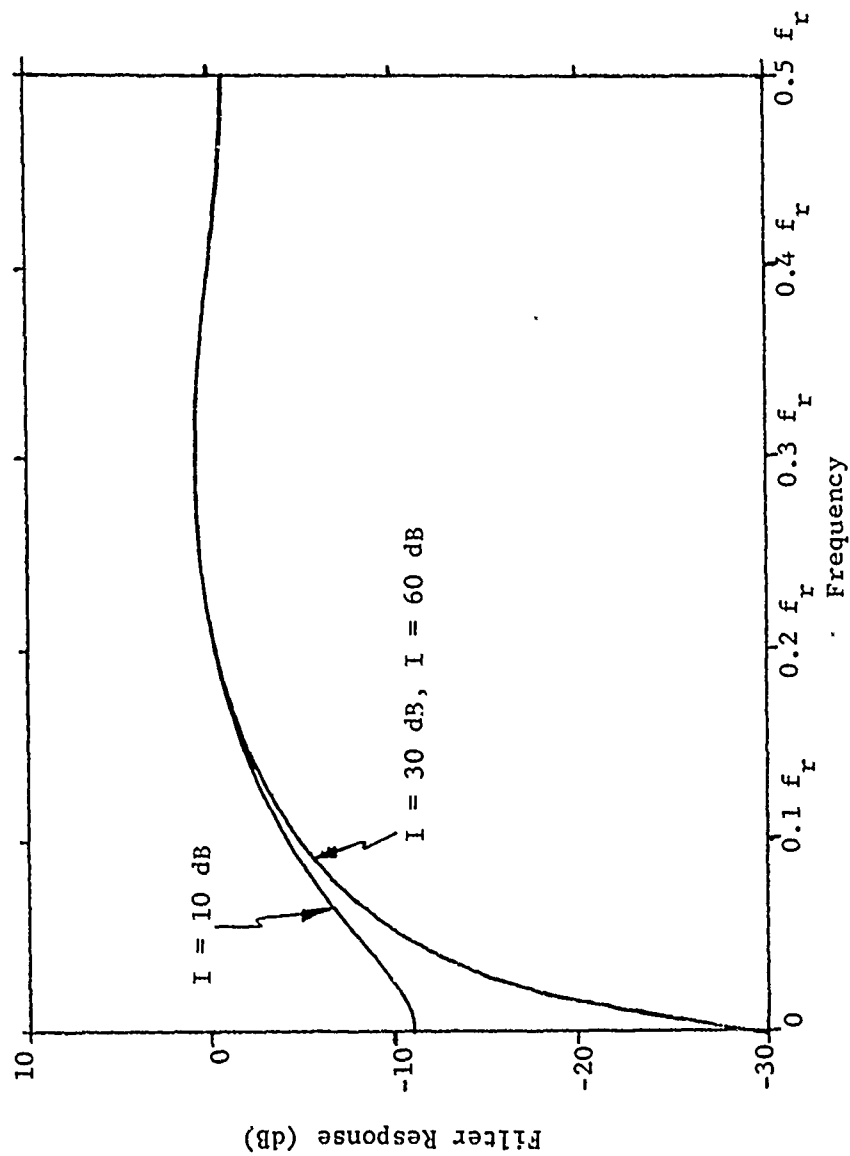


Figure 34. Comparison of responses of minimum rms filters designed for $I = 10, 30$, and 60 dB. $\eta = 0.1$, $\text{prf} = 5000$ pps, and $\sigma_c = 8.0$.

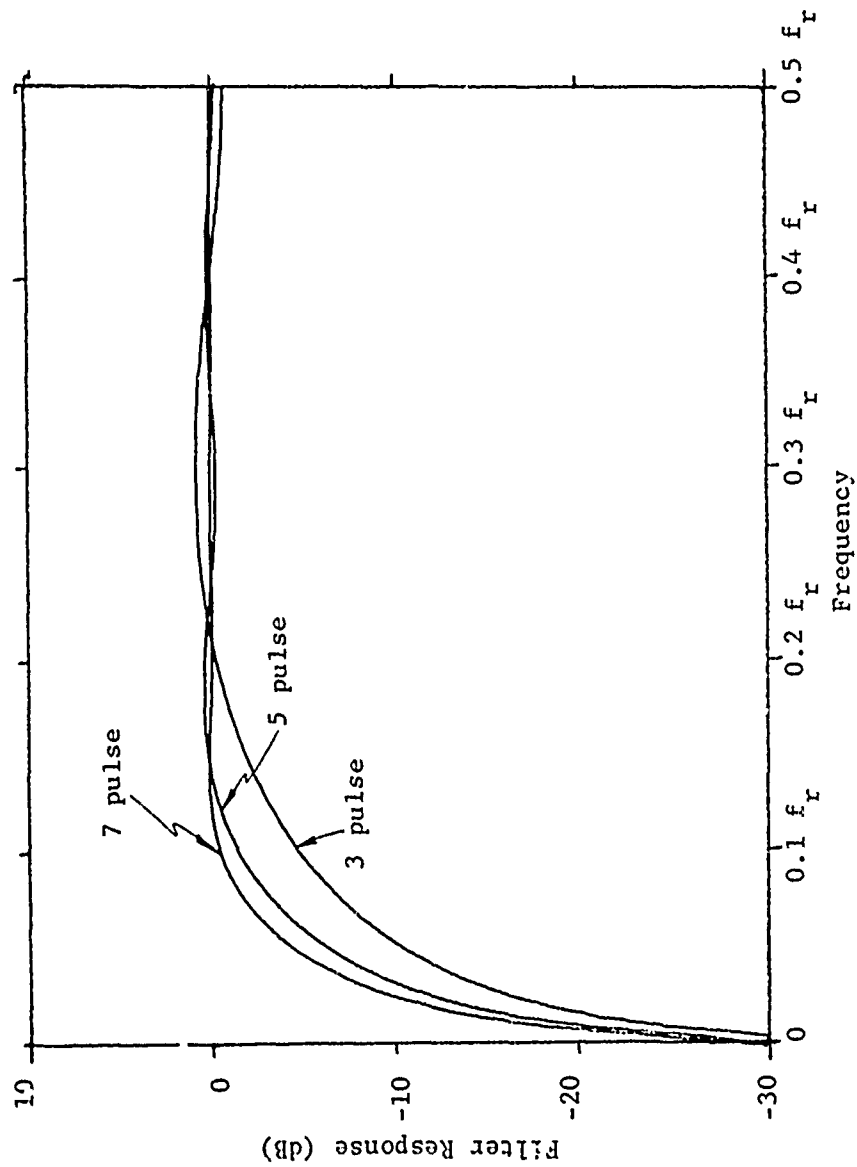


Figure 35. Comparison of minimum rms error filter responses for 3, 5, and 7 pulses processed. $I = 60$ dB, $\text{prf} = 5000$ pps, $\sigma_c = 8.0$, $\eta = 0.1$.

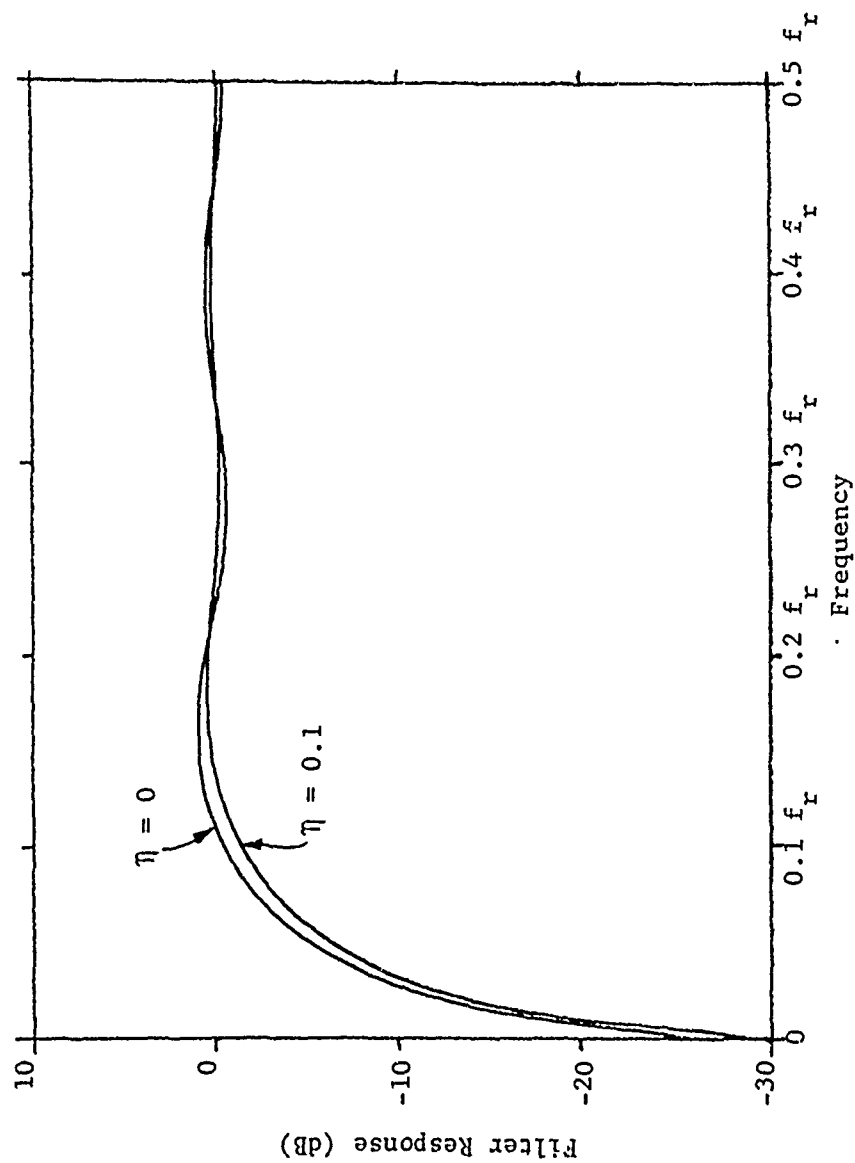


Figure 36. Comparison of responses of five-pulse minimum-rms-error filters for $\eta = 0$ and $\eta = 0.1$. $I = 60$ dB, $\sigma_c = 8.0$, $\text{prf} = 5000$ pps.

4. Maximally Flat Non-Recursive Digital MTI Filters

The digital MTI filters designed up to this point have had ripples in the pass band, with consequent variation in target detectability. This variation is objectionable in some cases; therefore, maximally flat non-recursive digital filter responses having a specified improvement factor have been developed for consideration for implementation in the EAR radar system.

By a "maximally flat" filter is meant one having a number of its derivatives with respect to frequency set equal to zero at some specified frequency or frequencies [41]. For the MTI case, it is also required that these filters have a certain specified amount of improvement in target-to-clutter ratio. In addition, the filter must have a non-zero amplitude specified at a given frequency, in order to prevent a solution which is identically equal to zero.

The procedure which was used to derive the maximally flat nonrecursive digital MTI filters is described below. As before, the power response of the filter is given by

$$G(\omega) = C_0 + 2 \sum_{q=1}^N C_q \cos q\omega T,$$

and the target-to-clutter improvement, I , is given by

$$= I \frac{C_0}{C_0 + 2 \sum_{q=1}^N C_q \exp(-2q^2 \pi^2 T^2 \sigma_c^2)}$$

Following the above discussion, choose a value for $I = \frac{1}{Y}$, and choose $G(\pi f_r) = 1$. Then there are $N-2$ derivatives which may be set equal to zero. The points at which to set these derivatives equal to zero were chosen to be $\omega = 0$ and $\omega = \pi f_r$. The way that these derivatives are apportioned between these two frequencies determines the shape of the filter characteristic.

A three-pulse canceller has only one derivative to set equal to zero; in order to obtain a high-pass filter characteristic this derivative must be zero for $\omega = \pi f_r$. For the three-pulse canceller, the equations for the C 's become

$$G(\pi f_r) = 1$$

$$\left. \frac{\partial^2 G(\omega)}{\partial \omega^2} \right|_{\omega = \pi f_r} = 0$$

$$I = \frac{1}{Y}$$

The filter response for $I = 60$ dB, $\sigma_c = 8$, and $T = 1/f_r = 1/5000$ is shown in Figure 37. Figure 38 compares this maximally flat three-pulse filter response with that of a minimum-rms-error three-pulse canceller, indicating the improved flatness of response obtained using a maximally flat filter response.

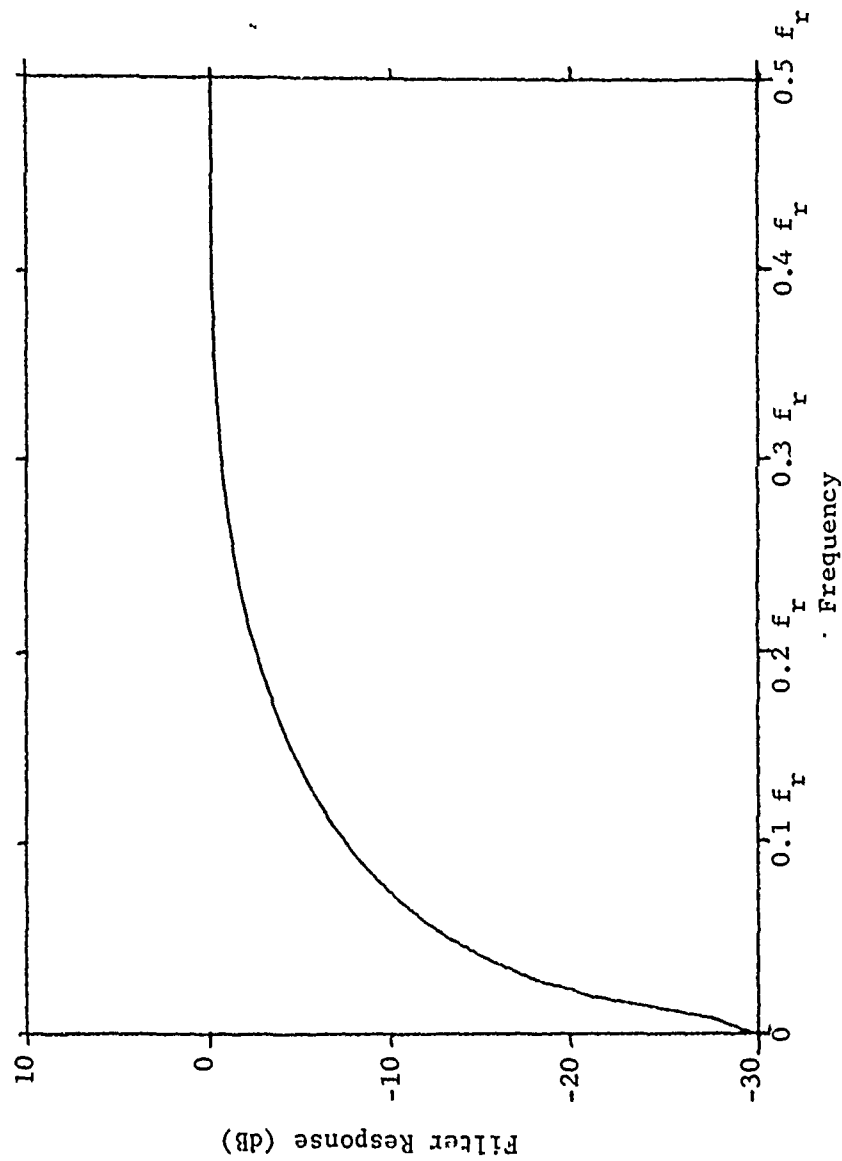


Figure 37. Maximally flat three-pulse MTI filter response. $I = 60$ dB.

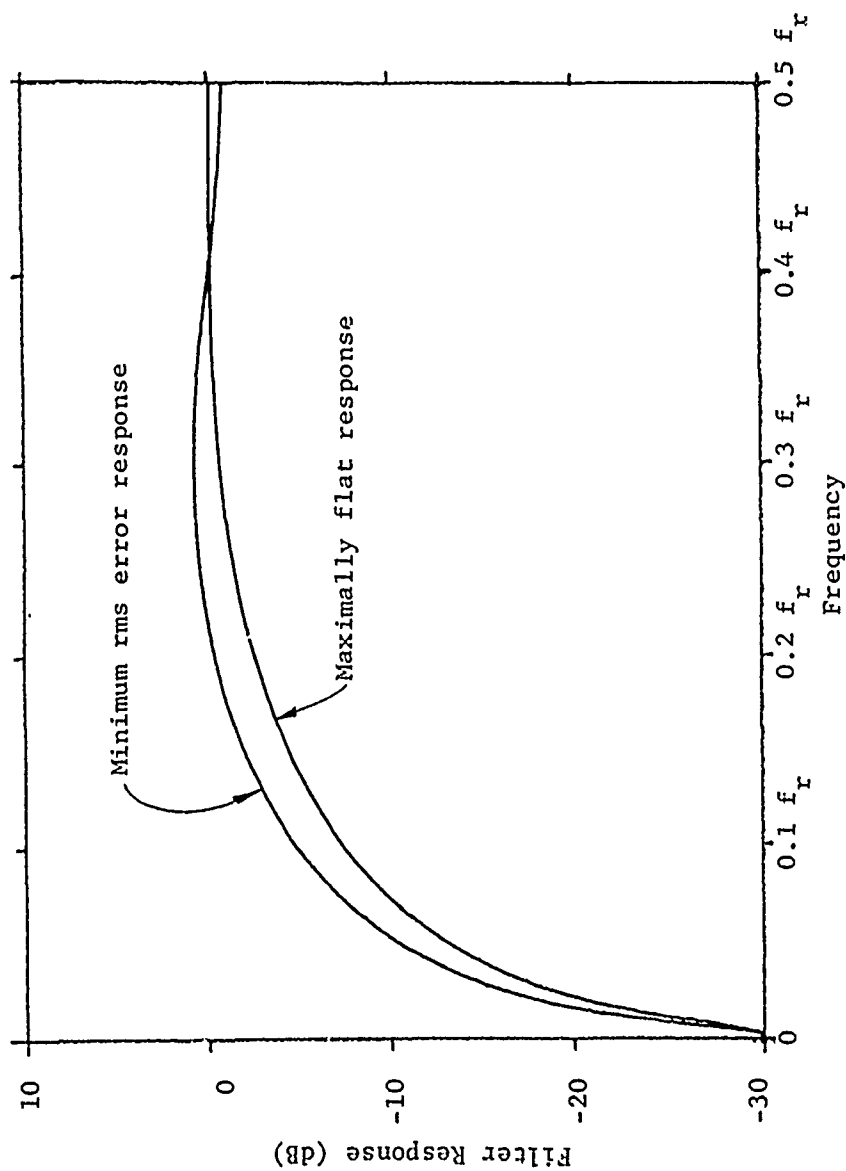


Figure 38. Comparison of responses for three-pulse maximally flat three pulse MTI filter ($I = 60$ dB) and minimum rms error MTI filter ($I = 60$ dB, $\eta = 0.1$, $\sigma_c = 8.0$, PRF = 5000).

If N pulses are processed, there are $N-2$ derivatives which may be set equal to zero, and these derivatives are specified at $\omega = 0$ and $\omega = \pi f_r$. Define the order, i , of the filter as being the number of derivatives set equal to zero at $\omega = 0$. Responses for filters with $i = 0$, and $N = 3$ and $N = 4$ are compared in Figure 39, where it may be seen that increasing N has little effect on the filter response. However, higher-order filters for $N > 3$, permit establishment of a stop band to reject slowly moving targets. Responses for $N = 4$ and $N = 5$ for various values of i are shown in Figures 40 and 41 to illustrate the shape of the pass and stop bands produced by various choices of N and i .

F. MTI Processors Using Staggered prf

One of the serious limitations of the systems discussed up to this point is that the filter responses exhibit so-called "blind speeds" -- target radial velocities for which the filter output is zero. These speeds are those for which the Doppler frequency is an integral multiple of the system prf.

If it is appropriately implemented, frequency agility may be used to reduce effects of blind speeds on system performance. An analysis of the effects of frequency agility on blind speeds is presented as Appendix D, where it is shown that this technique is effective only against targets having large radial velocities.

The other method for reducing the effects of blind speeds is the use of prf stagger, that is, varying the interpulse spacing from interval to interval. Use of stagger effects both the shape of the frequency response and the MTI improvement, I , of the system. An analysis of effects of prf stagger on conventional MTI processors will now be briefly discussed.

Changing the interpulse period by a fraction, ϵ , will greatly reduce the depth of the nulls of the filter response and provide, in some cases, a desirable response without blind speeds.

For a three-pulse filter having a stagger, ϵ , about the center pulse the impulse response, $h(t)$, is given by

$$h(t) = \delta(t + T(1-\epsilon)) - 2\delta(t) + \delta(t - T(1+\epsilon)) \quad ,$$

and the frequency response, $G(\omega)$, of this filter is given by the Fourier Transform of $h(t)$,

$$G(\omega) = 6 - 8 \cos \omega T \cos \omega T \epsilon + 2 \cos 2\omega T \quad .$$

Figure 42 shows the response of such a filter with values of ϵ ranging from 0 to 0.1, showing how the lower blind speeds are eliminated.

The reduction in I due to staggered prf may be determined as shown by Nathanson [48].

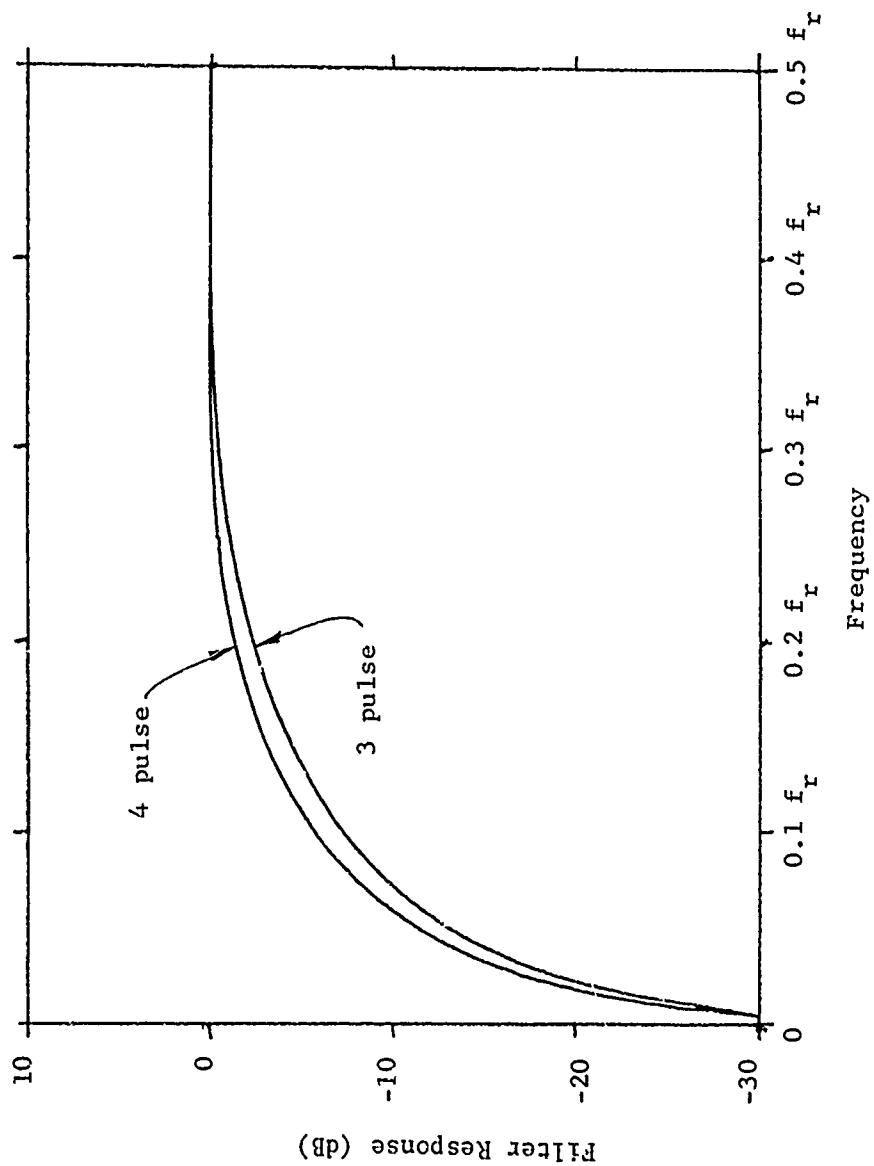


Figure 39. Maximally flat MTI filter responses for three and four pulses processed.

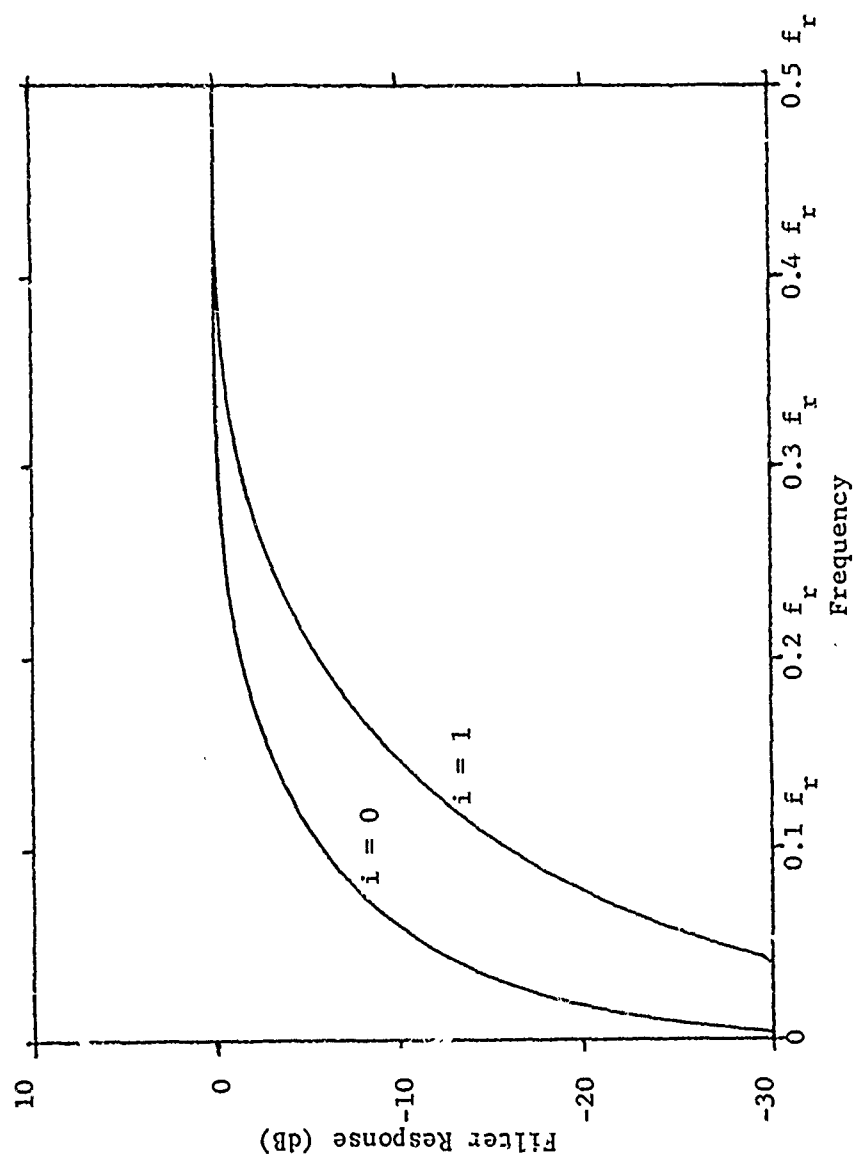


Figure 40. Maximally flat filter responses for a four-pulse MTI filter for $i = 0$ and $i = 1$.

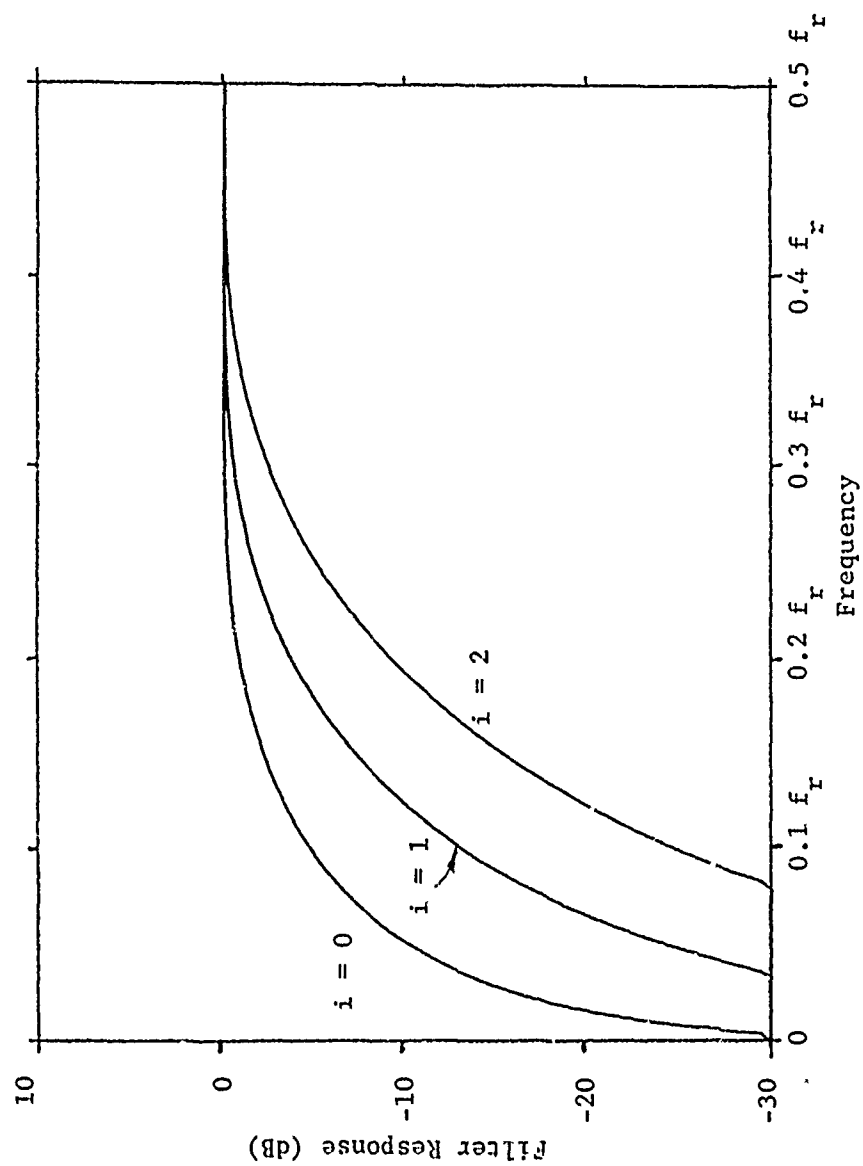


Figure 41. Maximally flat filter responses for a five-pulse NTI filter for $i = 0, 1$, and 2 .

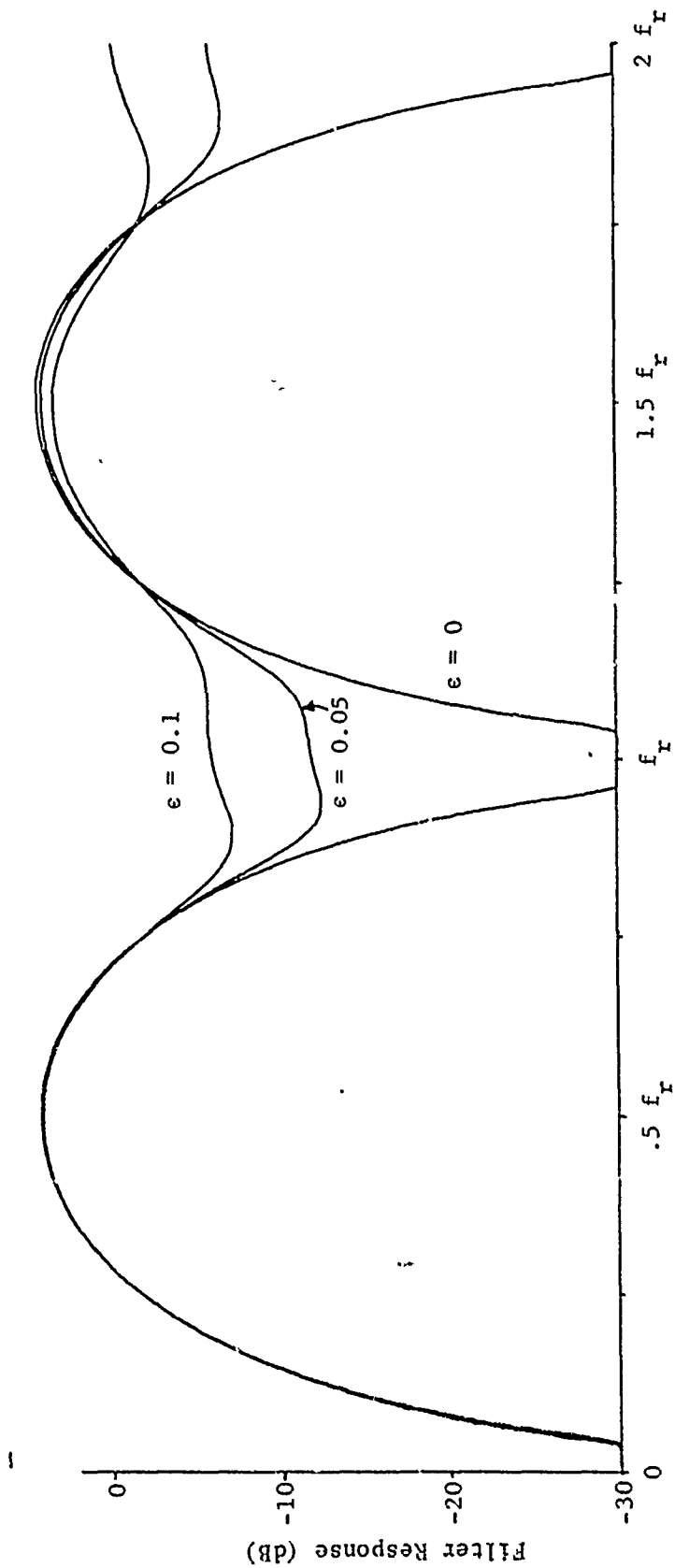


Figure 42. Filter response for a conventional three-pulse MTI filter when various values of stagger, ϵ , are used.

The residue, $E_r(t)$, from a conventional three-pulse canceller is

$$E_r(t) = E(t) - 2E(t-T) + E(t-T_1-T_2) \quad ,$$

where

$$E(t) = \text{sample at time, } t$$

$$T_1 = T(1 + \epsilon)$$

$$T_2 = T(1 - \epsilon)$$

Then the mean square value is given by

$$\overline{E_r^2(t)} = \overline{[E(t) - 2E(t-T_1) + E(t-T_1-T_2)]^2} \quad ,$$

which reduces to

$$= 6\overline{E^2(t)} - \frac{2}{3}[R(T_1) + R(T_2)] + \frac{1}{3}R(T_1 + T_2) \quad .$$

Let the normalized autocorrelation be defined as

$$\rho(\tau) = \frac{R(\tau)}{\overline{E^2(t)}}$$

where $R(\tau)$ is the autocorrelation function. Then,

$$\overline{E_r^2(t)} = 6\overline{E^2(t)} - \frac{2}{3}\overline{E^2(t)}(\rho(T_1) + \rho(T_2)) + \frac{1}{3}\overline{E^2(t)}\rho(T_1 + T_2) \quad ,$$

and

$$\frac{\overline{E_r^2(t)}}{\overline{E_r^2(t)}} = \text{Clutter Attenuation (I)} = \frac{1}{6 - 8(\rho(T_1) + \rho(T_2)) + 2\rho(T_1 + T_2)} \quad .$$

The stagger ratio, K , is defined as

$$K = T_2/T_1 \quad .$$

Therefore,

$$I = \frac{1}{6 - 8(\rho(T_1) + \rho(KT_1)) + 2\rho[T_1(1 + K)]} \quad .$$

The improvement, I_s , with staggered prf is I multiplied by the average gain (six)

$$I_s = \frac{1}{1 - \frac{4}{3}(\rho(T_1) + \rho(KT_1)) + \frac{1}{3}\rho[T_1(1 + K)]}$$

The loss due to staggering is [40]

$$\frac{I}{I_s} \approx \frac{4\sigma_T^2 (1 - K)^2}{3T^2 (1 + K)^2} + \frac{16}{(1 + K)^4} \left[K^2 - \frac{(1 - K)^4}{12} \right]$$

$$\sigma_T = \frac{\lambda}{4\pi\sigma_v},$$

where

λ = wavelength (meters)

σ_v = rms clutter velocity (m/sec)

So, L_s , the loss due to staggering is given by

$$L_s = \frac{\lambda^2 (1 - K)^2}{12T^2 \pi^2 \sigma_v^2 (1 + K)^2} + \frac{16}{(1 + K)^4} \left[K^2 - \frac{(1 - K)^4}{12} \right]$$

In Figure 43 I_s for a three-pulse canceller has been plotted for various stagger ratios.

Since both the frequency response curve and the MTI improvement, I , are affected by varying the interpulse period, the designs developed for the unstaggered case are not necessarily optimum for the staggered case as is illustrated in Figure 44. The results shown in Figure 44 illustrate the effects of prf stagger on the response of one of the minimum-rms error filters developed earlier; in fact its response might be considered less desirable than the conventional response shown in Figure 42.

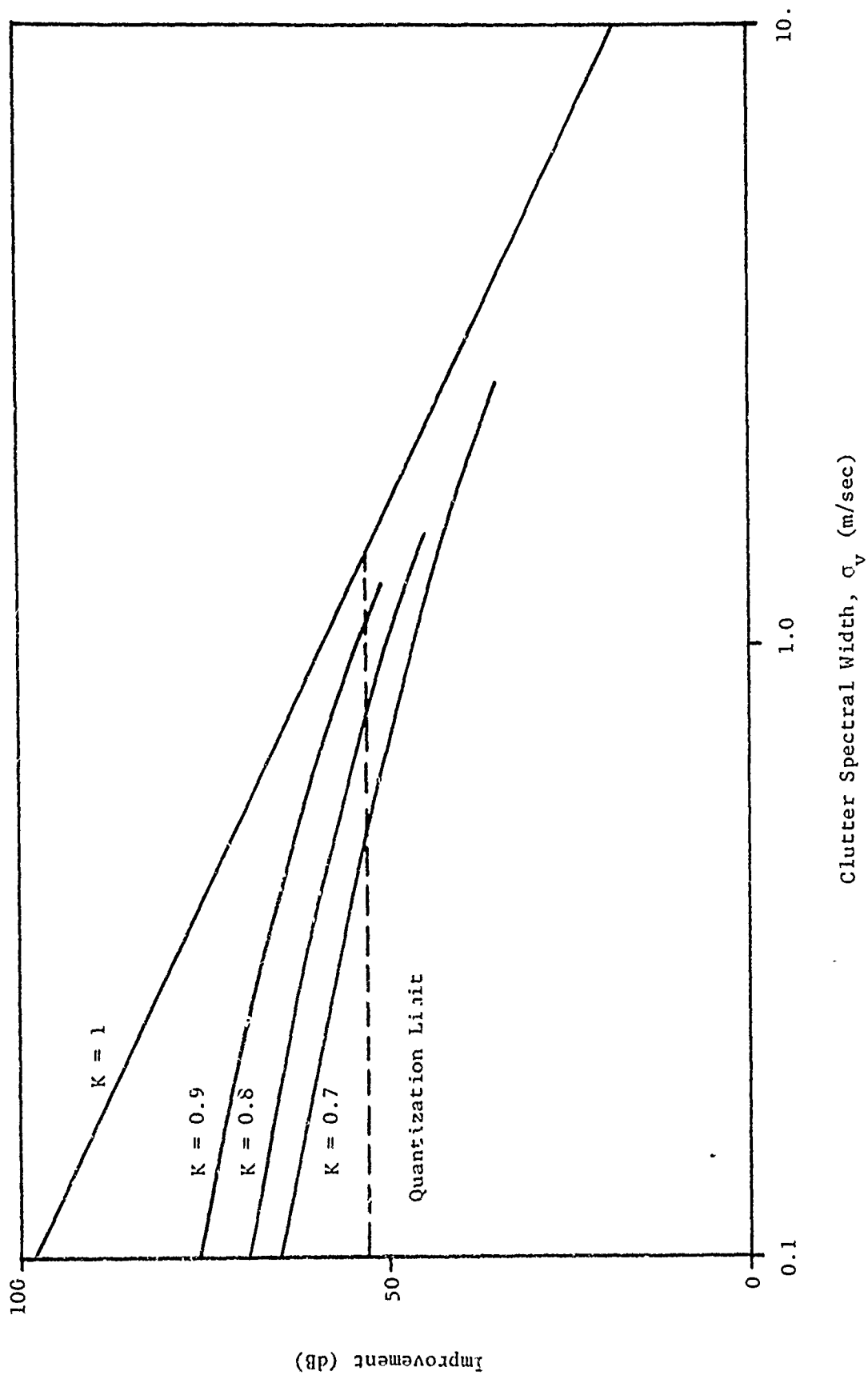


Figure 43. System improvement versus clutter spectral width for radar system with $f_r = 5$ kHz and $\lambda = 5.5$ cm, K = stagger ratio for staggered prf.

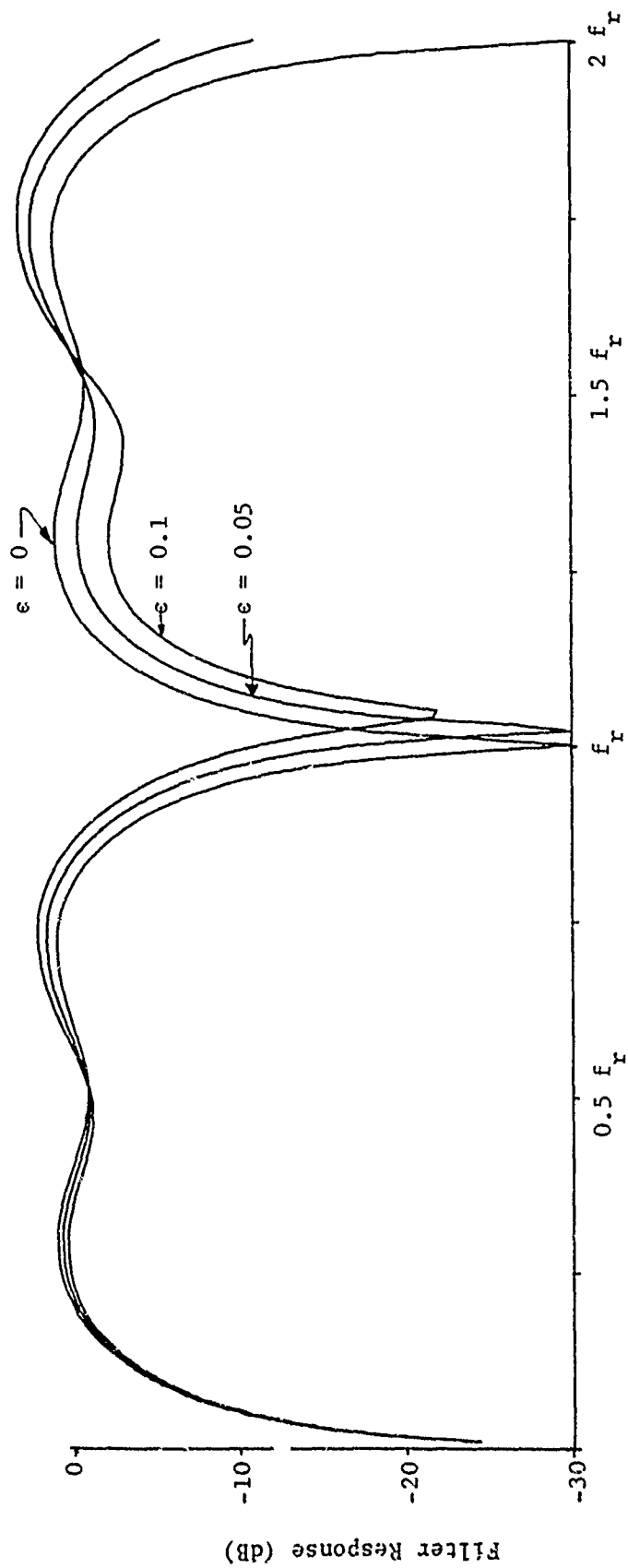


Figure 44. Response of an optimum unstaggered MTI filter when used with various amounts of prf stagger, ϵ .

VI. CONCLUSIONS AND RECOMMENDATIONS

A. Primary Conclusions

The free-space performance of the EAR system may be seriously affected by changes in Doppler frequency of the target. The region of optimum angle-tracking accuracy of the EAR system is approximately four to seven kilometers, depending upon the cross-section and physical size of the target. Clutter cancellation of the EAR system will primarily be limited by analog-to-digital conversion quantization noise.

The effect on system performance of changes in Doppler frequency of the target may be minimized by using samples with non-integral sample weights. The design procedures set forth in Section V produced significantly improved MTI processors for the unstaggered prf case, but very little has been done in the case of staggered prf.

System performance may be seriously limited by multipath returns when tracking low-flying targets. These tracking errors are significant for targets flying at altitudes less than approximately 1500 feet.

Frequency agility may be of appreciable help in reducing the effect of multipath returns on system performance. The effectiveness of frequency agility in reducing multipath-induced errors is a strong function of the frequency-agility bandwidth used, the target heights, and the antenna height. The 400-MHz bandwidth which may be possible with a modified EAR would significantly reduce these low-angle tracking errors, particularly for higher antenna heights.

B. Principal Recommendations

Based on the information studied during this program, the following recommendations are presented for the EAR development program.

(1) A flexible digital MTI filter or processor should be incorporated into the system. The performance obtainable by the selection of sample weights appears necessary if acceptable system operation over a wide range of target Doppler frequencies is to be achieved.

(2) Stagger of the prf should be incorporated into the EAR system concept in order to eliminate "blind speeds" of the system, and investigation of improved MTI filters for staggered systems should be initiated.

(3) Frequency agility should be incorporated into the EAR system, both to reduce free-space tracking errors due to target glint, and to reduce low-angle tracking errors due to multipath signals. Weighing of the received signals on the basis of the sum signal amplitude appears desirable.

Experimental evaluation of the EAR should be paralleled by careful theoretical studies as an aid in planning significant experiments and to assist in interpreting results of these experiments.

VII. REFERENCES

1. G. W. Ewell, N. T. Alexander, and E. L. Tomberlin, "Investigation of the Effects of Polarization Agility on Monopulse Radar Angle Tracking," Final Technical Report on Contract DAAH01-70-C-0535, Georgia Institute of Technology, June 1971.
2. J. L. Hatcher, H. G. Woods, and H. B. Buie, "Preliminary Action II Radar Hardware System Requirements," Report No. RE-TR-69-23, U.S. Army Missile Command, Redstone Arsenal, Alabama, November 1969.
3. D. K. Barton and H. R. Ward, Handbook of Radar Measurement, p. 24, Prentice-Hall, Inc., Englewood Cliffs, N.J., 1969.
4. Reference 1, Chapter IV.
5. Reference 1, Chapter V.
6. Reference 2, p. 10.
7. M. I. Skolnik, Introduction to Radar Systems, p. 502, McGraw-Hill, Inc., New York, New York, 1962.
8. S. M. Sherman, "Complex Indicated Angles Applied to Unresolved Radar Targets and Multipath," IEEE Transactions on Aerospace and Electronic Systems, Vol. AES-7, No. 1, pp. 160-170, January 1971.
9. Reference 1, p. 79.
10. D. O. North, An Analysis of the Factors Which Determine the Signal/Noise Discrimination in Radar, Technical Report PtR-6C, RCA Laboratories, Princeton, N. J., June 25, 1943.
11. J. Van Vleck and D. Middleton, "A Theoretical Comparison of the Visual, Aural, and Meter Reception of Pulsed Signals in the Presence of Noise," Journal of Applied Physics, Vol. 17, pp. 940-971, November 1946.
12. H. L. Van Trees, Detection, Estimation and Modulation Theory, Part I, p. 249, John Wiley and Sons, Inc., New York, New York, 1968.
13. T. S. George, Report No. 159, Philco Corp. Research Division.
14. B. M. Dwork, "Detection of a Pulse Superimposed on Fluctuation Noise," Proceedings of the IRE, Vol. 38, pp. 771-774, July 1950.

Preceding page blank

15. H. Urkowitz, "Filters for Detection of Small Radar Signals in Clutter," Journal of Applied Physics, Vol. 24, No. 8, pp. 1024-1031, August 1953.
16. A. W. Rihaczek, "Optimum Filters for Signal Detection in Clutter," IEEE Transactions on Aerospace and Electronics Systems, Vol. AES-1, No. 3, pp. 297-299, December 1965.
17. D. F. DeLong, Jr., and E. M. Hofstetter, "The Design of Clutter-Resistant Radar Waveforms with Limited Dynamic Range," IEEE Transactions on Information Theory, Vol. IT-15, No. 3, pp. 376-385, May 1969.
18. D. F. DeLong, Jr., and E. M. Hofstetter, "On the Design of Optimum Radar Waveforms for Clutter Rejection," IEEE Transactions on Information Theory, Vol. IT-13, No. 3, July 1967.
19. E. C. Westerfield, R. H. Prager, and J. L. Stewart, "Processing Gains Against Reverberation (Clutter) Using Matched Filters," IEEE Transactions on Information Theory, Vol. IT-6, pp. 342-348, June 1960.
20. H. L. Van Trees, "Optimum Signal Design and Processing for Reverberation Limited Environments," IEEE Transactions on Military Electronics, Vol. MIL-9, pp. 212-229, July 1965.
21. L. J. Spafford, "Optimum Radar Signal Processing in Clutter," IEEE Transactions on Information Theory, Vol. IT-14, No. 5, pp. 734-743, September 1968.
22. L. J. Spafford, Optimum Radar Signal Processing in Clutter, Ph.D. dissertation, Polytechnic Institute of Brooklyn, Brooklyn, N.Y., June 1967.
23. C. A. Stutt and L. J. Spafford, "A 'Best' Mismatched Filter Response for Radar Clutter Discrimination," IEEE Transactions on Information Theory, Vol. IT-14, No. 2, pp. 280-287, March 1968.
24. W. D. Rummier, "Clutter Suppression by Complex Weighing of Coherent Pulse Trains," IEEE Transactions on Aerospace and Electronic Systems, Vol. AES-2, No. 6, pp. 689-699, November 1966.
25. H. L. Van Trees, Detection, Estimation and Modulation Theory, Vol. 3, p. 278, John Wiley and Sons, Inc., New York, New York, 1971.
26. L. A. Wainstein and V. D. Zubakov, Extraction of Signals from Noise, Chapter 6, Prentice-Hall International, London, 1962.

27. Reference 12, Section 2.6.
28. I. Selin, "Detection of Coherent Radar Returns of Unknown Doppler Shift," IEEE Transactions on Information Theory, Vol. IT-11, pp. 396-400, July 1965.
29. L. E. Brennan, I. S. Reed, and W. Sollfrey, "A Comparison of Average Likelihood and Maximum Likelihood Ratio Tests for Detecting Radar Targets of Unknown Doppler Frequency," IEEE Transactions on Information Theory, Vol. IT-14, No. 1, pp. 104-110, January 1968.
30. J. Capon, "Optimum Weighing Functions for the Detection of Sampled Signals in Noise," IEEE Transactions on Information Theory, Vol. IT-10, pp. 152-159, April 1964.
31. H. R. Ward, "A Model Environment for Search Radar Evaluation," EASCON '71 Record, Electronics and Aerospace Systems Convention, pp. 164-171, October 1971.
32. W. W. Shrader, "An MTI Surveillance Radar Philosophy," EASCON '71 Record, Electronics and Aerospace Systems Convention, pp. 171-174, October 1971.
33. H. E. Kallman, "Transversal Filters," Proceedings of the IRE, pp. 302-310, July 1940.
34. L. R. Rabiner and R. W. Schafer, "Recursive and Nonrecursive Realizations of Digital Filters Designed by Frequency Sampling Techniques," IEEE Transactions on Audio and Electroacoustics, Vol. AU-19, No. 3, September 1971.
35. B. Gold and C. M. Rader, Digital Processing of Signals, Chapter 3, McGraw Hill Book Company, New York, New York, 1969.
36. R. M. Golden, Parametric Design of Digital Filters, Course Notes, Technology Service Corp., January 1970.
37. L. R. Rabiner, B. Gold, and C. A. McGonegal, "An Approach to the Approximation Problem for Nonrecursive Digital Filters," IEEE Transactions on Audio and Electroacoustics, Vol. AU-18, No. 2, pp. 83-106, June 1970.
38. D. W. Tufts, D. W. Rorabacher, and W. E. Moser, "Designing Simple, Effective Digital Filters," IEEE Transactions on Audio and Electroacoustics, Vol. AU-18, No. 2, pp. 142-158, June 1970.

39. H. D. Helms, "Digital Filters with Equiripple or Minimax Responses," IEEE Transactions on Audio and Electroacoustics, Vol. AU-19, No. 1, pp. 87-93, March 1971.
40. A. A. G. Requicha and H. B. Voelcker, "Design of Nonrecursive Filters by Specification of Frequency Domain Zeros," IEEE Transactions on Audio and Electroacoustics, Vol. AU-18, No. 4, pp. 464-470, December 1970.
41. B. Gold and K. L. Jordan, Jr., "A Direct Search Procedure for Designing Finite Duration Impulse Response Filters," IEEE Transactions on Audio and Electroacoustics, Vol. AU-17, No. 1, pp. 33-36, March 1969.
42. G. C. O'Leary, "Nonrecursive Digital Filtering Using Cascade Fast Fourier Transformers," IEEE Transactions on Audio and Electroacoustics, Vol. AU-18, No. 2, pp. 177-183, June 1970.
43. L. R. Rabiner, "Linear Program Design of Digital Filters," 1972 IEEE Convention Record, paper 6H.2, pp. 336-337, March 1972.
44. O. J. Jacomini, "Optimum Symmetrical Weighing Factors for a Video MTI Radar," IEEE Transactions on Aerospace and Electronic Systems, Vol. AES-7, No. 1, pp. 244-209, January 1971.
45. R. G. Martin, Optimum Synthesis of Transversal Filter Radar Moving-Target Indicator, Ph.D. Dissertation, The Johns Hopkins University, Baltimore, Maryland, 1970.
46. H. G. Daellenbach, and E. J. Bell, User's Guide to Linear Programming, Prentice Hall, Inc., Englewood Cliffs, N. J., 1970.
47. L. Weinberg, Network Analysis and Synthesis, p. 491, McGraw Hill Book Co., New York, New York, 1962.
48. F. E. Nathanson, Radar Design Principles, Chapter 9, McGraw Hill Book Company, New York, New York, 1969.
49. L. E. Brennan and I. S. Reed, "Optimum Processing of Unequally Spaced Radar Pulse Trains for Clutter Rejection," IEEE Transactions on Aerospace and Electronic Systems, Vol. AES-4, No. 3, pp. 474-477.
50. R. Roy and O. Lowenschuss, "Design of MTI Detection Filters with Nonuniform Interpulse Periods," IEEE Transactions on Circuit Theory, Vol. CT-17, No. 4, pp. 604-612, November 1970.

51. M. I. Skolnik (editor), Radar Handbook, Chapter 17 by N. W. Shrader, pp. 38-45, McGraw-Hill Book Co., New York, New York, 1970.
52. Reference 51, pp. 9-17.
53. Reference 51, pp. 12-35.
54. Mischa Schwartz, Information Transmission Modulation and Noise, p. 240, McGraw-Hill Book Co., New York, New York, 1959.
55. Athanasios Papoulis, The Fourier Integral and Its Applications, p. 104, McGraw-Hill Book Co., New York, New York, 1962.

APPENDICES

Preceding page blank

Appendix A

CONVENTIONAL THREE-PULSE MTI FILTERS

Consider the two-delay filter shown in Figure A-1. The impulse response of this configuration is

$$h(t) = \delta(t) - 2\delta(t - T) + \delta(t - 2T)$$

In the frequency domain

$$H(\omega) = 1 - 2e^{j\omega T} + e^{2j\omega T}$$

and

$$G(\omega) = H(\omega) \cdot H^*(\omega) = 16 \sin^4\left(\frac{\omega T}{2}\right)$$

It is interesting to examine the improvement in target-to-clutter ratio when this canceller is used as an MTI radar processor. This calculation will be made assuming a Gaussian frequency distribution of clutter power. The total received clutter power will be denoted by C .

Let target power be distributed uniformly in frequency, with a power of T_i . The input target-to-clutter ratio, r_i , is then

$$r_i = \frac{T_i}{C}$$

The output signal and clutter powers, T_o and C_o , must be computed, and the output target-to-clutter ratio, r_o , will then be

$$r_o = \frac{T_o}{C_o}$$

The improvement, I , if any, is then

$$I = \frac{r_o}{r_i} = \frac{T_o/C_o}{T_i/C}$$

Now,

$$C_o = \int_{-f_r/2}^{f_r/2} (\text{Clutter power spectral density}) \cdot G(\omega) d\omega$$

Preceding page blank

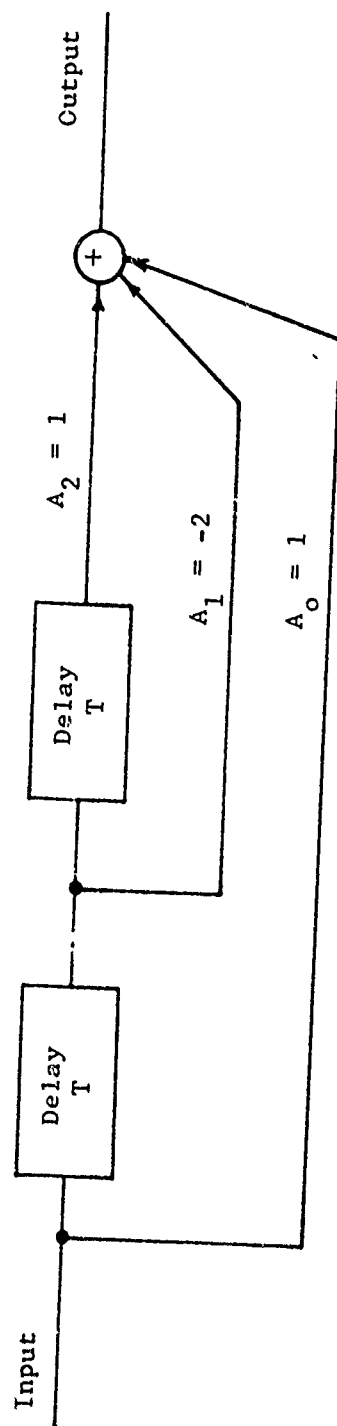


Figure A-1. Three-pulse MFI filter.

$$= \int_{-f_r/2}^{f_r/2} \frac{C}{\sigma_c \sqrt{2\pi}} \exp(-f^2/2\sigma_c^2) \cdot 16 \sin^4(\pi f T) df$$

where f_r = pulse repetition frequency

σ_c = clutter power standard deviation

T = interpulse period = $1/f_r$.

For small values of x

$$\sin x \approx x \text{ and } \sin^4 x \approx x^4.$$

Then

$$\begin{aligned} C_o &\approx \frac{16\pi^4 T^4 C}{\sigma_c \sqrt{2\pi}} \int_{-\infty}^{\infty} f^4 \exp(-f^2/2\sigma_c^2) df \\ &\approx 48\pi^4 T^4 \sigma_c^4 C. \end{aligned}$$

The signal power out of the filter is now computed,

$$\begin{aligned} T_o &= \frac{T_i}{\omega_r} \int_0^{\omega_r} 16 \sin^4(\omega T/2) d\omega \\ &= \frac{T_i}{2\pi f_r} \int_0^{f_r} 32\pi \sin^4 \pi f T df \\ &= 6T_i \end{aligned}$$

The output signal-to-clutter ratio, r_o , is

$$r_o = \frac{T_o}{C_o} = \frac{6T_i}{48\pi^4 T^4 \sigma_c^4 C},$$

and

$$I = \frac{r_o}{r_i} = \frac{1}{8} \left| \frac{f_r}{\pi \sigma_c} \right|^4 .$$

If it is often customary to define $\sigma_v = \sigma_c \lambda / 2$, where λ = wavelength (meters).

Representative values of σ_v are given in Table I, and Figure A-2 shows I plotted as a function of σ_v for values of $f_r = 5$ kHz and $F = 5.5$ GHz, where F = radar frequency.

Some sample calculations of the improvement obtainable can be made with the use of Table II.

If one assumes

$$\sigma_v = 0.22 \text{ (wooded hills, 20 kts)}$$

$$\lambda = 5.5 \text{ cm}$$

$$f_r = 5 \times 10^3 \text{ Hz}$$

then,

$$I = 82.9 \text{ dB.}$$

TABLE I
SUMMARY OF STANDARD DEVIATIONS OF THE CLUTTER SPECTRUM [52]

<u>Source of Clutter</u>	<u>Wind Speed (knots)</u>	<u>σ_v (m/sec)</u>
Sparse Woods	Calm	0.017
Wooded Hills	10	0.04
Wooded Hills	20	0.22
Wooded Hills	25	0.12
Wooded Hills	40	0.32
Sea Echo	--	0.7
Sea Echo	--	0.75 - 1.0
Sea Echo	8-20	0.46 - 1.1
Sea Echo	Windy	0.89
Chaff	--	0.37 - 0.91
Chaff	25	1.2
Chaff	--	1.1
Rain Clouds	--	1.8 - 4.0
Rain Clouds	--	2.0

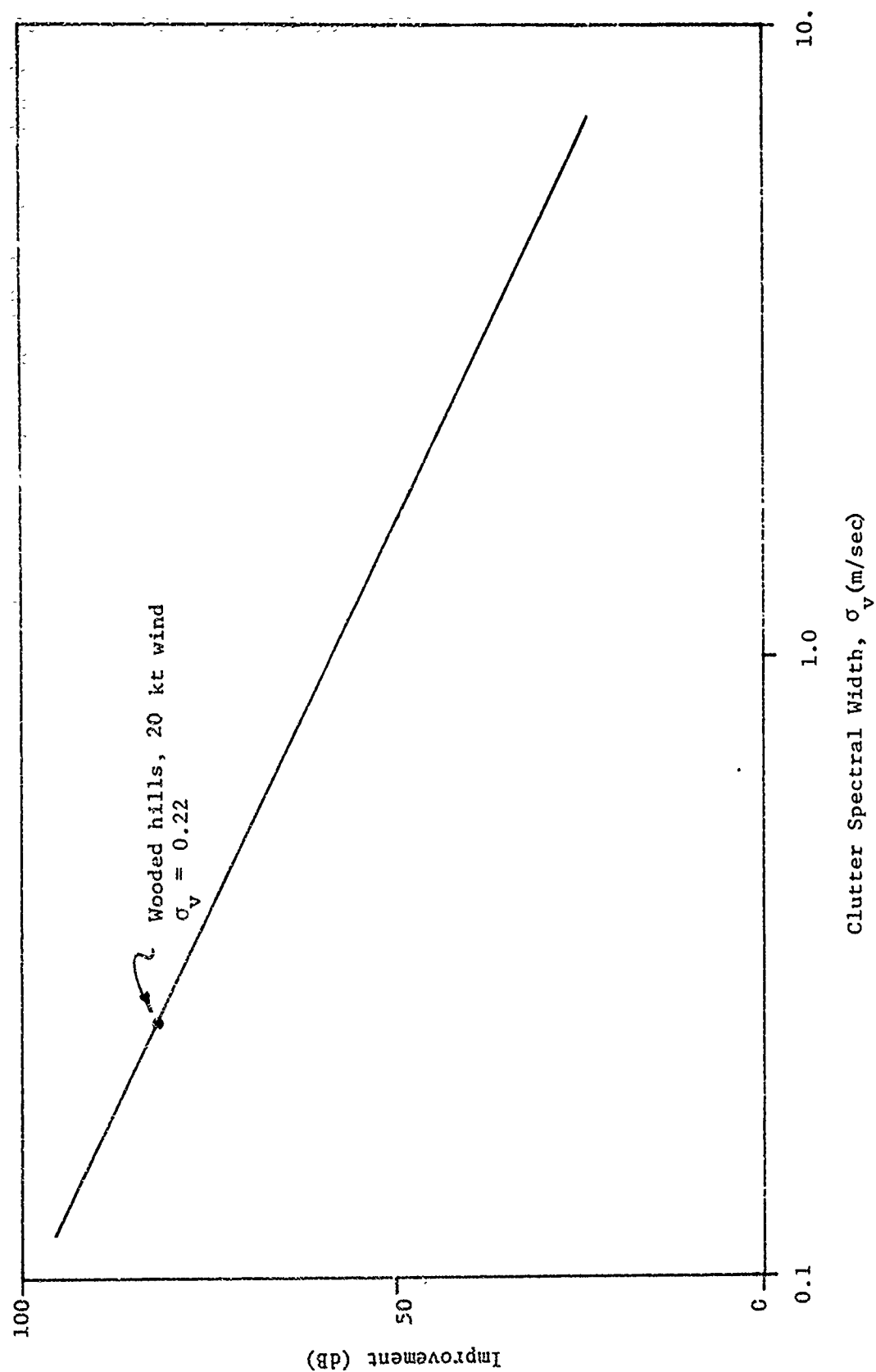


Figure A-2. System improvement versus clutter spectral width for radar system with $f_r = 5$ KHz and $\lambda = 5.5$ cm.

Appendix B

LIMITATION IN IMPROVEMENT FACTOR CAUSED BY ANALOG-TO-DIGITAL CONVERSION

Since radar systems using digital processing must operate with a finite number of bits, errors are introduced by the process of analog-to-digital (A/D) quantization; these errors impose a limit on the MTI improvement that can be obtained. In a system for which E is the value of the least-significant bit, there is a possible error $\pm E/2$ in each conversion. This error has a uniform probability density if the least-significant bit is uncorrelated.

Let the error in quantization be e , and

$$\bar{e} = 0$$

$$\sigma_e^2 = \int_{-E_0/2}^{E_0/2} (x^2/E_0) dx = E_0^2/12,$$

where σ_e^2 is the quantization noise power.

In a nonrecursive filter such as those studied earlier, the noise power out of the filter due to quantization, P_n , is

$$P_n = \frac{E_0^2}{12} \sum_{n=0}^N A_n^2.$$

It has been shown [53] that if the filter output is from -1 to +1, the pulse-to-pulse signal deviation due to quantizer noise is

$$\frac{1}{(2^M - 1) \sqrt{1.5}},$$

where M is the number of A/D converter bits.

The limit this imposes on the improvement factor, I , is

$$I = 20 \log (2^M - 1) \sqrt{1.5}.$$

Since in a two-channel MTI there are two independent errors, then at the output,

$$I = 20 \log (2^h - 1) \sqrt{.75}.$$

For a nine-bit A/D converter, this is 52.9 dB, and for a nine-bit plus sign conversion (ten bits) this is 58.9 dB.

Appendix C

RANGE TRACKING

In conventional radar systems using analog signal processing, the so-called split-gate range tracker is often used to track a desired target in range. In a radar using digital signal processing, however, the conventional split-gate range tracker cannot be used, since received signals are sampled at discrete points. Nevertheless, the information obtained from these discrete samples may be used to perform a range-tracking function.

Consider a representative received pulse (figure C-1) which is sampled at points spaced Δ units of time apart. The current estimate of pulse position we designate by t_o and the pulse amplitude at t_o by Σ_o . Associated with Σ_o are two other samples, Σ_e and Σ_l , which occur at times $t_o - \Delta$ and $t_o + \Delta$ respectively. These three samples may now be used to calculate the error in range, ϵ_r , between t_o and some point on the received pulse. A number of computational algorithms are possible; one which appears very similar to the analog split-gate range-tracking scheme is

$$\epsilon_r = K \frac{\Sigma_l - \Sigma_e}{\Sigma_o} ,$$

where K is a proportionality constant. Another algorithm which has been proposed by the General Electric Company is

$$\epsilon_r = K \frac{\Sigma_l - \Sigma_o}{\Sigma_l + \Sigma_o} .$$

A brief analysis of the performance of these two range tracking algorithms has been undertaken. There are a number of variables in such an analysis that affect system performance, for example: the particular algorithm, the transmitted pulse shape, the receiver bandpass, and the sample spacing. In order to simplify the analysis, a rectangular transmitted pulse and a Gaussian filter response were assumed.

The first step in the analysis was to calculate the received pulse shape for a rectangular transmitted pulse and the appropriate receiver bandpass. A Gaussian filter was assumed since this closely approximates the response which will probably be implemented in the EAR system.

The frequency response of a Gaussian filter is given by [54]

$$H(\omega) = A_o e^{-0.35(\omega/\omega_c)^2} ,$$

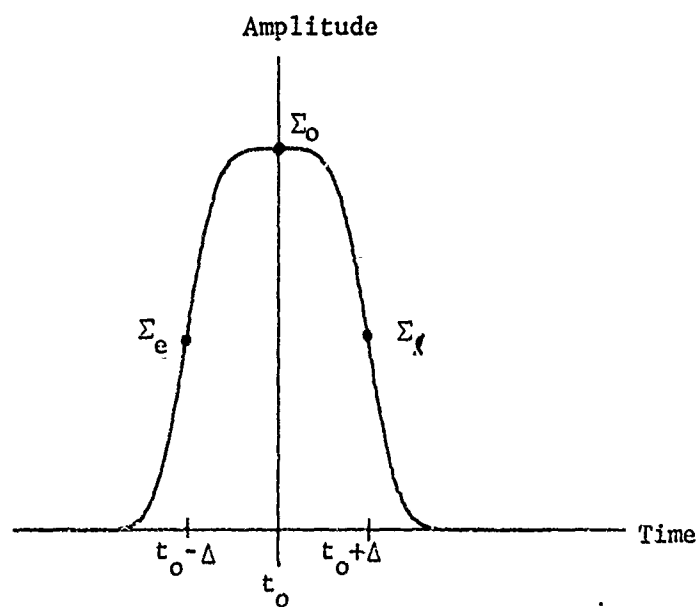


Figure C-1. Representative received pulse shape showing the samples used in the range-tracking algorithms.

where,

$H(\omega)$ = voltage output of the filter,

A_0 = a scale factor,

ω = angular frequency ($2\pi f$)

ω_c = 3-dB video bandwidth of the filter (in radians),

and the filter delay has arbitrarily been set equal to zero. In the above expression, ω_c , the 3-dB video bandwidth, is equivalent to half the 3-dB bandwidth at the IF frequency.

The response of such a Gaussian filter, $a(t)$, to a unit step function is [55]

$$a(t) = \frac{A_0}{2} \left(1 + \operatorname{erf} \frac{\omega_c t}{2/0.35} \right),$$

where

$$\operatorname{erf} x = \frac{2}{\sqrt{\pi}} \int_0^x e^{-y^2} dy.$$

Therefore, the filter response, $f(t)$, to a rectangular pulse of width, T , is given by

$$f(t) = \frac{A_0}{2} \left(1 + \operatorname{erf} \frac{\omega_c t}{2/0.35} \right) - \frac{A_0}{2} \left(1 + \operatorname{erf} \frac{\omega_c (t - \tau)}{2/0.35} \right),$$

or

$$f(t) = \frac{A_0}{2} \left\{ \operatorname{erf} (0.845 \omega_c t) - \operatorname{erf} [0.845(t - \tau) \omega_c] \right\}$$

This information was used to calculate sample values Σ_e , Σ_o , and Σ_{ϵ} . The range error was then calculated using each algorithm. Results are plotted as functions of ϵ/K versus normalized time error t/τ . The condition $t/\tau = 0$ corresponds to the on-target sample coinciding with the leading edge of the rectangular pulse input to the filter, while $t/\tau = 1$ corresponds to the trailing edge. Figure C-2 shows ϵ/K as a function of t/τ for the case $f_{3dB}\tau = 1$ (f_{3dB} is the IF 3-dB bandwidth) and sample spacing $\Delta/\tau = 1$. Figure C-3 is the same type of presentation for $f_{3dB}\tau = 2$. The actual performance of the EAR system probably lies somewhere between these two cases.

The performance of the two tracking algorithms in the presence of receiver noise is an important system design consideration. While an exact analysis is beyond the scope of this project, an approximate analysis gives useful.

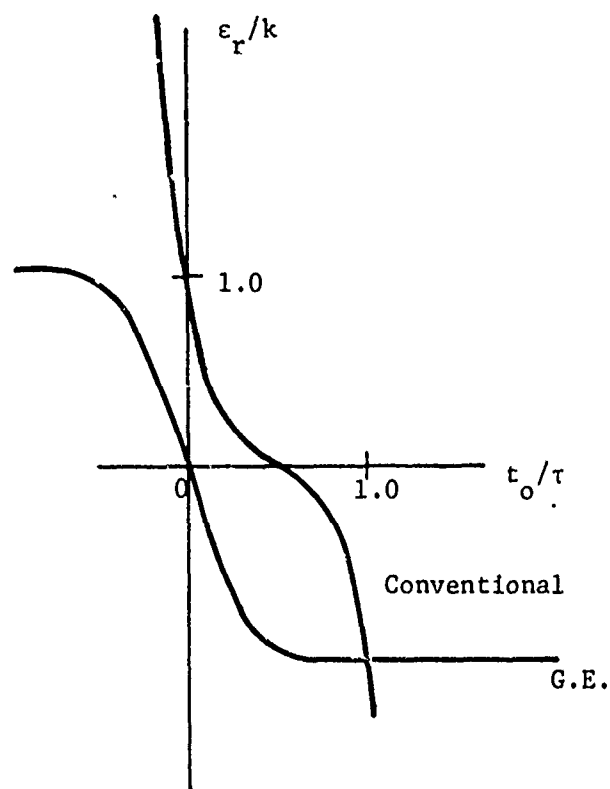


Figure C-2. ϵ_r/k as a function of t_o/τ for $f_{3dB} \tau = 1$ and $\Delta/\tau = 1$.

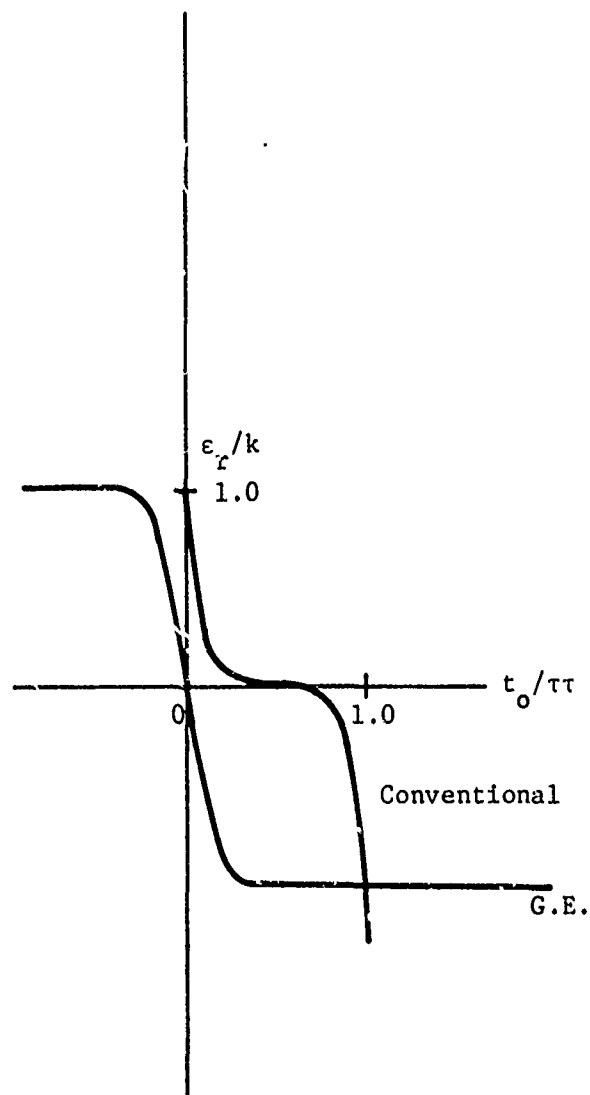


Figure C-3. ϵ_r/k as a function of t_o/τ for $f_{3dB}\tau = 2$ and $\Delta/\tau = 1$.

insight into the performance of the two algorithms.

Assume n_e , n_o , and n_l are the noise voltages associated with Σ_e , Σ_o , and Σ_l , respectively. Then for the conventional tracking algorithm

$$\epsilon_r = K \left[\frac{(\Sigma_l + n_l) - (\Sigma_e + n_e)}{\Sigma_o + n_o} \right] .$$

Assume the signal-to-noise ratio is greater than one, such that

$$\Sigma_o + n_o \approx \Sigma_o .$$

Then

$$\epsilon_r \approx K \left[\frac{\Sigma_l - \Sigma_e + n_l - n_e}{\Sigma_o} \right] .$$

If n_e and n_l are uncorrelated, and their noise powers are both equal to n , and the range tracker is on target ($\Sigma_l - \Sigma_e = 0$), then the rms range error due to noise, σ_{rn} is given by

$$\sigma_{rn} \approx \left(\frac{\sqrt{2n}}{\Sigma_o} \right) .$$

If S/N is the signal-to-noise power ratio, then

$$\sigma_{rn} = K \left[\frac{\sqrt{2}}{\sqrt{S/N}} \right] .$$

While strictly true only for large S/N , the general prediction, that range errors are directly related to K and inversely related to the signal-to-noise ratio, appears to be indicative of the performance for other cases as well.

Figures C-2 and C-3 show that ϵ/K is a much more nonlinear function of range error for the conventional algorithm than for the General Electric algorithm. They also show that the conventional algorithm is relatively insensitive to small variations in position about the true pulse location, particularly for the case $f\tau = 2$, as evidenced by the small slope of ϵ_r/K at $t/\tau = 0.5$. Because of the nonlinearity of the conventional algorithm, it would appear that any assumed value of K for this system would be only approximately correct over the region $0 \leq t/\tau \leq 1$; it appears that this average K would closely approximate the value of K for the General Electric algorithm, so the noise performance would be approximately the same for the two cases. These results indicate substantial advantages in using the algorithm proposed by General Electric. Realistic values of K for the two algorithms are comparable, indicating comparable noise performance. The greater linearity of the General Electric algorithm and the fact that it remains bounded for large errors offer substantial advantages. Partially offsetting this advantage is the fact that the conventional algorithm tracks with a sample on the center of the pulse, thus providing the maximum signal-to-noise ratio.

Appendix D

EFFECTS OF FREQUENCY AGILITY ON BLIND SPEEDS

Changing the carrier frequency of MTI radar has no effect on the frequency response of the filters, but the target blind speeds, V_B , are shifted slightly, since

$$V_B = N \frac{0.29 \text{ prf}}{F} \text{ (knots) } N = 1, 2, \dots$$

prf = pulse repetition frequency (Hz)

F = radar frequency (GHz).

In a frequency-agile radar the blind speeds vary from pulse to pulse, yielding a velocity response that is the sum of the output at each frequency.

Figures D-1 and D-2 show the response for a frequency-agile radar operating with two frequency step sizes. Figure D-1 is for 50-MHz step size and Figure D-2 is for 31.25-MHz step size. The starting frequency is 5.3 GHz, and the stopping frequency is 5.6 GHz for Figure D-1 and 5.8 GHz for Figure D-2.

It may be noted that a marked change is made in the velocity response without benefit of pulse staggering, but approximately 20 dB nulls are present at the lower blind speeds.

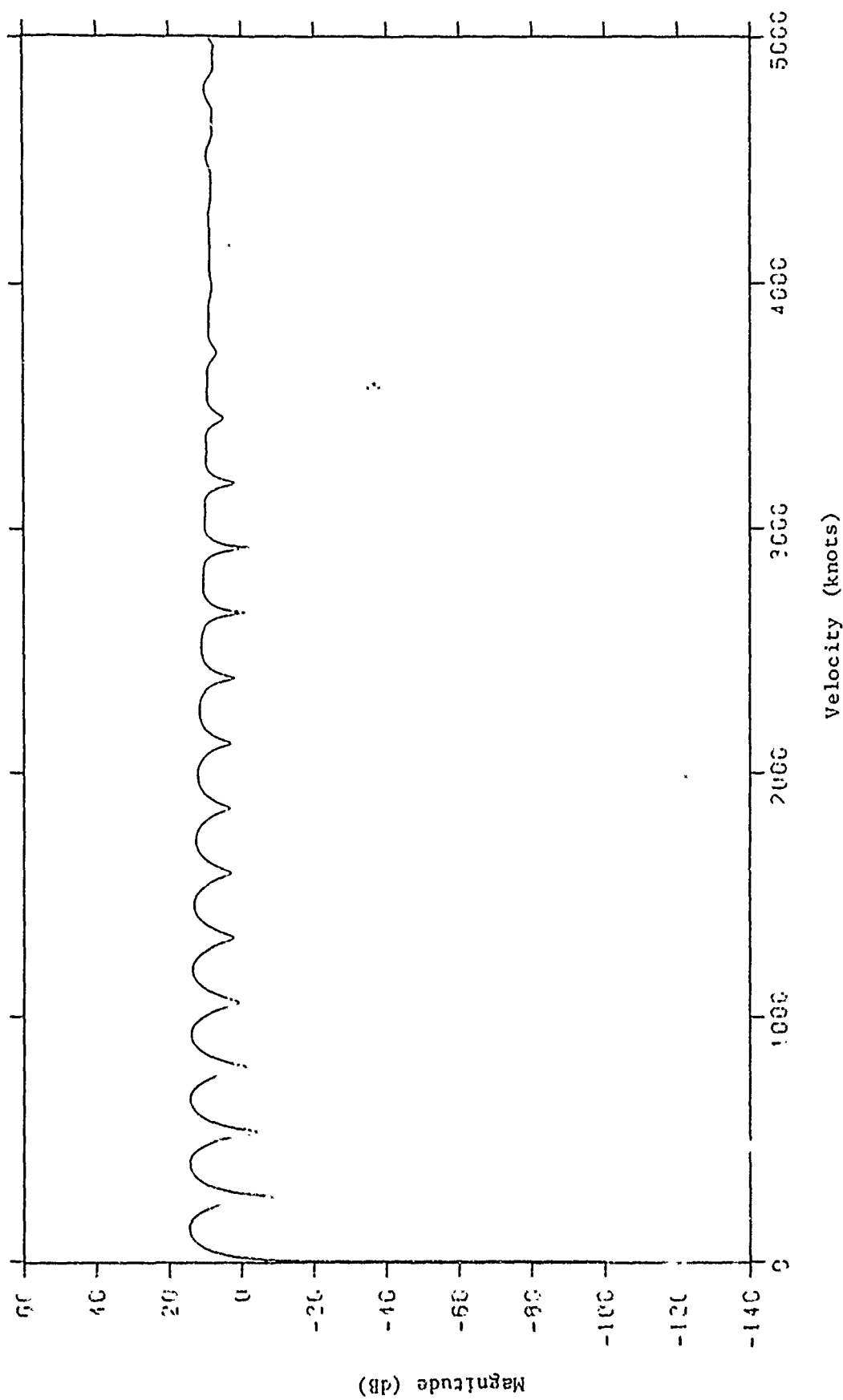


Figure D-1. Velocity response for frequency-agile radar using three-pulse MTI filter.
 $F_{\text{start}} = 5.3 \text{ GHz}$, $F_{\text{final}} = 5.6 \text{ GHz}$, Step = 0.05 GHz.

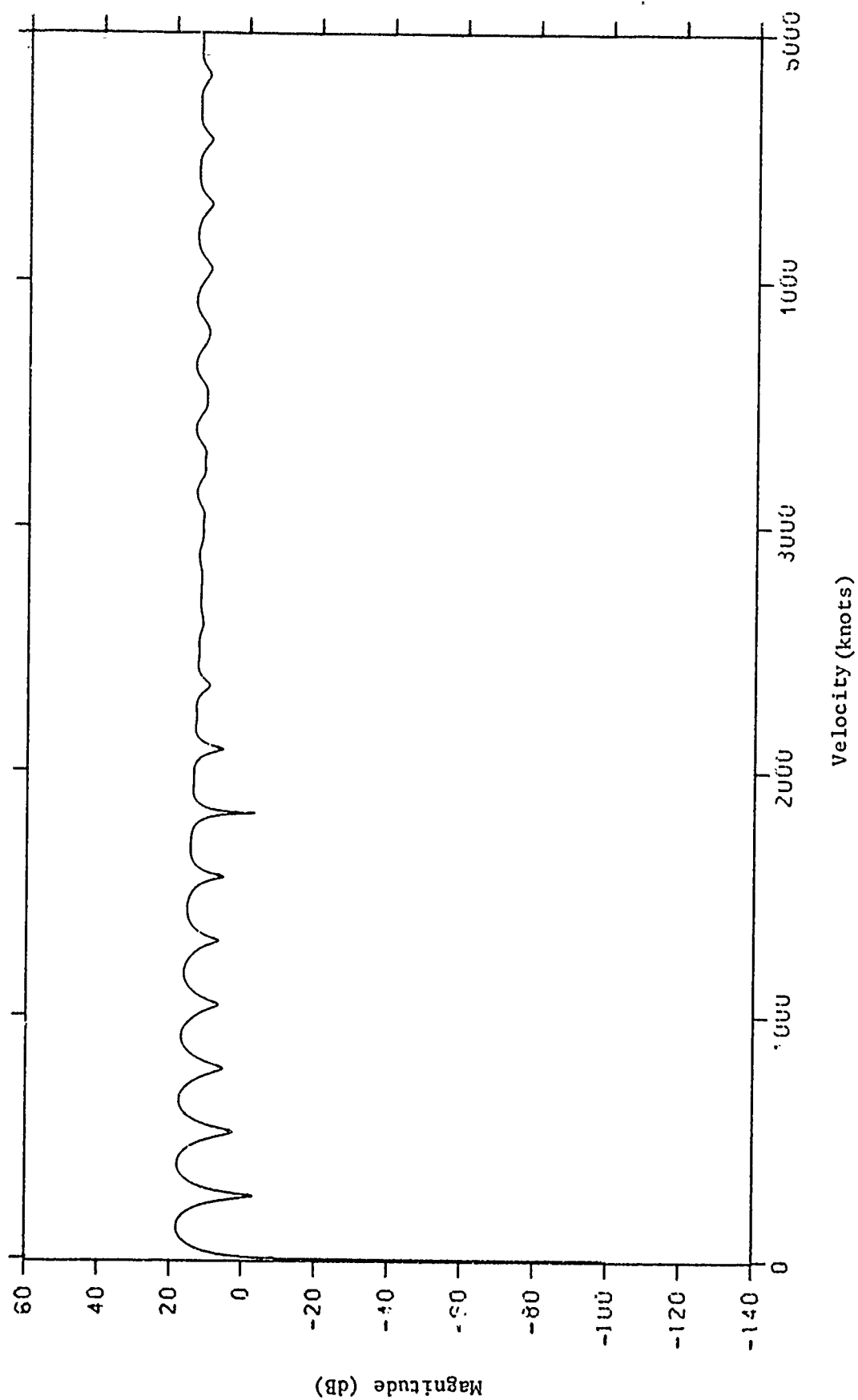


Figure D-2. Velocity response for frequency-agile radar using three-pulse MTI filter.
 $F_{\text{start}} = 5.3 \text{ GHz}$, $F_{\text{final}} = 5.8 \text{ GHz}$, Step = 0.03125 GHz .

Appendix E

COMPUTER PROGRAM

In this appendix is presented the FORTRAN V computer program used in the computation of multipath errors in the EAR system. The subroutines listed are representative of those employed in the generating data for this report; however, various slightly modified versions were used as necessary to produce special outputs.

```

      DIMENSION IBUF(5000),VTITLE(12),HTITLE(12)
      CALL PLOTS(IBUF(1),5000,2)
      WRITE(6,900)
900  FORMAT('ONO PREDICTION FILTER, FREQUENCY AGILE')
      DIMENSION NARRAY(5000),X(1000),ERRFT(1000)
      DIMENSION SLOGG(1000)
      PI=ATAN2(0.,-1.)
      RD=180./PI

100  FORMAT( )
101  FORMAT('ENTER HA,HT,RSTART,V,PRF,FREQ(GHZ),RHO')
102  FORMAT(' BYE')
      PI02=PI/2.
      IDSTRT=-200
      IDSTOP=200
      ILAST=400
      ICNT=400
      THSCAN=0.
      WRITE(6,800)
800  FORMAT('ENTER THANT,DLEVEL')
      READ(5,100) THANT,DLEV
      RHO=0.
      AKS=.85934
10  WRITE(6,101)
      READ(5,100,END=999,ERR=999) HA,HT,RSTART,V,PRF,FREQ,RHO
      WRITE(6,940)
940  FORMAT('ENTER FSTART,FSTOP,FSTEP')
      READ(5,100) FSTART,FSTOP,FSTEP
      RANGE=RSTART+6000.
      THIS=ASIN((HT-HA)/RANGE)
      THSCAN=(THANT-THIS*RD)
      DELTAT=450/PRF
      T=0.
      IFREQ=INT((FSTOP-FSTART)/FSTEP)+1
918  CONTINUE
      TO=T
      FREQ=FSTART-FSTEP
      DO 20 I=1,3
      FMO=FMO(450,IFREQ)
      FREQ=FREQ+FMO)*FSTEP
      ALAM=.9843/FREQ
      THSCAN=THSCAN+ANGERR
      CALL ERRO(HA,THANT,HT,RANGE,ALAM,ANGERR,V,RHO,TH,THSCAN,T,FREQ,
      C      FSTART,FSTOP,FSTEP,PRF,DLEV,SLOGG(I))
      T=T+DELTAT
      XX=THSCAN+THANT
      X(I)=XX+ANGERR
      ERR=XX-TH
      ERRFT(I)=RANGE*ERR/RD

```

Figure E-1. Main Computer program.

```

Y=RANGE*COS(THT/RD)-V*6.*DELTAT/3.6
RANGE=SQRT(Y**2+(HT-HA)**2)
20 CONTINUE
LCNT=200
LCT=LCNT-3
DO 40 I=1,LCT
FREQ=FREQ+FV03*FSTEP
ALAM=.9843/FREQ
THSCAN=THSCAN+ANGERR
CALL ERRO(HA,THANT,HT,RANGE,ALAM,ANGERR,V,RHO,THT,THSCAN,T,FREQ,
C FSTART,FSTOP,FSTEP,PRF,DLEV,SLOGG(I+3))
T=T+DELTAT
XX=THANT+THSCAN
X(I+3)=XX+ANGERR
ERR=XX-THT
ERRFT(I+3)=RANGE*ERR/RD
Y=RANGE*COS(THT/RD)-V*6.*DELTAT/3.6

RANGE=SQRT(Y**2+(HT-HA)**2)
FREQ1=FREQ+.000001
IF(FREQ1.GE.FSTOP) FREQ=FSTART-FSTEP
40 CONTINUE
CALL DIST(NARRAY,ERRFT,IDSTRT,IDSTOP,LCNT,ICNT,IOVER,IUNDER)
WRITE(6,928)
928 FORMAT('ENTER 1 TO PLOT DATA')
READ(5,100) NPLOT
NCNT=NCNT+1
IF(NPLOT.NE.1) GO TO 923
IF(NCNT.GT.1) GO TO 929
DO 777 I=1,12
VTITLE(I)= '
777 CONTINUE
VTITLE(1)='ERROR '
VTITLE(2)='(FEET)'
VLBND=-400.
VUBND=400.
926 FORMAT(12A6)
WRITE(6,927)
927 FORMAT('ENTER TITLE FOR HOR AXIS')
READ(5,926) HTITLE
929 HLBND=T0
HUBND=T
CALL SIMPL(ERRFT,LCNT,VLBND,VUBND,HLBND,HUBND,VTITLE,HTITLE)
923 CONTINUE
MM=MM+LCNT
WRITE(6,920) RANGE,MM
920 FORMAT('RANGE =',F7.1,' FEET,',I5,' ITERATIONS')
WRITE(6,919)
919 FORMAT('ENTER 1 TO CONTINUE ')
READ(5,100) NCONT
IF(NCONT.EQ.1) GO TO 918
999 CONTINUE
CALL PLOT(10,.0,.999)
END

```

Figure F-1. (contd.)

```

COMPLEX FUNCTION GAIN(TH,SCANTH,N)
THSCAN=ABS(SCANTH)
COMPLEX T,ARG
PI02=ATAN2(1.,0.)
PI=2*PI02
R0=180./PI
THZERO=.73 + .27*(THSCAN/40.)
F=1.5 - .5*(THSCAN/40.)
THM=(TH-THZERO)/R0
THP=(TH+THZERO)/R0
UM=F*33.9*PI*SIN(THM)
UP=F*33.9*PI*SIN(THP)
TM=F*PI02*72.8*COS(UM)/(PI02**2-UM**2)
TP=F*PI02*72.8*COS(UP)/(PI02**2-UP**2)
ARG=CMPLX(0.,PI02)
IF(N.EQ.1) T=TM+TP
IF(N.EQ.2) T=(TM-TP)*CEXP(ARG)
GAIN=T
RETURN
END

```

Figure E-2. Subroutine GAIN

```

SUBROUTINE DIST(NARRAY,X,ISTART,ISTOP,ICOUNT,ICNT,I0VER,IUNDER)
DIMENSION NARRAY(5000)
I0VER=0
IUNDER=0
DIMENSION X(1)
K=0
100 FORMAT('DISTRIBUTION RANGES FROM ',I6,' TO ',I6,'.')
101 FORMAT('OTHER WERE ',I4,' POINTS THAT WERE OUT OF RANGE OF THE DI
DISTRIBUTION ARRAY')
102 FORMAT('D MEDIAN IS ',I5)
103 FORMAT('D ',I4,' POINTS WERE UNDER, ',I6,' POINTS WERE OVER.')
NBINS=ISTOP-ISTART
IF(ISTOP.LE.ISTART) GO TO 999
IF(NBINS.GT.5000) GO TO 999
IBOT=ISTOP
ITOP=ISTART
DO 10 I=1,NBINS
10 NARRAY(I)=0
DO 20 I=1,ICOUNT
IX=INT(X(I)+0.5)-ISTART
IF(X(I).LT.0.) IX=INT(X(I)-.5)-ISTART
IF(IX.GT.ITOP) ITOP=IX
IF(IX.LT.IBOT) IBOT=IX
IF(IX.GT.NBINS) I0VER=I0VER+1
IF(IX.LT.1) IUNDER=IUNDER+1
IF((IX.GT.NBINS).OR.(IX.LT.1)) GO TO 30
NARRAY(IX)=NARRAY(IX)+1
GO TO 20
30 K=K+1
20 CONTINUE

ICNT=ICOUNT-K
IBOT=IBOT+ISTART
ITOP=ITOP+ISTART
WRITE(6,100) IBOT,ITOP
SUM=0.
DO 40 I=1,NBINS
K=I
SUM=NARRAY(I)/FLOAT(ICNT)+SUM
IF(SUM.GE..5) GO TO 999
40 CONTINUE
999 CONTINUE
K=K+ISTART
RETURN
END

```

Figure 6-1. Subroutine DIST.

```

SUBROUTINE STNDEV(X,ICOUNT)
DIMENSION X(1)
S=0.
SQ=0.
DO 10 I=1,ICOUNT
S=S+X(I)
XSQ=X(I)**2
SQ=SQ+XSQ
10 CONTINUE
XAVG=S/ICOUNT
XSQAVG=SQ/ICOUNT
SD=SQRT(XSQAVG-XAVG**2)
WRITE(6,100) XAVG
100 FORMAT('0 AVERAGE IS',F6.1)
WRITE(6,200) SD
200 FORMAT('0 STANDARD DEVIATION IS',F6.1)
RETURN
END

```

Figure E-4. Subroutine STNDEV.

```

SUBROUTINE ERRO(HA,THANT,HT,RANGE,ALAM,ANGERR,V,RHO,TH1,THSCAN,T,
C      FREQ,FSTART,FSTOP,FSTEP,PRF,OLEV,SLOG1)
COMPLEX T3,T4,T5,T6,T7,T8,T9,T10,T11,T12
DIMENSION XANG(100),DLOG(100),SLOG(100)
COMPLEX GAIN,EXP,RATIO
COMPLEX T1,T2,T6,T7,S,D
AKS=.845+.335*(THSCAN/30.)
DELTAT=1/PRF
PI=ATAN2(0.,-1.)
RD=180./PI
X=0.
IF(FREQ.GE.FSTOP-FSTEP) FREQ=FSTART-FSTEP
DO 10 I=1,48
IMOD=MOD(I,3)
IF(IMOD.EQ.0) FREQ=FREQ+FSTEP
IF(IMOD.EQ.0) ICNT=1
IF(IMOD.NE.0) ICNT=ICNT+1
ALAM=.9843/FREQ

TH1=ASIN((HT-HA)/RANGE)
TH1=TH1*RD
YY=SQRT(RANGE**2-(HT-HA)**2)
THIM=-ATAN2((HA+HT),Y)
THIM=THIM*RD
Y=YY-V*DELTAT/.6
RANGE=SQRT(Y**2+(HT-HA)**2)
DELTAR=4.*PI*HA*(HA+HT)/(ALAM*RANGE)
THBEAM=THANT+THSCAN
TH1=TH1-THBEAM
TH2=THIM-THBEAM
EXP=CMPLX(0.,-DELTAR)
T1=GAIN(TH1,THSCAN,1)
T2=GAIN(TH2,THSCAN,1)
T6=GAIN(TH1,THSCAN,2)
T7=GAIN(TH2,THSCAN,2)
T8=T6*RCS(TH1)
T9=RHO*CEXP(EXP)*T6*RCS(TH1)
T10=RHO*CEXP(EXP)*T7*RCS(TH2)
T11=RHO*RHO*CEXP(2*EXP)*T7*RCS(TH2)
D=T8+T9+T10+T11
DMAG=CABS(D)
IF(DMAG.LT.1E-10) DMAG=1E-10
DLOG(I)=20*ALOG10(DMAG)
T3=T1*RCS(TH1)
T4=RHO*CEXP(EXP)*T1*RCS(TH1)
T5=RHO*CEXP(EXP)*T2*RCS(TH2)
T12=RHO*RHO*CEXP(2*EXP)*T2*RCS(TH2)
S=T3+T4+T5+T12

```

Figure E-5. Subroutine ERRO.

```

SMAG=CABS(S)
IF(SMAG.LT.1E-10) SMAG=1E-10
SLOG(I)=20*ALOG10(SMAG)
RATIO=D/S
XANG(I)=AKS*AIMAG(RATIO)
DELSL=SLOG(I-3)-SLOG(I)
IF(DELSEL.GT.DLEV) XANG(I)=XANG(I-1)
X=X+XANG(I)
1  FORMAT()
FREQ1=FREQ+.000001
IF((FREQ1.GT.FSTOP).AND.(ICNT.EQ.3)) FREQ=FSTART-FSTEP
10 CONTINUE
SLOG1=SLOG(I)
T=T+.01
ANGERR=X/48
RETURN
END

```

Figure E-5. (contd)

```

FUNCTION RCS(TH)
DATA RD/57.29578/
THR=TH/RD
THR1=180*TH/RD
T1=COS(THR)**2
T2=COS(THR1)
RCS=T1.
RETURN
END

```

Figure E-6. Subroutine RCS.

APPENDIX F

FREQUENCY RESPONSE OF NONRECURSIVE DIGITAL FILTERS

The nonrecursive digital filter is illustrated in Figure F-1. This processor is typified by simplicity of analysis, economical hardware implementation, and short settling time.

The output of the filter is formed from a weighted sum of the previous $N + 1$ input samples, where N is the number of delay elements. It follows directly from Figure F-1 that $h(t)$, the impulse response of the filter, is given by

$$\begin{aligned} h(t) &= A_0 \delta(t) + A_1 \delta(t-T) + A_2 \delta(t-2T) + \dots + A_N \delta(t-NT) \\ &= \sum_{k=0}^N A_k \delta(t-kT), \end{aligned} \quad (1)$$

where $\delta(t)$ represents a unit impulse, and A_n is the weight of the N th sample.

To compute the complex frequency response of the network, $H(\omega)$, the Fourier Transform is applied to (1), yielding

$$H(\omega) = \sum_{k=0}^N A_k e^{-jk\omega T}. \quad (2)$$

The power response of the filter, $G(\omega)$, is then

$$G(\omega) = H(\omega) \cdot H^*(\omega) = C_0 + 2 \sum_{q=1}^N C_q \cos(q\omega T), \quad (3)$$

$$\text{where } C_q = \sum_{j=0}^{N-q} A_j A_{j+q} \quad 0 \leq q \leq N.$$

Equation 3 will be recognized as a truncated Fourier Series, whose coefficients are simple combinations of the filter coefficients.

Preceding page blank

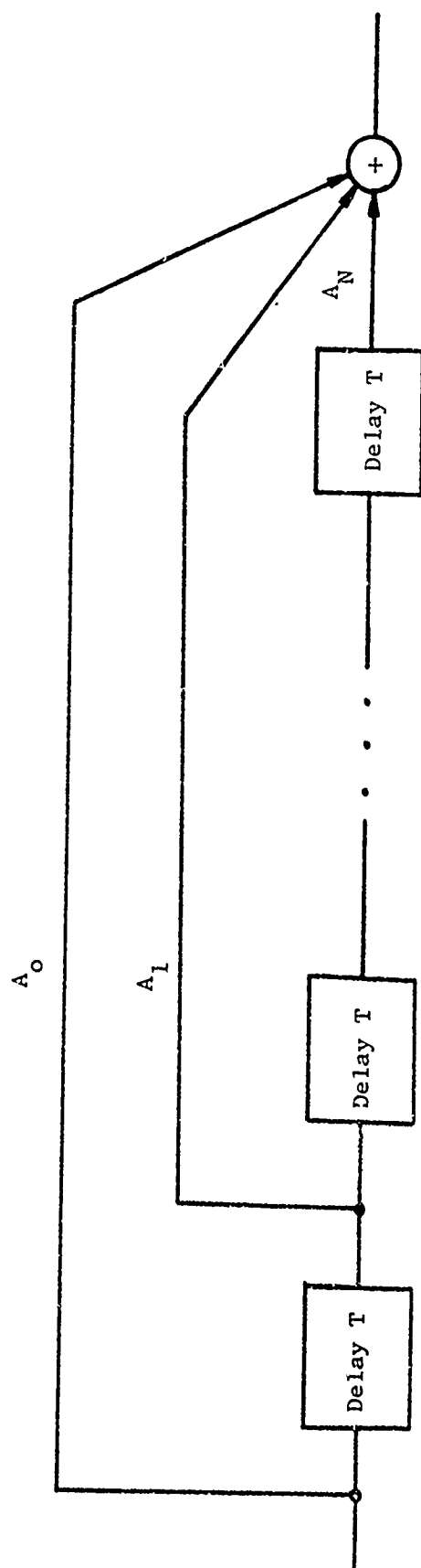


Figure F-1. General form of nonrecursive digital filters.